1-1-2012

High Intensity Focused Ultrasound and Microbubble Induced Tissue Ablation: Effect of Treatment Parameters on Thermal Lesion Volume and Temperature

Sonal Bhadane
Ryerson University

Follow this and additional works at: http://digitalcommons.ryerson.ca/dissertations

Part of the Atomic, Molecular and Optical Physics Commons

HIGH INTENSITY FOCUSED ULTRASOUND AND MICROBUBBLE INDUCED TISSUE ABLATION: EFFECT OF TREATMENT PARAMETERS ON THERMAL LESION VOLUME AND TEMPERATURE

By

Sonal Bhadane

B.Sc. Medical Radiation Sciences,

University of Toronto, 2008

A thesis

presented to Ryerson University

in partial fulfillment of the

requirements for the degree of

Master of Science

in the Program of

Biomedical Physics

Toronto, Ontario, Canada, 2012

© Sonal Bhadane 2012

Author's Declaration

I hereby declare that I am the sole author of this thesis. This is a true copy of the thesis, including any required final revisions, as accepted by my examiners.

I authorize Ryerson University to lend this thesis to other institutions or individuals for the purpose of scholarly research I further authorize Ryerson University to reproduce this thesis by photocopying or by other means, in total or in part, at the request of other institutions or individuals for the purpose of scholarly research.

I understand that my thesis may be made electronically available to the public.

High intensity focused ultrasound and microbubble induced tissue ablation: effect of treatment parameters on thermal lesion volume and temperature

Master of Science, 2012

Sonal Bhadane

Biomedical Physics

Ryerson University

ABSTRACT

Microbubble agents have been shown to increase therapeutic effect of HIFU (High intensity focused ultrasound). Here, the effects of treatment parameters on lesion volume and temperature are investigated. *Ex vivo* tissue was treated with a 2 MHz HIFU beam in absence and presence of the Artenga® microbubbles at varying HIFU focal intensities (600-2300 W/cm^2), microbubble concentrations, and exposure durations (3-10 s). The temperature was measured at 1 mm from focus using a K-type thermocouple. Thermal lesion volume was measured based on an ellipsoid model. Microbubbles increased the lesion volume and peak temperature achieved with HIFU. At 2316 W/cm^2 intensity, the lesion volume increased by 2-folds, and the peak temperature increased by 16 °C with microbubbles. This effect depended on microbubble concentration, ultrasound intensity and exposure duration. Lower intensities and shorter time durations were required at higher microbubble concentrations to ablate the tissue. It was concluded that the efficacy of the HIFU therapy in combination with microbubbles can be controlled through ultrasound/ microbubble exposure parameters.

Keywords: High intensity focused ultrasound, microbubble, thermal lesion

Acknowledgments

TABLE OF CONTENTS

LIST OF TABLES

LIST OF FIGURES

LIST OF APPENDICES

CHAPTER 1

INTRODUCTION AND BACKGROUND

1.1. CANCER

Cancer is the general name for a group of more than 100 diseases where cells in a part of the body begin to grow abnormally and uncontrollably (Canadian Cancer Society, 2011). Although there are many kinds of cancer, they all start because abnormal cells grow out of control. In 2007, cancer surpassed cardiovascular and cerebrovascular diseases as the leading cause of death in Canada. Estimated by the Canadian cancer statistics, 40% of Canadian women and 45% of men will develop cancer during their lifetimes. An estimated 1 out of every 4 Canadians is expected to die from cancer (Canadian Cancer Society, 2011). Human efforts have made great strides in the treatment of cancer. A century ago the chances of someone surviving cancer was negligible. Today two out of every three people diagnosed will still be alive at the end of five years. It is evident by the ever-increasing number of survivors that cancer treatment continues to improve, although the 'cure' for cancer has been far more elusive than once hoped (Frenkel, 2008). Cancer treatment has improved in part due to the increase in understanding of cellular, genetic and molecular mechanisms, which provide targets for interventions to prevent, detect, eliminate and control the disease (von Eschenbach, 2004). When the disease is local, surgery and radiation therapy are commonly used to treat cancer with a radical intent. Technological advancements in imaging and non-invasive treatments bring new therapeutic possibilities to the field (Alongi, 2011). Among the minimally invasive treatment methods that have been developed, thermal therapy is the most investigated technology in the new panorama of solid tumor treatment based on ultrasound (ter Haar, 2001; Kennedy, 2005).

1.2. THERAPEUTIC ULTRASOUND

Therapeutic ultrasound is generally described as the use of ultrasound for applications other than imaging or diagnostics (Frenkel, 2006). In diagnostic ultrasound, biological effects are undesirable and hence the energy deposition in tissues is meant to be minimal. Whereas application of therapeutic ultrasound is based on depositing ultrasound energy to specifically

create beneficial effects. These effects can be mild and non-destructive, like those generated for physiotherapy healing (Warden et al., 2006), or more extreme and destructive, such as thermal ablation of tumors (Kennedy, 2005). The mechanisms of interaction between ultrasound energy and various cells and tissues for producing therapeutic effects are typically divided into thermal and non-thermal mechanisms (Mitragotri, 2005). The three most important ultrasound mechanisms (heat generation, acoustic cavitation, and acoustic radiation forces) for creating bio-effects will briefly be covered in later sections.

1.2.1. APPLICATIONS OF THERAPEUTIC ULTRASOUND

In 1927 it was recognized that ultrasound could produce lasting change in biological systems. This was the start of both ultrasound therapy and safety studies (Wood and Loomis, 1927). Tissue heating due to ultrasonic energy absorption has been used with therapeutic intent in many conditions. Recently it has been realized that benefit may also be obtained from the non-thermal effects that occur as ultrasound travels through tissue. Therapeutic ultrasound applications can generally be divided based on the direct effects of ultrasound energy deposition and the enhanced delivery of therapeutic agents (Frenkel, 2008).

Ultrasound therapies can broadly be divided into low power and high power therapies where low power applications include sonophoresis, sonoporation, gene therapy, sonothrombolysis, bone healing and wound healing. High power therapies encompasses physiotherapy, Histotripsy, high intensity focused ultrasound (HIFU) and lithotripsy. Apart from physiotherapy uses, ultrasound therapies are currently not widespread. This section will describe the most frequently used applications of ultrasound for therapy as well as those for which research is currently most active.

1.2.1.1: LOW POWER THERAPIES

Sonophoresis: Sonophoresis is defined as increase in the penetration of pharmacologically active drugs through the skin by using ultrasound (Frenkel, 2011; ter Haar, 2007). Transdermal (through skin) drug delivery offers an attractive alternative to conventional drug delivery methods such as oral administration and percutaneous injection. Mechanisms involved in sonophoresis are unclear. It is believed that the stratum corneum (outermost layer of epidermis)

serves as a barrier that limits the penetration of agents through the skin. Ultrasound application temporally renders the skin permeable by non thermal effects such as acoustic cavitation or streaming thereby allowing the enhanced perfusion (Bommannan et al., 1992a, b; Ziskin and Michlovitch, 1986; Mitragotri and Blankschtein, 1995; Tezel and Mitragotri, 2003; Mitragotri et al., 1995; Frenkel, 2011).

Sonoporation: The phenomenon by which ultrasound may transiently alter the structure of the cellular membrane, and thus allow enhanced uptake of low and high molecular weight molecules into the cell is called sonoporation (ter Haar, 2007). Presently, large number of studies seek a synergistic effect between ultrasound and different drugs. There is a growing evidence that cavitation either induced in tissue by the ultrasound exposure or facilitated by microbubbles introduced into the tissue, is instrumental in enhancing drug delivery (Unger et al., 2004; Dijkmans et al., 2004). Bubbles (explained in a later section) increase the local absorption of ultrasound and oscillate or resonate in response to the pressure field. Depending on the driving parameters and the bubble size, they may break up, releasing a shock wave and creating microjets locally inducing mechanical effects. These bubbles may be used in a number of ways to aid drug delivery. Drugs may be encapsulated within the bubble; they may be incorporated into the shell or incorporated into it by ligands embedded into the lipid membrane. Microbubbles have also been constructed with a multilayered shell-containing drug. If these bubbles can be accumulated within the target volume, ultrasound can destroy them locally, releasing the drug (ter Haar, 2007; Unger et al., 2004).

Gene therapy: Gene therapy involves facilitating the transfer of genes into diseased tissues and organs using ultrasound. The main goal is to increase the delivery efficiency of exogenous nucleic acid to the intended target. Ideally the gene expression would be enhanced in the target while having no effect in non-target tissues. Ultrasound has been shown to enhance gene transfer into cells *in vitro* (Bao et al., 1997; Kim et al., 1996; Lawrie et al., 1999; Tata et al., 1997). This has also been demonstrated *in vivo* (Bao et al., 1998; Bednarski et al., 1997). The exposure levels required to destroy microbubbles for enhanced gene therapy lie in the diagnostic range (Huber et al., 1999). Ultrasound-enhanced gene therapy is a rapidly evolving field.

Sonothrombolysis: Sonothrombolysis technique uses ultrasound to aid the dissolution of blood clots either on its own or in combination with microbubble contrast agents and fibrinolytic drugs (ter Haar, 2007). The mechanisms for the enhancement of the thrombolytic effect are poorly understood, but a number of processes have been suggested. It has been proposed that acoustic streaming may facilitate the permeation of the drug into the clot, or that the mechanical action of the ultrasound affects the fibrin mesh, allowing better access for the drug. There is also evidence that cavitation may be key in producing effects. Microstreaming occurring around oscillating bubbles in the vicinity of the cell membrane will also alter the cellular environment (Rosenschein et al., 1997, Rosenschein et al., 1999; Yock and Fitzgerald, 1997; Schafer et al., 2005).

Bone healing and wound healing: There is some evidence in the literature that low intensity ultrasound can enhance repair rates and reduce healing times (Dyson and Brookes, 1983; Pilla et al., 1990). Dyson and Brookes (1983) showed in their experiments in rat fibulae that when ultrasound exposures are carried out during the inflammatory and early proliferative phases of bone repair following fracture, healing can be accelerated, with direct ossification being observed. Mechanisms that have been proposed are signal transduction, gene expression enhancement, blood flow changes, tissue modeling or re-modeling effects or micro-mechanical stresses. There is experimental and some clinical evidence of the beneficial effects of very low ultrasound intensities on bone repair (Warden, 2006; ter Haar, 2007).

1.2.1.2 HIGH POWER THERAPIES

Physiotherapy: Physiotherapy ultrasound is used mainly in the treatment of soft tissue injuries, for the acceleration of wound healing, the resolution of edema and softening of scar tissue. It is also used, amongst other things, for musculoskeletal injuries, muscle relaxation pain relief etc. (ter Haar, 2007). The mechanism of action is known to be thermal. A non-focused beam with low-level energy deposition is typically used for physiotherapy (Byl, 1995).

Lithotripsy: Lithotripsy has been the most common treatment for kidney stones since 1980s and continues to be the favored method for uncomplicated, upper urinary tract calculi, even with the advent of percutaneous surgical techniques. Ultrasound induced shock waves are used to disintegrate kidney and gallbladder stones. Main mechanisms studied in lithotripsy are erosion

(coleman et al., 1987), shear (Lokhandwalla et al., 2001), and circumferential compression (Eisenmenger, 2001). These mechanisms may all be activated to differing degrees by either the lithotripter shock pulse or the subsequent collapse of cavitation bubbles excited by the pulse (ter Haar, 2007).

Histotripsy: Histotripsy is a promising extracorporeal ultrasound technology that produces nonthermal tissue fractionation by cavitation (converting the targeted tissue into an a cellular liquid) (Lake et al., 2008). Cavitation occurs when intense ultrasound pulses induce extreme pressure changes within the targeted tissue, resulting in the formation of a localized, highly dynamic cluster of microbubbles. These bubbles oscillate and violently collapse, producing localized stresses that mechanically fractionate and subdivide the targeted tissue, resulting in cellular destruction (Fry et al., 1970; Tran et al., 2003; Xu et al., 2004; Parsons, Cain and Fowlkes, 2004; Xu et al., 2005; Roberts et al., 2006; Kieran et al., 2007; Hall et al., 2007).

High intensity focused ultrasound: More pronounced effects are generated as the rate of energy being deposited in the tissue increases. Lynn and Putnam (1944), and Lynn et al. (1942), were the first to demonstrate that focused ultrasound beams could produce regions of highly localized biological effect. High intensity focused ultrasound (HIFU) was developed for local tissue destruction in the brain for Parkinson's disease by Fry (1958), and Fry et al. (1955). Use of HIFU for cancer therapy, was first suggested by Burov (1956). Early use was made of HIFU in the treatment of Parkinson's disease (Fry and Fry, 1960) and for a number of ophthalmological problems, including the treatment of glaucoma and retinal tears (Coleman et al., 1985a–c; Lizzi et al., 1978). The further development of these applications was inhibited by the introduction of L-dopa for treatment of Parkinsonism, and of lasers for eye surgery. It was not until the 1990s that HIFU began to be used more widely due to the advent of advanced imaging techniques for targeting and monitoring. The revival of interest was largely fuelled initially by the search for non-invasive treatments of benign prostatic hyperplasia (BPH) (ter Haar, 2006). Other uses of HIFU include the preclinical studies that demonstrated how these exposures can accelerate the recovery of sciatic nerve injury (Mourad et al., 2001). Higher energy deposition rates are presently being used to ablate solid tumors, such as prostate cancer (Thuroff et al., 2003) and uterine fibroids (Stewart et. al. 2003). These types of exposures, which produce irreversible cell death by the process of coagulative necrosis, are also being evaluated in clinical trials for treating

5

breast and kidney tumors (Wu, 2003), liver tumors (Kennedy et al., 2004), testicular cancer (Kratzik et al., 2006), and for palliation in patients with bone cancer (Catene et al., 2007). The same types of HIFU exposures, generating high levels of heat, are also presently being developed for controlling hemorrhage (Zderic and Vaezy, 2007).

1.2.2. HIFU DEVICES

Extracorporeal devices: During last 20 years, many prototype extracorporeal devices have been used in feasibility studies (Visioli et al., 1999; Vallancien et al., 1996; Kohrmann et al., 2002). However, at present the use of only 2 commercially available devices has been reported in the medical literature (Gianfelice et al., 2003; Wu et al., 2004). China designed and developed the first commercially available extracorporeal device –JC focused ultrasound (Chongqing HIFU Technology Company, Chongqing, China). It has 12-cm-diameter plane lead-zirconate-titanate disc transducer with an aluminium alloy lens with focal length of 10 to 16 cm. It is driven at 0.8, 1.2, or 1.6 MHz. It operates at relatively high intensities (up to 20,000 W/cm^2) and also has a built-in 3.5-MHz diagnostic scanner (Wu, Chen and Bai, 1999). The majority of the published clinical data comes from work with this device. A second extracorporeal device is MRI-compatible, 10-cm-diameter focused transducer with an 8-cm radius of curvature, operating at 1.5 MHz (GE Medical Systems, Milwaukee, Wisconsin) (Hynynen et al., 2001). This device is only licensed for use with uterine fibroids. It is being installed in many centers worldwide.

Transrectal Devices: There are 2 commercially available transrectal devices. They are undergoing multicenter evaluation to assess their role in the management of prostate cancer (Leslie and Kennedy, 2006). The Sonablate 500 transrectal device (Focus Surgery; Milpitas, California) uses a 4-MHz curved lead-zirconate-titanate transducer with a dimension of 3.0 x 2.2 cm for treatment. The central, circular, 12-mm-diameter portion is used for imaging. The focal length can be 3.0, 3.5, 4.0, or 4.5 cm. The intensity at the focus is 1680 to 2000 W/cm^2, depending on the focal length (Madersbacher, 1993). The second transrectal device is the Ablatherm (Technomed International, Lyon, France) system. This device includes a bed, ultrasound power generator, a probe-positioning system, cooling system for preservation of the rectal wall, and the ultrasound scanner (Chaussy and Thuroff, 2000). There is a treatment and imaging endorectal probe that incorporates both a bi-plane imaging probe that works at 7.5 MHz

and uses a rectangular phased-array transducer focused at 4.0 cm that is driven at a working frequency of between 2.25 and 3.0 MHz with a spatially averaged intensity of 1000 W/cm^2.

1.2.3 HIFU LIMITATIONS:

Safety is paramount in developing any new technology. It is important to consider the safety, side effects, and limitations of the treatment. A clear knowledge of expected and hazardous side effects is critical in order to achieve regulatory approval and for a patient to give fully informed consent for a procedure. HIFU has been investigated extensively in small and large animals. It has been shown to be successful for the treatment of liver tumors in the former (ter Haar, Rivens and Chen, 1991) and in the selective destruction of normal liver, bladder, muscle, and kidney in the latter (Chapelon et al., 1992; Vaughan et al., 1994). Small-animal studies have also shown that HIFU does not increase the risk of tumor metastasis (Oosterhof et al., 1997).

Studies involving transrectal HIFU for the treatment of prostate cancer have recorded side effect profiles (Leslie and Kennedy, 2006). The most serious complication described is rectal wall injury. This can lead to the formation of a rectourethral fistula. Although, after improvements in device-design and safety features such as rectal wall cooling, this particular complication occurs very rarely at less than 1%. The other side effects are disease specific, with urinary incontinence (<5%) and impotence (≈50%) being the most common. The general consensus from all studies to date has been that extracorporeal and transrectal HIFU are both safe and acceptable to patients.

The adverse effects of the HIFU process have been reported in previous studies. First, on the basis of clinical experiences in China (Wu et al., 2004) it can be seen that the duration of HIFU treatment is long. The procedure takes several hours and the patients must lie on the therapy platform, making them uncomfortable and causing unnecessary deposition of energy in the surrounding tissues. This procedure may cause adverse events such as skin burns, transient pain, and nerve injury. Kennedy et al. (2004) reported that the most severe treatment-related adverse events were transient pain and superficial skin burns in their study for the HIFU treatment of 11 patients with liver tumors. Second, a few live cells may be left in the targeted area after HIFU ablation. Spaces between extremely small focal regions of HIFU may result in the survival of a few cells in the focal area (Gelet et al., 1999). Third, ablation and blocking of micro vessels

smaller than 0.2 mm in diameter is achievable with HIFU, but it is less effective with vessels 0.2 mm in diameter and larger because rapid blood flow may reduce HIFU energy absorption, preventing it from depositing sufficient energy in the target zone within a short time (Wu et al., 2004). These adverse effects may be due to small throughput and long treatment time. Therefore, HIFU energy deposition should be enhanced in a much shorter time. Factors related to HIFU energy deposition in HIFU therapy consist of the acoustic intensity of transducers, energy absorption characteristics of tissues and the exposure duration. Theoretically, elevating acoustic intensity or prolonging duration of sonication can change small throughput. However, there is always a risk of depositing more energy to the overlying tissue. The resulting effect is a longer ablation time for patients with an increase in the incidence of adverse effects and the technical difficulty of providing treatment. Many studies have focused on how the tissue characteristics of acoustic absorption can be changed to make energy deposition more efficient (Clement et al., 2004; Wang et al., 1998). In order to enhance the HIFU ablation efficiency, heating, cavitation, and mechanical events in the target tissues should be enhanced (Melodelima et al., 2004; Poliachik et al., 1999; Feng et al., 2005). Several types of materials such as iodized oil, porphyrin, and ultrasound contrast agents have been investigated for enhancing energy deposition in tissue in the past (Chen et al., 1997; Kessel et al., 1994). In particular, ultrasound contrast agents have been intensively studied to enhance the effect of HIFU therapy (Chen et al., 1997).

1.3 MICROBUBBLES

1.3.1 GENERAL PROPERTIES OF MICROBUBBLES

Microbubbles are comprised of micron sized spherical cavities filled by a gas. A coating material such as phospholipids, surfactant, denatured human serum albumin or synthetic polymer stabilizes the microbubbles for medical purposes (Cosgrove, 2006). Gas is less dense than a liquid or solid, hence, microbubbles comprise of a low-density region or pocket. This property of low density of microbubbles has a number of potentially important medical applications. These include site-specific delivery, treatment of thrombosis and pulmonary delivery (Crum et al., 1992). Ultrasound can be used to exploit the diagnostic and therapeutic applications of microbubbles. Sound travels more slowly in gas than in liquid. The difference in sound speed

and density of microbubbles compared to soft tissue creates an acoustic impedance mismatch between the bubble and surrounding tissue and blood. Microbubbles reflect the ultrasound energy; therefore they are used as contrast agents for ultrasound imaging. Microbubbles also lower the threshold for cavitation with ultrasound. Microbubbles can be used as therapeutic cavitation nuclei with ultrasound. Cavitation is generally easier to produce at lower frequencies of ultrasound (Apfel et al., 1991, Crum et al., 1992). Microbubbles must be sufficiently smaller in size compared to red blood cells to allow for easy passage through the capillaries during intravascular applications. Microbubbles should be sufficiently stable to circulate for a long enough period of time in order to reach the target site. The stability of microbubbles in liquid (e.g., a biological fluid such as the blood) depends upon the surrounding medium temperature, pressure, the solubility and composition of the gas in the microbubble, the concentration of dissolved gases and the coating material surrounding the microbubble (Unger et al., 2006). Uncoated air filled microbubbles rapidly dissolve within blood. Lipid coated microbubbles are more stable. Microbubbles comprised of high molecular weight perfluorocarbon gases have a longer life time in the blood (Unger et al., 2006).

1.3.2 FREE BUBBLES AND ENCAPSULATED MICROBUBBLES

The activity associated with air or gas bubbles, pockets and cavities under excitations of acoustic waves is referred to as "acoustic cavitation". Free bubbles are usually cavities filled with air or gas vapor from surrounding liquid (Wu and Nyborg, 2008). They have no artificial boundaries to prevent leakage of air or gas from the bubbles unlike encapsulated microbubbles (EMB). They are unstable in a liquid for various reasons. They may be dissolved into the liquid because of the Laplace pressure that is the pressure difference between the inside and the outside of the bubble, imbalance due to the surface tension or they may float to the top of the liquid and disappear under the influence of gravitational force (Wu and Nyborg, 2008). They may also coalesce into larger bubbles. Those microscopic bubbles may grow in volume during ultrasonic excitation via a process called "rectified diffusion" (Crum, 1980). Rectified diffusion is a phenomenon where the influx of gas during the expansion of a bubble exceeds outflux during contraction.

EMBs are commercially available for diagnostic US imaging, and therefore are also called ultrasound contrast agents (UCAs). Their acoustic impedance is very different from that of the

soft-tissue. Several cardiac and vascular ultrasound contrast agents are commercially available: Optison® (GE Healthcare, Princeton, NJ) and Definity® (Lantheus Medical Imaging, Inc, Billerica, MA) in the U.S.A. SonoVue^{TM} (Bracco diagnostic inc, Milan, Italy) in Europe. Other agents undergoing regulatory approval include EchoGen® (Sonus Pharmaceuticals, Bothell, WA, USA), SonoVue® (Bracco Diagnostics, Milan, Italy), Imagent® (Imcor Pharmaceutical, Sandiego, CA, USA), Sonazoid® (Nycomed-Amersham, Oslo, Norway), Quantison® (Quadrant, Ltd, Nottingham, UK) and Artenga® (Artenga inc, Ottawa, Canada). The first generation products Albunex® and Echovist® have been replaced by the new generation agents Optison® and Levovist®. All the vascular contrast agents are intravenously injectable. Optison® has been approved by the United States Food and Drug Administration (FDA) for clinical applications in the USA. Optison® contains micron-size denatured albumin microspheres filled with octafluoropropane. The microbubble concentration in a suspension offered by the vendor is 5–8×10^8 μbubbles/mL, and the mean measured diameter of the microbubbles is 2–5 μm. EMBs are not only useful as contrast agents but also widely used in therapeutic applications (Wu and Nyborg, 2007). This thesis presents a novel therapeutic application of the Artenga® EMB in combination with HIFU exposure.

1.4 HIFU OVERVIEW

High intensity focused ultrasound (HIFU) beams may be used to destroy tissue volumes noninvasively within the body without damage to surrounding tissues. Compared to diagnostic ultrasound, HIFU has significantly higher time-averaged intensities in the focal region of the ultrasound transducer (Dubinsky et al., 2008). Typical diagnostic ultrasound transducers deliver ultrasound with time-averaged intensities of approximately 0.1–100 mW/cm^2 and compression and rarefaction pressures of 0.001–0.003 MPa. HIFU transducers deliver ultrasound with intensities in the range of 100–10,000 W/cm^2 to the focal region, with peak compression pressures of up to 30 MPa and peak rarefaction pressures up to 10 MPa (Dubinsky et al., 2008).

1.4.1 PHYSICS OF HIFU

Focused ultrasound has widely been used to localize acoustic energy in a small volume of tumor. The focused ultrasound field is usually produced using a high power piezo-electric material

(such as lead zirconate titanate [PZT]) formed into either a single element spherical-shaped concave radiator or an array that can be driven electronically to produce focus (Wu and Nyborg, 2008). Figure 1.1 shows simple focusing achieved by a spherical-shaped concave radiator. This type of focusing transducer is usually a piezoelectric ceramic whose front surface is of spherical shape of a given radius of curvature *(ROC)*. The aperture diameter of the transducer is *D*. The geometrical center of the sphere is at *C*. The dimensions of the curved front surface have the following relationship;

D/2 =(ROC) sin α

h = ROC (1 − cos α), Where *h* is the depth of the concave surface

f number = *ROC / D*
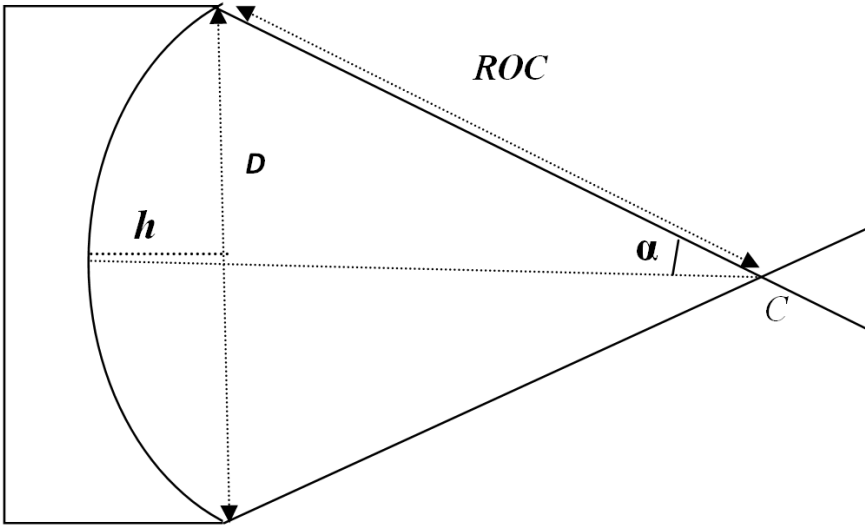
Figure 1.1: Illustration of a focusing acoustic radiator.

The focus of a single element transducer lies on its central axis near its center of curvature. It has been mathematically demonstrated by O'Neil (1949) that the greatest intensity takes place near but not exactly at C (geometrical focus). The magnitude of focusing, expressed by the ratio of the intensity at C to the average intensity at the radiating surface, is equal to $(2\pi h /\lambda)$. In other words, decreasing f number increases the sharpness of the focusing (Wu and Nyborg, 2008).

Furthermore, it also decreases the distance between the physical focus and the geometrical focus C. The plane that contains C and is normal to the axis of the sound field is called the focal plane. The focal length is defined as distance F (Wu and Nyborg, 2008).

A cigar-shaped focal volume (an ellipsoid of revolution around the central axis) is formed with HIFU. The size depends on the frequency used, with its width decreasing with increasing frequency for a given absorbed energy (ter Haar, 2011). At 1.7 MHz, using a 10 cm diameter transducer with a focal length of 14 cm produces focal lesion approximately 1.5 mm in diameter and 15 mm long. The precise shape of the lesion depends on the tissue acoustic properties, ultrasound intensity and exposure time, and the transducer geometry. The optimum frequency for a treatment at any depth is a compromise between the need to keep the attenuation in the tissue path overlying the target low in order that sufficient energy reaches this volume, and the necessity of having adequate absorption at the focus to ensure the required temperature rise (ter Haar, 2011). Several factors determine whether an effective lesion will be formed. These include the thermal properties of the targeted tissue, the acoustic properties of the tissue that the beam will pass through, and the presence of blood vessels that, if close to the focus, can act as heat sinks reducing the rate of temperature rise (Zang et al., 2005).

1.4.2 HIFU ABLATION AND ITS MECHANISM

High power megahertz ultrasound in tissue can be brought to a tight focus at a certain distance from its source; this can be used to therapeutic benefit. High temperatures can be generated within the focal region, while the surrounding areas remain largely unheated (ter Haar, 1995; ter Haar and Coussios, 2007). It has been shown that, at 1.7 MHz, when focal peak intensities of $1500 Wcm^2$ are held for 1–2 s, temperatures in excess of $56\ ^{\circ}C$ are achieved in *ex vivo* liver tissue (ter Haar, 1995). Instantaneous coagulative necrosis occurs and hence cell death with a margin of 6–10 cells between live and dead cells at the edge of the focal zone (ter Haar, 1995; ter Haar and Robertson, 1993). The ablated volume reflects the focal region of the beam, and it is typically an ellipsoid of length $\sim$ 1 - 2 cm and diameter $\sim$ 1 - 2mm, depending on the transducer geometry and frequency, and HIFU output exposure power and time.

Ultrasound beam propagating through tissue loses energy due to ultrasonic attenuation caused by both scattering and absorption of the tissue (Frenkel, 2011). The absorption of ultrasonic energy causes a local temperature rise in tissue if the rate of heating exceeds the rate of cooling. The energy levels carried in the HIFU beam are several orders of magnitude greater than those of a clinical diagnostic ultrasound beam, within a wide range of frequencies from a few hundred kilohertz to a few tens of megahertz (ter Haar, 2007). When the intensity of the ultrasound beam is increased and focused onto a tight spot the temperature at the focus rises rapidly above a certain limit (Figure. 1.2), it leads to effective cell killing even for very short exposures (ter Haar et al., 1991; Hill et al., 1995). Very little damage to overlying or surrounding tissue occurs during HIFU lesioning. There are two main mechanisms that are directly involved in the tissue damage induced by HIFU exposure. The first is a thermal effect from the conversion of mechanical energy into heat in the tissue, and the second is acoustic cavitation.
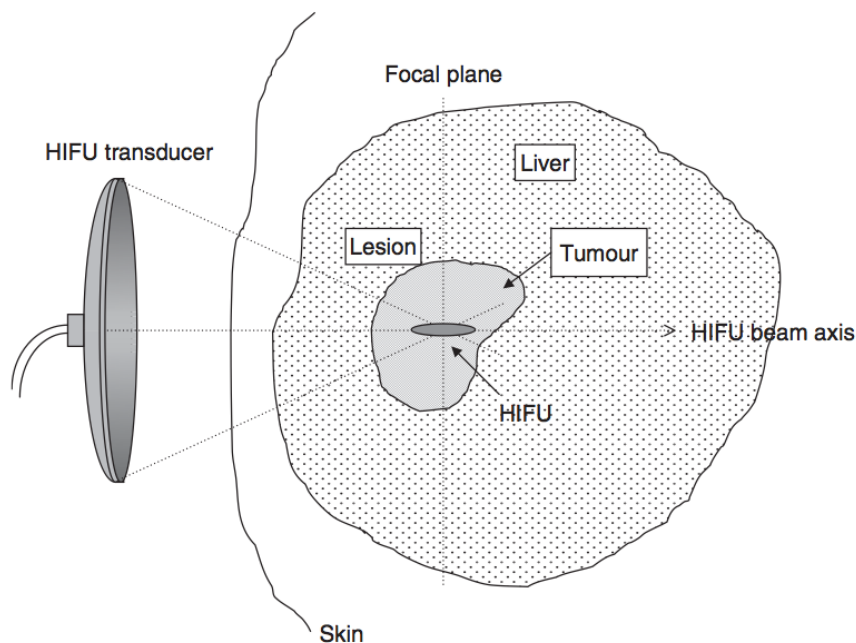
Figure 1.2: Diagrammatic illustration of the principle of HIFU. High-intensity ultrasound waves are generated by a transducer outside the body and focused onto a small region deep within tissue. HIFU-induced heating causes cell death by thermal necrosis within the focal volume, but leaves tissue elsewhere in the propagation path unaffected. Adapted from ter Haar and Coussios 2007.

The predominant mode of ablation with HIFU is heating. Absorption of ultrasound results in the conversion of ultrasonic energy to heat. Acoustic cavitation is the second mechanism of HIFU induced tissue damage. Cavitation is relatively unpredictable. It depends on many independent variables such as frequency, intensity pulse shape and length and the degree of presence of particles and voids in the medium (Hynynen, 1991).

During HIFU exposure, it would be difficult to identify distinctly thermal effect from mechanical effect. In practice, the two effects occur simultaneously within tissue. Hence, the coagulation necrosis induced by HIFU can be considered as the result of biological effects from a combination of mechanical stresses and thermal damage on the tissue (Brujan et al., 2005).

Thermal effect is generally considered as the predominant mechanism of tissue ablation with HIFU. However, as clinical experience improves, there is increasing interest in using cavitation to optimize HIFU treatments and this is currently under extensive investigation. Specifically, inducing cavitation during exposures can improve the rate of heating through enhanced absorption (Tran et al., 2003, Sokka et al., 2003, McDannold et al., 2006, Brujan et al., 2005, Parsons et al., 2006).

1.4.3 ACOUSTIC MECHANISMS

1.4.3.1 THERMAL MECHANISMS

Therapeutic applications of ultrasound depend on the direct interaction of the sound field with the tissue to produce the desired beneficial bioeffect. The thermal effect depends on the temperature achieved and the duration of HIFU exposure. If the temperature rise is above a threshold of 56°C and the exposure time is at least 1 second, irreversible cell death will be induced through coagulation necrosis (Hill et al., 1995). The coagulation necrosis is characterized by cell death mainly due to protein denaturation, which is caused by an infarct such as excessive heat (Frenkel, 2011). Typically, a steep temperature gradient is created between the focus and normal non-focal surrounding tissue, and therefore a sharp demarcation between the treated and untreated tissue is typically found in histological examinations of HIFU lesions with a very narrow boundary between live and necrosed (dead) cells (Figure. 1.3).

Ultrasound-induced temperature rise is dependent on several factors, including tissue properties (e.g., absorption coefficient, density, perfusion rate, etc.), ultrasound exposure parameters (e.g., frequency, pressure amplitude, pulse duration, pulse repetition frequency (PRF), etc.). Thus, the generation of heat in tissues can typically be controlled through proper exposure planning (Humphrey, 2006).

The acoustic energy removed from the wave by absorption is deposited in the medium as heat at a rate q_v per unit volume where (Humphrey, 2006)

$$q_v = 2\,\alpha_a\,I \tag{1}$$

where I, is the intensity of the wave at the focus in W/cm^2, and α_a is amplitude absorption coefficient in dB cm $^{-1}$MHz $^{-1}$. Due to this heat deposition the temperature T at a point in the field will rise at a rate given by

$$\frac{dT}{dt} = \frac{2\alpha_a I}{\rho_0 C_p} \tag{2}$$

Where C_p is specific heat capacity in J/Kg.Kelvin of the medium at a constant pressure in Pascal.
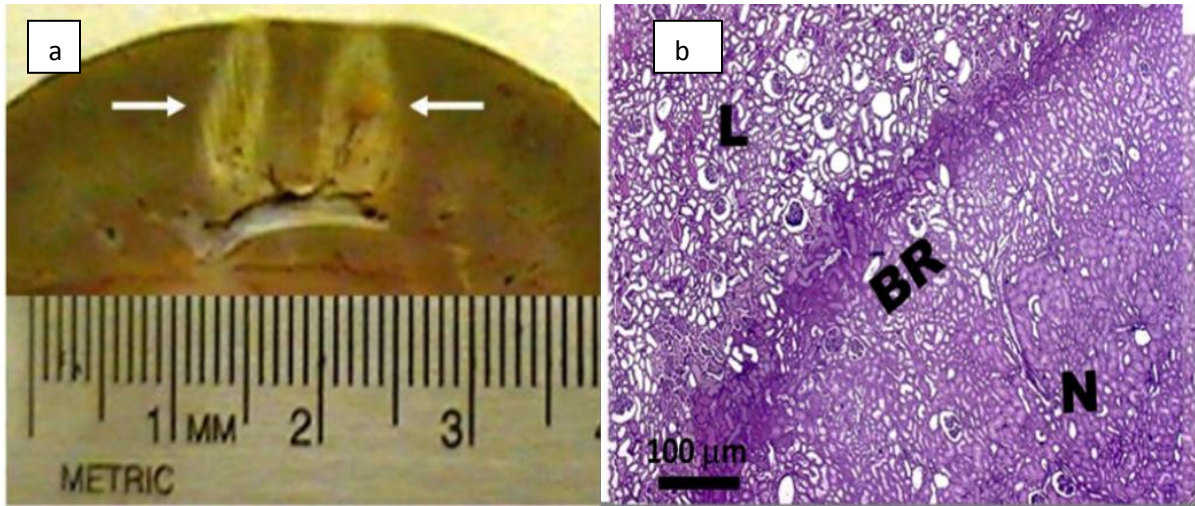
Figure 1.3: HIFU induced ablation. (a) HIFU lesions created in porcine kidney in vivo. Two isolates are identified by the arrows. (b) Histological section of the lesion showing the very

sharp boundary region (BR) between the live (L) and necrosed (N) cells. Adapted from Frenkel 2011.

Once the temperature of the medium rises above the ambient value, convection, conduction and radiation will result in heat being transferred from warmer to cooler regions (Humphrey, 2006). In addition, an extra process of perfusion occurs in tissue. Perfusion is described as the process by which heat is removed from warmer regions by blood flowing through capillaries and blood vessels and redistributed to cooler regions (Humphrey, 2006). The temperature elevation in a region subjected to an acoustic disturbance is a direct result of acoustic power absorption in the region of interest. For soft tissues these processes can be described by using the Pennes bio-heat transfer equation (Kang and Yoon, 2005):

$$\rho_t C_t \frac{\partial T}{\partial t} = K_t \nabla^2 T - w_b C_b (T - T_\infty) + q_v \qquad (3)$$

where ρ, C, and K are the density, the specific heat, and the thermal conductivity with the subscripts t and b referring to tissue and blood, respectively, T is the temperature of the tissue, T_∞ is the arterial blood temperature, and t is the time. Here the first term on the right-hand side accounts for heat diffusion while the second term accounts for blood perfusion losses with w_b being the perfusion rate. The term q_v is the rate of acoustic power deposition per unit volume given by Equation. (1).

Thermal Lesion: Thermal lesion is usually used to determine the extent of the lesioned tissue (Sapareto and Dewey, 1984). The thermal dose can be defined as the time (t) required to produce an isoeffect at temperature T to the time (t 43) which would be required to produce the same effect at 43 ⁰C. Tissue exposed for more than the equivalent of one hour at 43 ⁰C is considered "lesioned". Depending on the cell type, this is roughly equivalent to 3 logs of cell kill in a typical cell survival experiment and has been shown to induce tissue necrosis in-vivo (Linke et al. 1967). The boundaries of the thermal isodose curves delineate the lesion shape and size. A threshold for the denaturing of tissue protein (thermal coagulation necrosis), is calculated according to the thermal dose (*TD*) formulation. The thermal dose concept has been proposed to quantify the relationship between treatment efficacy and the temperature of the target as a

function of time. Sapareto and Dewey (1984) proposed the following relationship between the tissue thermal dose $TD43(t)$ (also known as cumulative equivalent minutes (CEM) at 43 °C) as a function of treatment temperatures, $T(t)$, and time t

$$TD43(t) = \int_0^t R^{43 - t(t)} \, dt'$$ (4)

where the empirical constant R = 0.5 $t >=$ 43 C and R = 0.25 t < 43 C (Sapareto and Dewey, 1984).

The thermal dose required to create a thermal lesion is equivalent to the thermal dose of a 240-min exposure at 43°C (Wu and Nyborg, 2008). This definition originated from the hyperthermia protocol, when the tissue was heated to a temperature of 43–45°C during a long exposure of several hours (Wu and Nyborg, 2008). However, it has been shown that this model gives good estimations of the thermal lesion for the higher temperatures caused by HIFU, which include 10 s at 53 ºC, 1 s at 57 ºC, and 0.1 s at 60 ºC. In HIFU treatments, the temperature commonly exceeds 70 ºC in about 1–4 s. Thus, tissue necrosis occurs almost immediately (Wu and Nyborg, 2008).

1.4.3.2 NON - THERMAL MECHANISMS

Acoustic Cavitation: Acoustic cavitation term is used to refer to a range of complex phenomena that involve the creation, oscillation, growth and collapse of bubbles within a medium (Humphrey, 2007). The cavitation behavior can be broadly classified into one of two categories: stable cavitation and inertial cavitation. The behavior of the bubble will depend on the frequency, pressure amplitude, bubble radius and environment surrounding the bubble. When an existing bubble is exposed to an ultrasonic field the acoustic pressure acts as a driving force that drives the bubble and results in the bubble radius varying. The bubble behaves as an oscillator with stiffness and inertia. The gas within the bubble provides the stiffness. As the gas is compressed it provides a force that resists the compression. The liquid surround the bubble provides the inertia and moves with the bubble wall. As a result the bubble has a natural resonant frequency f_r. For the case of a spherical air bubble of radius R_0 in water (assumed to be incompressible and inviscid) a simple calculation based on linear oscillations gives (Humphrey, 2007).

$$fr\,Ro \approx 3\,Hz.m\ (Ro \geq 10\,\mu) \qquad\qquad (5)$$

When the bubble is exposed to an ultrasound field at its resonance frequency, it exhibits its maximum response. The resonance frequency is dependent on the initial size of the bubble. The maximum expansion of a non-inertial cavity typically does not exceed twice the equilibrium radius. The response of the bubble can be nonlinear and is dependent on variables including the acoustic pressure amplitude, exposure frequency, and size of the bubble. The damping of the bubble oscillations occurs through viscous dissipation, sound radiation, and thermal conduction mechanisms (Young, 1989; Flynn, 1964; Leighton, 1994).

Stable cavitation: Oscillating bubbles can display a range of other behavior. One possibility is rectified diffusion: described as the slow growth of an oscillating bubble owing to a net flow of gas into the bubble over many acoustic cycles (Humphrey, 2007). This is the process by which the bubble's equilibrium radius grows with time and the bubble surface area is larger on the expansion phase than on the compression phase. This results in more gas diffusing into the bubble when the pressure inside is low than the diffusion of the gas out when the pressure is high. Acoustically driven bubble oscillations can result in heat production, microstreaming of fluid near the bubble, and localized shear stresses. The processes described so far are all classified as non-inertial cavitation (Humphrey, 2007).

Inertial cavitation: At sufficiently high exposure amplitudes, a bubble may expand to a maximum radius greater than twice its initial radius and then collapse rapidly to a small fraction of its initial radius (Humphrey, 2007). The relatively slow expansion is followed by a rapid collapse phase driven by the inertia of the spherically converging liquid. During this collapse phase, the gas temperature inside the bubble rises significantly as it is compressed to a small fraction of its original volume. As a result, shocks can be generated in the surrounding liquid. These processes can potentially create free radicals (Bradley, 1962). Various parameters determine the violence of the collapse of the inertial cavity. These include acoustic frequency, pressure amplitude, and initial bubble radius. The response of an inertial cavitation to an acoustic field is highly nonlinear, such that a small increase in acoustic pressure amplitude can change the bubble response from a non-inertial cavitation to an inertial cavitation. The acoustic pressure at which the transition occurs is often called the threshold for inertial cavitation. Extremely high

temperatures and pressures can be achieved at the minimum radius of the inertial bubble collapse (Flynn, 1982). Some models predict maximum collapse temperatures exceeding thousands of degrees Kelvin (Flynn, 1964; Flynn, 1982). These high temperatures and pressures are localized near the collapsing bubble. They are temporally limited to the duration of the collapse. Generally for a given pressure amplitude and bubble radius, the maximum collapse pressure in the bubble decreases as the frequency of exposure increases (Flynn, 1982).

The motion of the bubble wall may become supersonic during inertial collapse. This may generate a spherically diverging shock wave in the liquid medium surrounding the collapsing bubble. An asymmetrical collapse can occur near solid boundaries (Delius et al., 1990). Asymmetric collapse can result in the formation of high-speed, fluid microjets that impinge on the solid boundary. These microjets likely play a role in the fragmentation of kidney stones with lithotripter shock waves (Bailey et al., 1999).

In a given liquid, for a particular spherical bubble nucleus, the occurrence of inertial cavitation depends on the acoustic pressure amplitude, the acoustic frequency and bubble radius. The surface tension forces in smaller bubbles prevent the initial growth so the bubbles do not grow enough. On the other hand, large nuclei can grow initially, however they do not collapse sufficiently to generate high temperatures. For a given bubble radius and frequency, there is a threshold pressure required for inertial cavitation. Figure 1.4 illustrates the transition threshold between inertial and non-inertial cavitation, based on the calculations of Apfel and Holland (1991). If within one period of the applied waveform, the bubble collapsed and generated a temperature in the gas in excess of 5000 K, they assumed inertial cavitation. The calculations show that for any frequency there is a minimum peak rarefactional pressure p_{opt} that is required to generate inertial cavitation. This will only occur for bubbles with an initial radius R_{opt}. For example from figure 1.4, for a 10MHz wave the minimum rarefactional pressure to induce inertial cavitation is about 0.84 MPa.
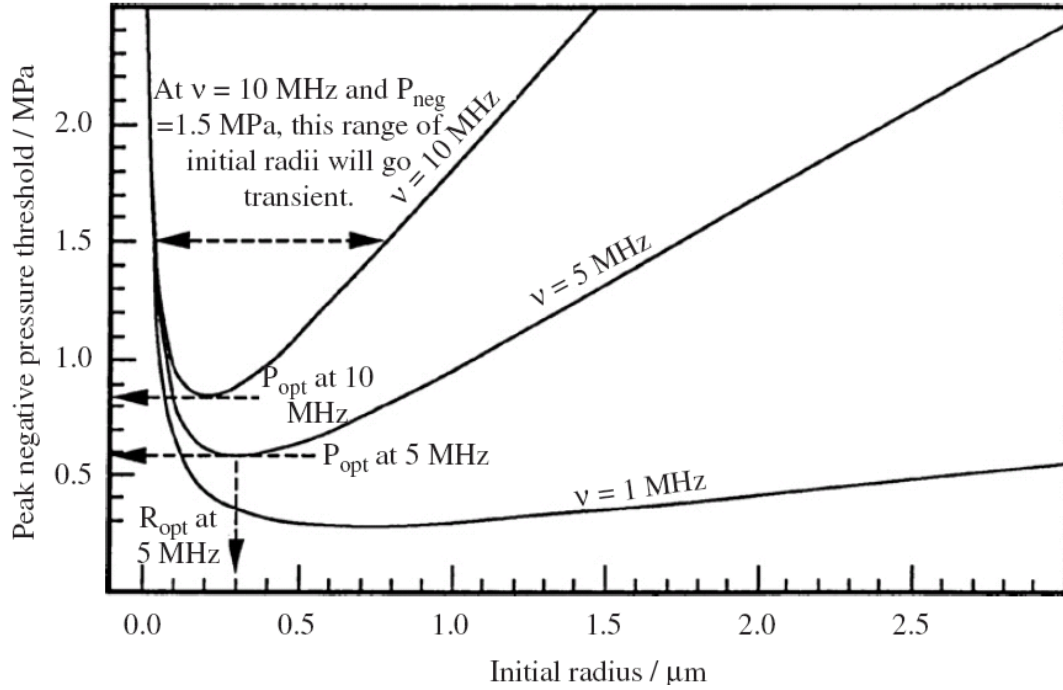
Figure 1.4: Apfel and Holland (1991) predicted the theory for the threshold for inertial cavitation. The minimum peak negative (rarefactional) pressure required to produce inertial cavitation within one period is plotted as a function of initial bubble radius and frequency (after Apfel and Holland (1991) and Leighton (1994). Adapted from Humphrey 2006.

Acoustic Streaming: The unidirectional circulation that may be set up by an acoustic field in a fluid is called acoustic streaming. It arises due to bulk fluid flow induced due to acoustic field propagating in the fluid medium. This results from a transfer of momentum to the liquid as it absorbs energy from the acoustic field (Hill et al., 2002; Kaneko, 2005). The velocity gradients associated with this fluid motion may be quite high, especially in the vicinity of boundaries within the field, and the shear stresses set up may be sufficient to cause changes and/or damage. The streaming velocity is dependent on factors including the absorption coefficient, speed of sound, kinematic viscosity, intensity, beam geometry, and nonlinear propagation (Nightingale et al., 1995; Miller and Thomas, 1996; Yu et al., 2004).

Acoustic force and radiation torque: A steady, time-averaged force called the acoustic radiation force typically acts upon an object in an acoustic field. This force results from a transfer of momentum from the sound field to the object (Rooney and Nyborg, 1972). Techniques that

employ radiation force are frequently used in methods to calibrate ultrasonic fields (Kissoff, 1965; Rooney, 1973; Hasegawa and Yosioka, 1975; Dunn et al., 1977). The magnitude of the radiation force depends on characteristics of both the sound field and the object in the field. The radiation force exerted by a plane wave on a perfectly reflecting target is twice that of a perfectly absorbing target (Cobbold, 2007). Radiation forces can also displace contrast agents to the wall of blood vessels in laboratory animals (Dayton et al., 1999). Radiation force is the underlying mechanism for phenomena such as radiation torque, acoustic streaming, acoustic levitation, and acoustic fountain effects (Dayton et al., 1999). Radiation torque can result in the rotation or spinning of symmetrical particles, whereas asymmetrical particles may rotate to a preferential orientation in the sound field.

1.4.4 APPLICATION OF MICROBUBBLES IN HIGH INTENSITY FOCUSED ULTRASOUND.

The use of HIFU as a tool for the treatment of cancer has been investigated for many decades. Given the present condition, improvements in HIFU are needed for clinical applications. Clinical studies are under way to enlarge focal spots and enhanced tissue coagulation volume by improving energy deposition in HIFU (Takegami et al., 2005). It has been reported that microbubble contrast agents are important for enhancing the therapeutic efficacy of HIFU as they may enhance tissue heating. The absorption of energy as ultrasound propagates through a medium produces a heating effect. In tissue, the rate of absorption increases with frequency (Hill et al. 2004). The presence of bubbles can enhance this heating effect owing to their ability to generate higher harmonics of the excitation frequency (Coussios and Roy, 2008). Bubbles will also dissipate energy as heat due to viscous friction in the surrounding liquid. The size of the bubble, the physical properties of the surrounding liquid, and the frequency and intensity of the ultrasound field will determine the relative significance of each of these dissipation mechanisms (Hilgenfeldt et al., 2000; Coussios and Roy, 2008). In addition to these parameters, the concentration of bubbles present, the pulse repetition frequency/ duty cycle, and proximity to blood vessels will determine the magnitude of the temperature rise generated (Coussios et al., 2007; Hariharan et al., 2007). Focalized high temperature rises are essential in HIFU surgery for tissue ablation.

Takegami et al. (2005) showed in *in vivo* experiments that target tissue was heated more quickly with the use of Levovist® contrast agent during the first 20 s than it was without the use of microbubbles. After 60 s of exposure, no significant difference in temperature elevation was seen between the group with contrast agent and the group without. The primary reason for this may be that microbubbles in the focal lesion were exhausted within the first 20 s of HIFU ablation. It was recommended that additional stable microbubbles are needed if higher temperatures are to occur in ablated tissues (Takegami et al., 2005).

It is well known that the presence of microbubble contrast agents enhances cavitation activity under certain *in vitro* conditions. The bubble implosion can lead to the production of high-velocity liquid jets, free radical species, shock waves, and strong shear forces that can damage cells. As has been known, hemolysis caused by cavitation usually does not occur in human whole blood because of high-density cells and few cavitation nuclei. Poliachik et al., (1999) exposed human whole blood samples with and without contrast agent to focused ultrasound. The exposure of 2360 W/cm^2 intensity for 1 s with a contrast agent concentration of 0.28 mL per milliliter of whole blood resulted in measurable cavitation and a 6-fold increase in hemolysis compared with outcomes in control. The conclusions of Williams and Miller (1989) attributing blood damage *in vivo* to heating of tissue and not to cavitation were confirmed. Tran et al. (2005) showed that the addition of a contrast agent decreased threshold duration and threshold intensity for bioeffect. Another study by Brayman et al. (1995) showed that twice as much hemolysis in whole blood could be achieved with contrast agents as without. These studies show that microbubbles may be effective in assisting ultrasound therapy.

Cavitation and hemolysis occurrences are proportionate to contrast agent concentration, HIFU acoustic intensity, and duration of HIFU exposure, when the microbubbles are added to the blood. Increasing the concentration of Albunex® from 1% to 10% did not improve hemolysis in canine whole blood in a study by Miller and Thomas (1989). However, decreasing the concentration to 0.1% significantly decreased hemolysis, but with the same apparent threshold. Adding microbubbles can reduce exposure time and decrease the acoustic power of HIFU to some extent, but it results in a similar outcome. Microbubbles also appear to lower cavitation thresholds by serving as cavitation nuclei in the blood (Thomas and Miller, 1989).

Recent studies have shown that *in vivo* infusion of microbubble contrast agents in experimental animals increased the tissue volume of coagulation necrosis and, thus, improve the therapeutic efficacy of HIFU treatment. Yu et al. (2004) used a lipid-coated perflupropane microbubble agent in rabbit kidney. They noticed a 3.1- to 3.4-fold increase in volume of necrosis produced by HIFU exposure compared to HIFU exposure without a microbubble. In another study by Kaneko et al. (2005) Levovist® was shown to increase the volume of necrosis 2.8-fold in rabbit liver, but the pathologic changes caused by HIFU with Levovist® were the same as those seen in control. In a study by Sokka et al. (2003) bubble-enhanced exposures showed a faster elevation in temperature within the first 4 s and higher temperatures overall than were observed in exposures without bubbles. Two to 3 times larger coagulated regions were noticed in the gas bubble enhanced group. These were more spherical in shape, and closer to the transducer than were control exposures. This showed that gas bubbles might be used reliably to create significantly larger lesions *in vivo* (Sokka et al., 2003).

The potential of stabilized microbubbles for aiding tissue ablation during ultrasound therapy in canine kidneys have been explored (Tran et al., 2003). Overall intensity of tissue damage threshold was reduced by factor of 2 and duration of tissue damage threshold was reduced approximately by factor of 100, respectively. It was concluded from this study that stabilized microbubbles acting as cavitation nuclei may make acoustic cavitation more predictable and practical for noninvasive ultrasound surgery (Tran et al., 2003).

1.5 HYPOTHESIS AND THESIS OUTLINE

Current study aims to investigate the effect of the HIFU treatment parameters – microbubble concentration and ultrasound exposure conditions on *ex vivo* tissue model. We have measured the lesion volume and peak temperature rise in absence and presence of microbubbles to identify the optimal conditions of microbubble induced HIFU treatments.

Hypothesis:

The efficacy of the HIFU therapy in combination with microbubbles can be controlled through ultrasound/ microbubble exposure parameters.

Specific aims of the study are

- To measure the temperature rise and lesion volume in HIFU therapy without and with microbubbles under constant microbubble conditions and varying ultrasound exposure intensities
- To measure the temperature rise and lesion volume in HIFU therapy without and with microbubbles under constant ultrasound exposure intensities and varying microbubble concentration
- To measure the temperature rise and lesion volume in HIFU therapy without and with microbubbles under constant ultrasound intensities and constant microbubble concentration with varying ultrasound exposure duration

Overview of the experiments

Chapter 2 is divided into 2 parts. The first part describes development and testing of the image guided HIFU system and the experimental setup. Second part describes the experimental procedure that includes HIFU treatment with and without microbubbles at various ultrasound intensities, microbubble concentration and ultrasound exposure duration. Chapter 3 describes the results of the experiments in chapter 2. Chapter 4 is dedicated to discussion and explanation of the results. It also includes the conclusion and summary of the thesis along with suggestions for future work.

CHAPTER 2

MATERIALS AND METHODS

Ex vivo tissue was treated with image guided HIFU (2-MHz frequency) in absence and presence of microbubbles. Artenga® microbubbles (concentration of around 10^9 microbubbles/ml, mean bubble diameter of 2-4 microns) were injected at the HIFU focus prior to ultrasound treatment. The temperature was measured using K type thermocouple. Lesion volume was estimated using the ellipsoid volume. Experiments were conducted at varying ultrasound intensities (600 to 2400 W/cm^2), microbubble concentrations (0 to 100%, 0.2 ml microbubble concentration) and exposure durations (3 to 10 seconds).

We constructed the image guided HIFU system prior to conducting any experiments. The purpose of this image guided HIFU system was to enable us to visualize the focal area for HIFU treatment.

2.1 DEVELOPMENT AND TESTING OF IMAGE GUIDED HIFU SYSTEM

The ultrasound imaging probe was attached to the HIFU transducers to provide real time guidance and monitoring during HIFU applications. The alignment of the imaging probe and the HIFU transducer was accomplished using hydrophone measurements with a 3D computer-controlled motion system. After construction of the image-guided HIFU system and its output power characterization, a tissue-mimicking gel phantom as well as an *ex vivo* tissue model (chicken breast tissue) were utilized to test the image-guided HIFU system.

2.1.1 IMAGING AND HIFU TRANSDUCER, COUPLING TANK AND DRIVING ELECTRONICS

2.1.1.1 TRANSDUCERS

Imaging system

HIFU therapy was guided by a SONIX RP® clinical imaging system (Ultrasonix Medical Corp., Richmond, BC, Canada) (figure 2.1a). Grey scale B mode images were acquired using EC9-5/10 Endovaginal microconvex Transducer (Ultrasonix Medical Corporation, Richmond, BC, Canada) with band width of 5-9 MHz. Imaging was used to locate the HIFU focus (Figure 2.1b).
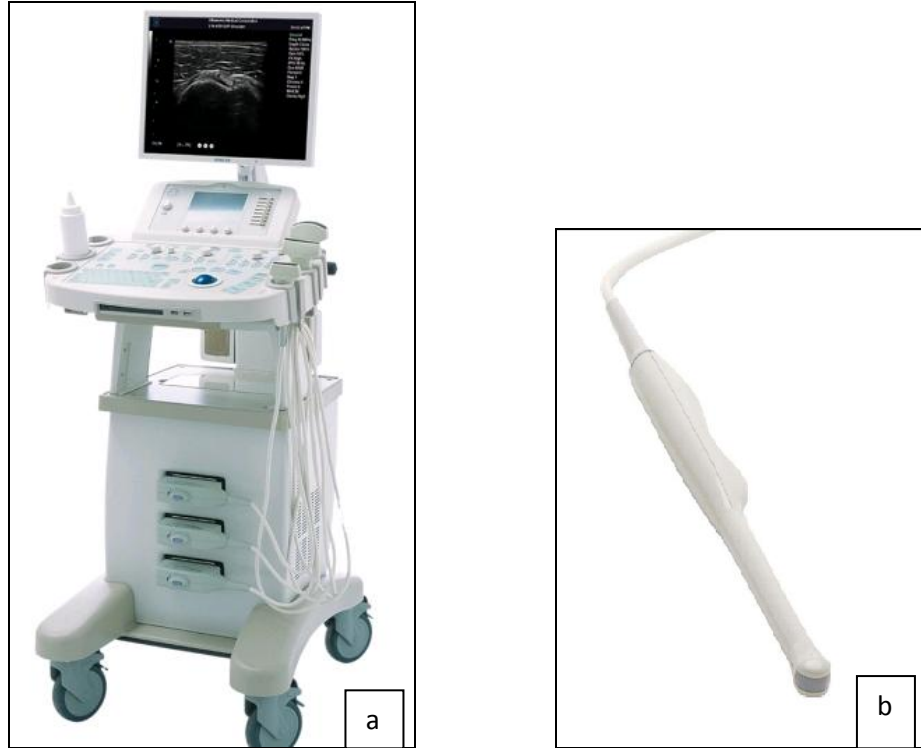
Figure 2.1: (a) Sonix RP (b) EC9-5/10Endovaginal microconvex Transducer

HIFU Transducer

The HIFU transducer used in the project was a spherically concaved, handheld HIFU transducer (Figure 2.2) made of special high power Lead Zirconate Titanate piezoelectric material (PZT-4 crystal, Boston Piezo-Optics Inc., Bellingham, MA). The resonance frequency of the transducer is 2.2 MHz with aperture diameter of 5 cm and radius of curvature 7.5 cm (Figure 2.3). The f-number of the crystal (defined as ratio between the radius of curvature and the aperture diameter) is therefore 1.5, which makes this transducer a moderately focused one. The white housing component of the HIFU transducer, shown in figure 2.2 is an in-house design made of ultra-high-molecular-weight (UHMW) polyethylene material. This prototype is immersed in a coupling water tank that is filled with degassed water prior to conducting experiments.
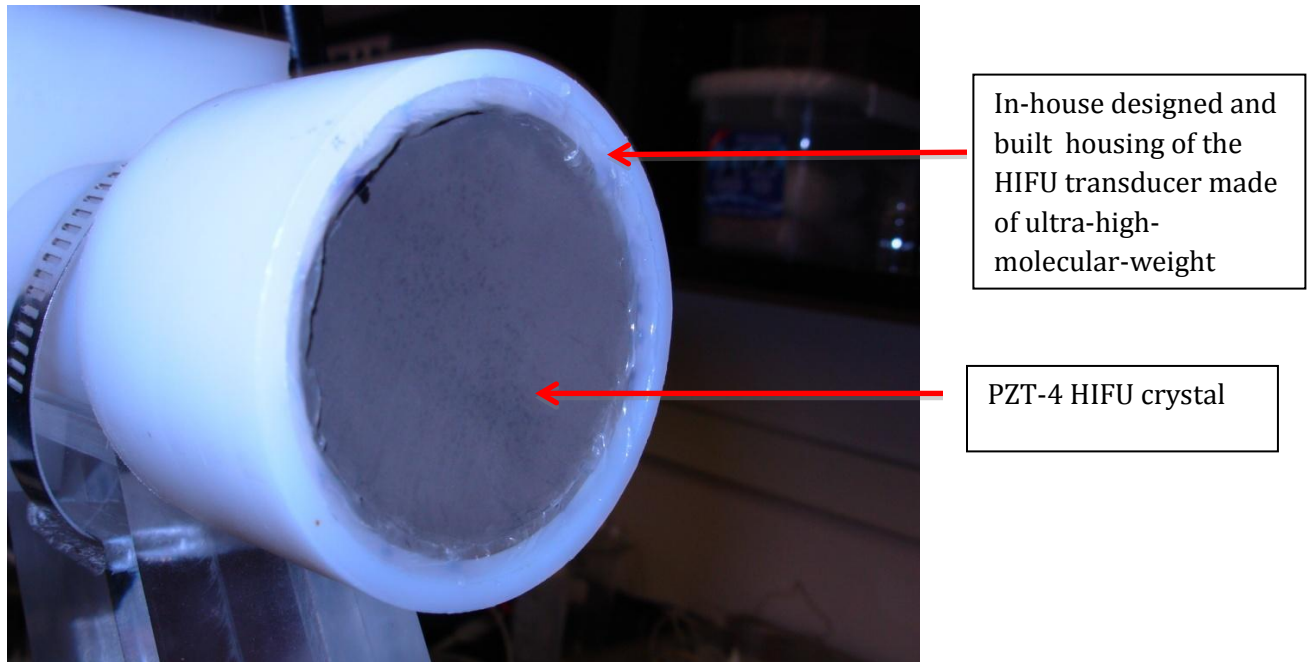
Figure 2.2: HIFU transducer prototype with white ultra-high-molecular-weight (UHMW) polyethylene housing the PZT4 crystal.
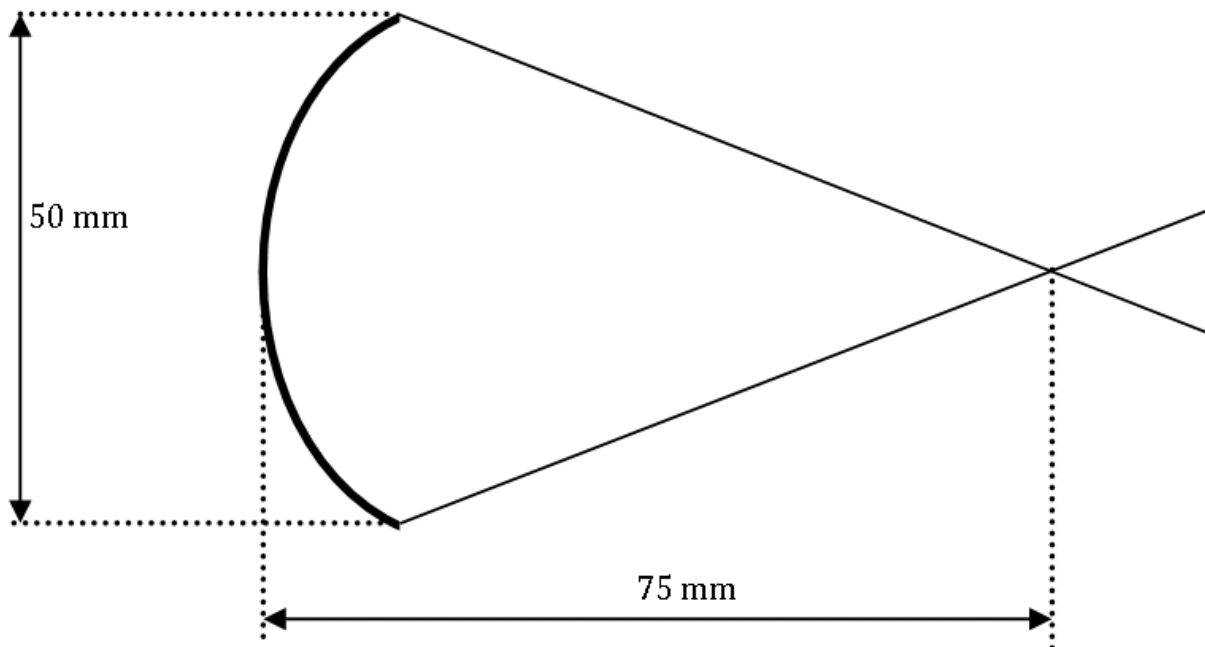
Figure 2.3: Schematic diagram of HIFU transducer used in current study showing its aperture diameter (5 cm) and radius of curvature (7.5 cm).

2.1.1.2 Coupling water Tank

A coupling water tank, shown in figure 2.5, was used in this experiment to couple the HIFU transducer to phantom or tissue. The tank is made of a transparent poly methyl methacrylate (also known as acrylic) with dimensions 10 cm in height, 22 cm in length and 13 cm in width (Figure 2.4). An acoustic window of approximately 8 x 6.5 cm was cut out at the base of the tank. A 127 μm silicon rubber membrane (Dow Corning Corporation Medical Products, Midland, MI), covered this acoustic window to permit the ultrasonic waves to propagate from the transducer surface to a medium of interest. Usually a coupling gel was applied between the medium of interest and the membrane (Figure 2.6).
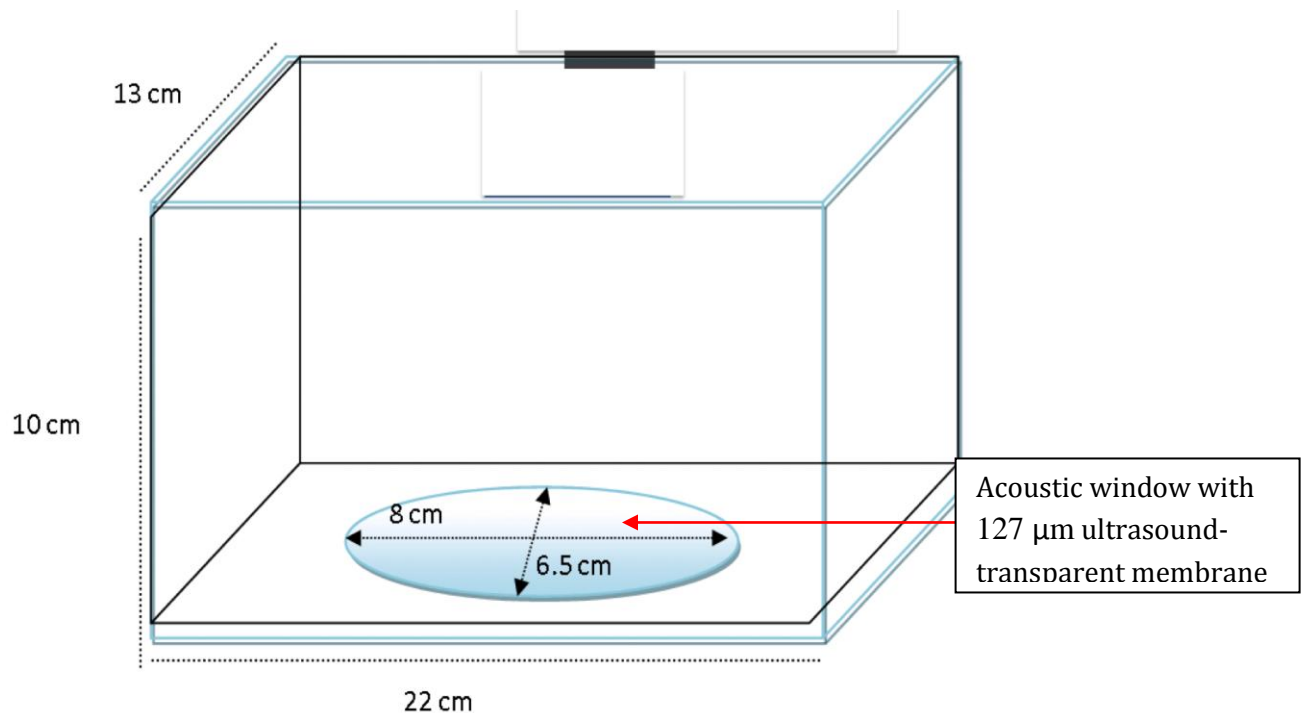
Figure 2.4: Schematic representation of the coupling tank with acoustic window.

Acrylic coupling water tank

Acoustic window with ultrasound-transparent membrane
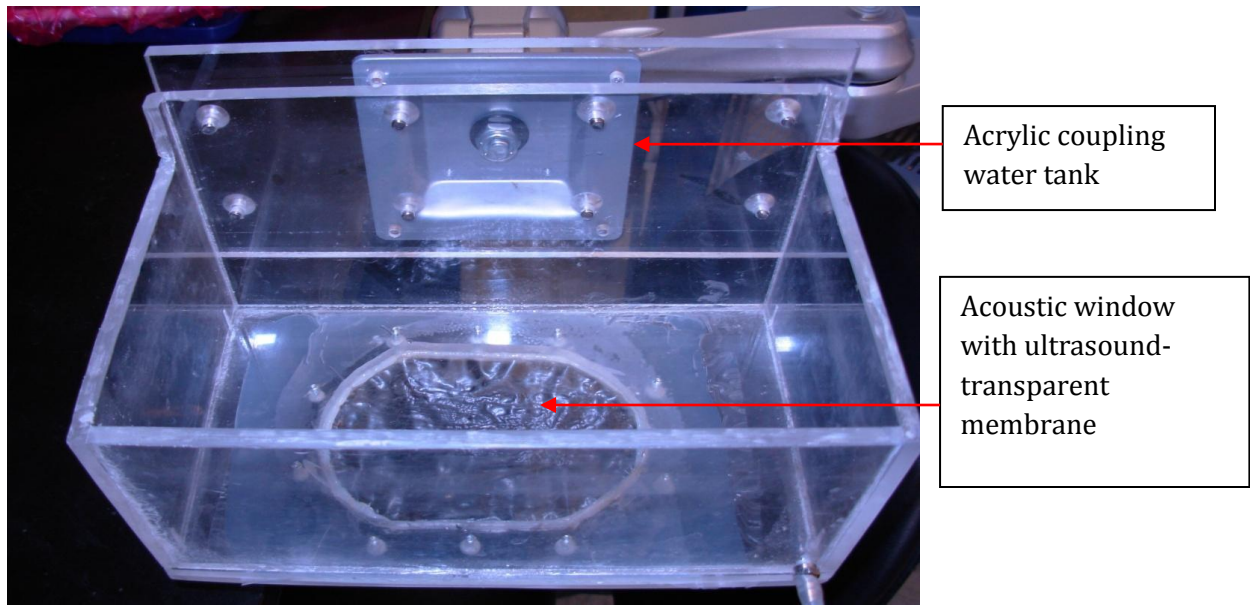
Figure 2.5: Coupling water tank

HIFU transducer

Imaging probe

Coupling tank with water

Acoustic Window with Ultrasound transparent membrane
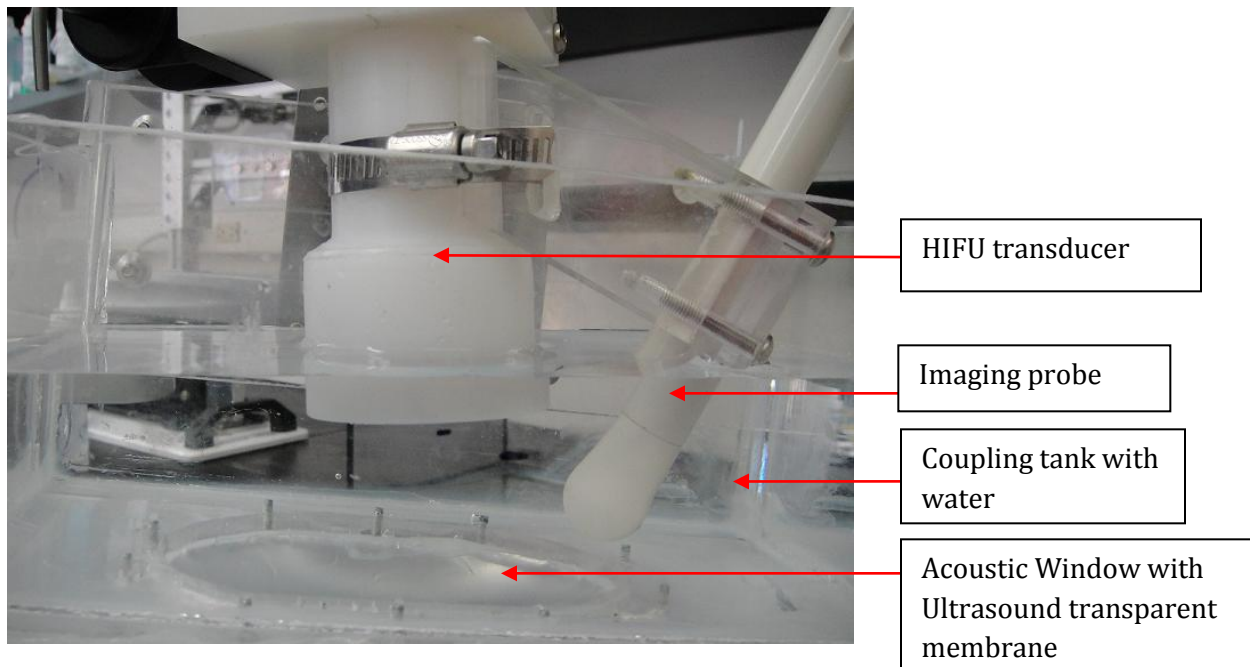
Figure 2.6: HIFU transducer inserted in the Coupling water tank

2.1.1.3 DRIVING ELECTRONICS

An Arbitrary Function Generator (AFG3101) (Tektronix Inc, Beaverton, OR, USA) was used to provide a continuous-wave sinusoidal signal to a radio frequency (RF) power amplifier (2100L, Electronics and Innovation Ltd., Rochester, NY) which, in turn, was connected to the HIFU transducer, as shown by the block diagram in figure 2.7. The actual driving electronics are shown in figure 2.8.
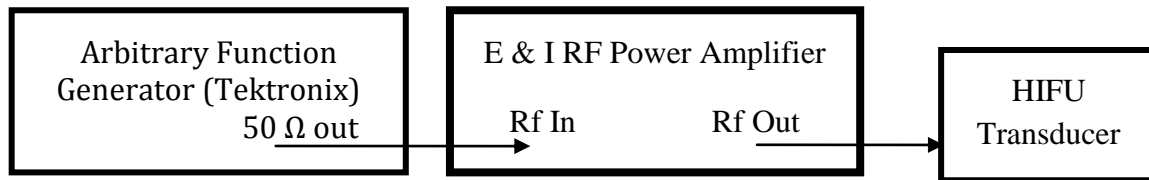
Figure 2.7: Block diagram illustrating the connections between the HIFU system and its driving electronics.
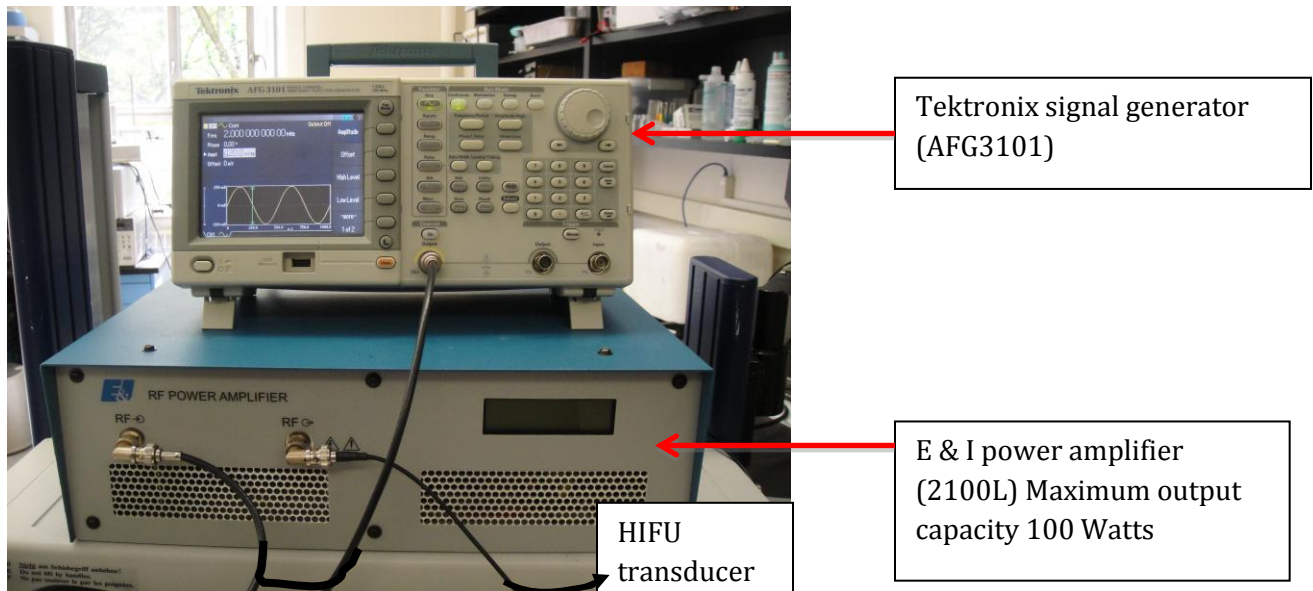
Figure 2.8: The HIFU system driving electronics.

Figure 2.9 represents the schematic diagram of the treatment setup for Image guided HIFU for *ex vivo* tissue. Figure 2.10 shows the actual representation of the complete setup.
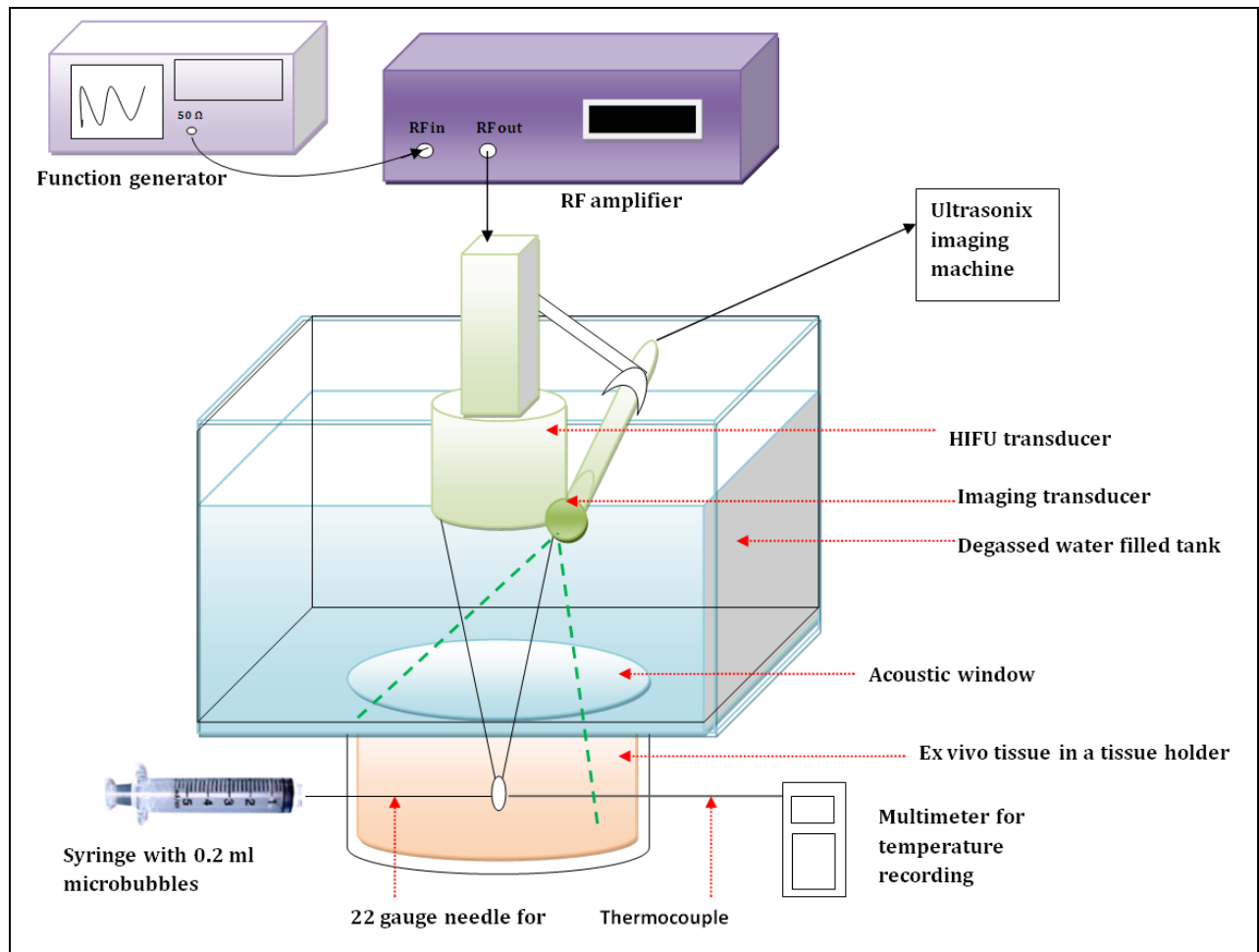
Figure 2.9: Schematic diagram of the image guided HIFU transducer treatment setup showing the driving electronics, HIFU and Imaging transducers and tissue holder.
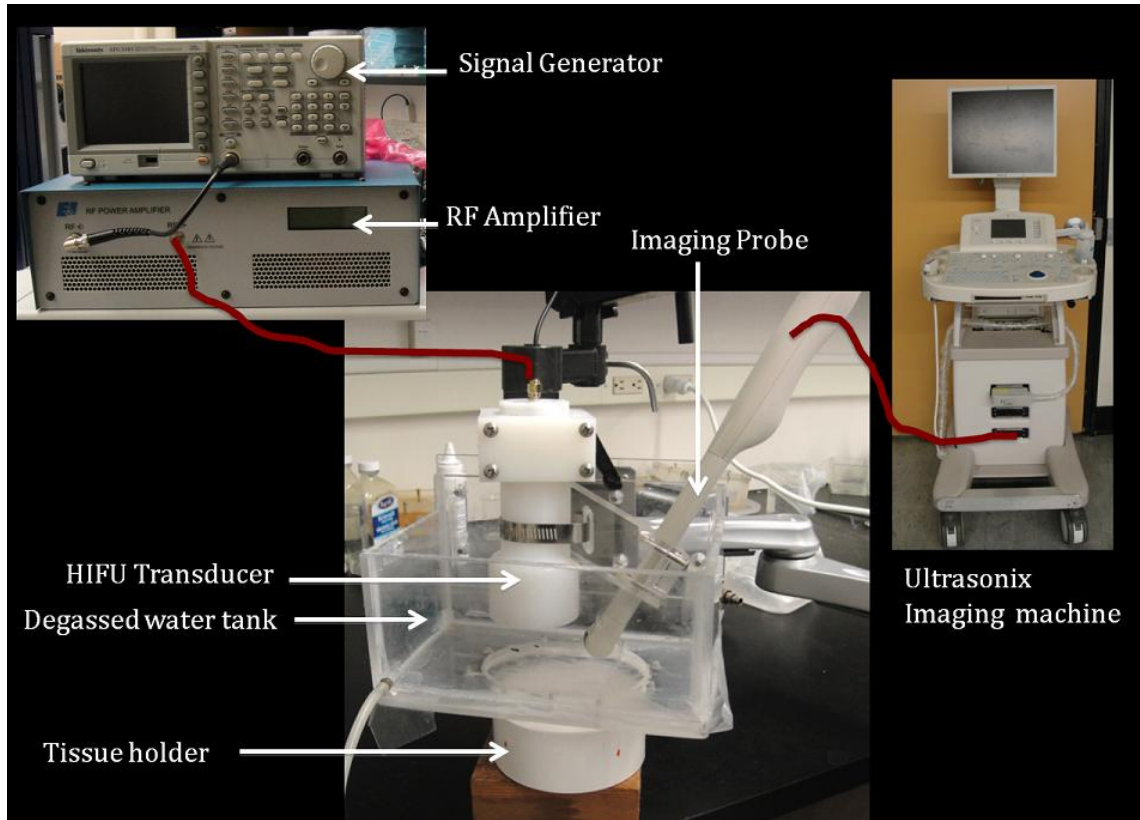
Figure 2.10: Image guided HIFU system

2.1.2 ULTRASOUND POWER MEASUREMENTS

Acoustic output power of the HIFU transducer was measured using a calibrated acoustic power meter to determine the dose delivered by the HIFU therapy. Along with ultrasonic field simulations, we also determined the focal intensities of varying HIFU exposures by measuring the ultrasound power for a given input voltage. A calibrated radiation force balance power meter (RFB-2000, Onda Corp., Sunnyvale, CA) was utilized in this study to measure the total acoustic power of HIFU transducer. The RFB-2000 system consists of an acrylic water tank with support base (figure 2.11). In the water tank, a stainless steel sensor holds an acoustic target, which can be a flat absorbing target or a brush target. For HIFU transducers, a brush target is utilized as it is sensitive to high levels of acoustic power (up to 100 W) and can withstand the high power without breaking or damaging the target (Onda Corp. 2008). The procedure to use the power meter is explained in the device's operating manual (Onda Corp. 2008). Figure 2.12 shows the actual setup of the Onda equipment.
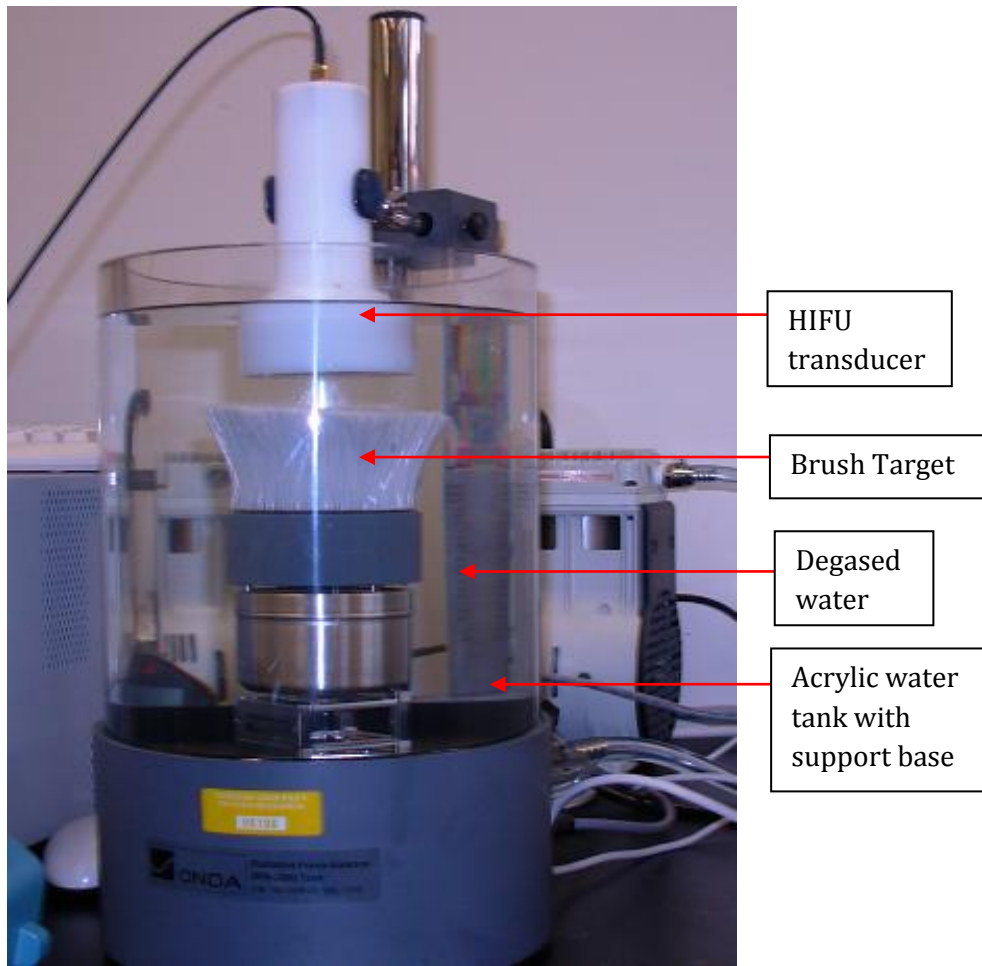
Figure 2.11: Onda RFB-2000 acoustic power meter with Acrylic water tank with support base, HIFU transducer and Brush target. (Figure partially duplicated from Onda Corp. 2008).
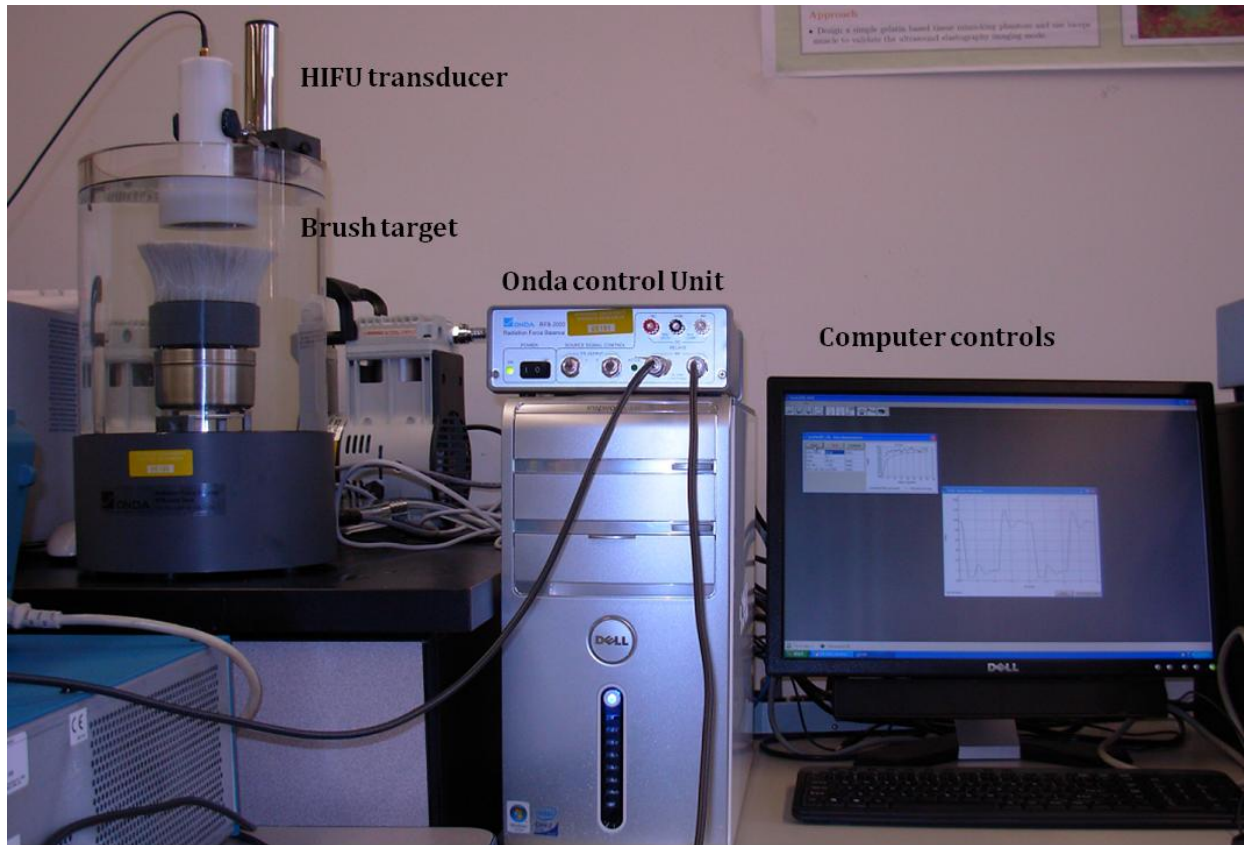
Figure 2.12 Onda Calibration systems. (Figure partially duplicated from Onda Corporation, 2008).

2.1.3 ULTRASOUND FIELD SIMULATION PROGRAM

A MATLAB based ultrasound field simulation code called LATS (Linear Acoustic and Temperature Simulator) (Butt and Tavakkoli, 2011) was used to simulate the ultrasonic field propagation and interaction with tissue by predicting the intensity profiles and temperature responses in a user-defined calculation volume (Appendix A). The medium properties as well as transducer geometries and characteristics are specified in order to accurately represent the experimental scenario. The details of the simulation can be obtained from the user manual by Butt and Tavakkoli (2011).

2.1.4 ALIGNMENT OF IMAGING AND THERAPY TRANSDUCER

The imaging and therapy transducers were aligned by synchronizing the imaging plane with the therapy field in such a way that the HIFU geometric focus lies in the B-mode ultrasound imaging plane. This was accomplished by using a 3D computer-controlled motion system (Daedal MC 5300 Controller, Parker Hannifin corp., Rohnert Park, CA) to micro-position a calibrated needle hydrophone (Precision Acoustics Ltd., Dorchester, Dorset, UK) placed in a water tank filled with degassed water and facing the desired transducer (figures 2.13, 2.14 and 2.15). Micro positioning of the needle hydrophone in HIFU field was done in 3D space in order to precisely locate the tip of the hydrophone at the focal spot of the HIFU transducer. The hydrophone was scanned in X and Y plane from -5.00 mm to +5.00 mm with step a size of 0.5 mm at an axial distance of 75 mm from transducer element. This was repeated at several axial distances. The hydrophone was moved in X, Y and Z plane to find its maximum voltage signal at the focal point. The hydrophone voltage was measure on a Tektronix TDS 1012 Digital Phosphor Oscilloscope (Tektronix Inc., Beaverton, OR, USA). Once the focal point was found, and XY scan was performed to create a map of the ultrasound field (figure 2.16).

After the position of the focal spot of the HIFU transducer was located, the precise position of the hydrophone tip was utilized in a B-mode (Figure 2.13), real-time ultrasound imaging to confirm that both the imaging and therapy transducers were aligned as well as to mark the focal spot using a template (Figure 2.18) overlaid on the screen of the ultrasound imager. In subsequent experiments, the template was overlaid on the ultrasound imager screen to estimate the location of the HIFU geometric focus during HIFU procedures, thereby guiding the HIFU focal energy to the desired region in the volume of interest.
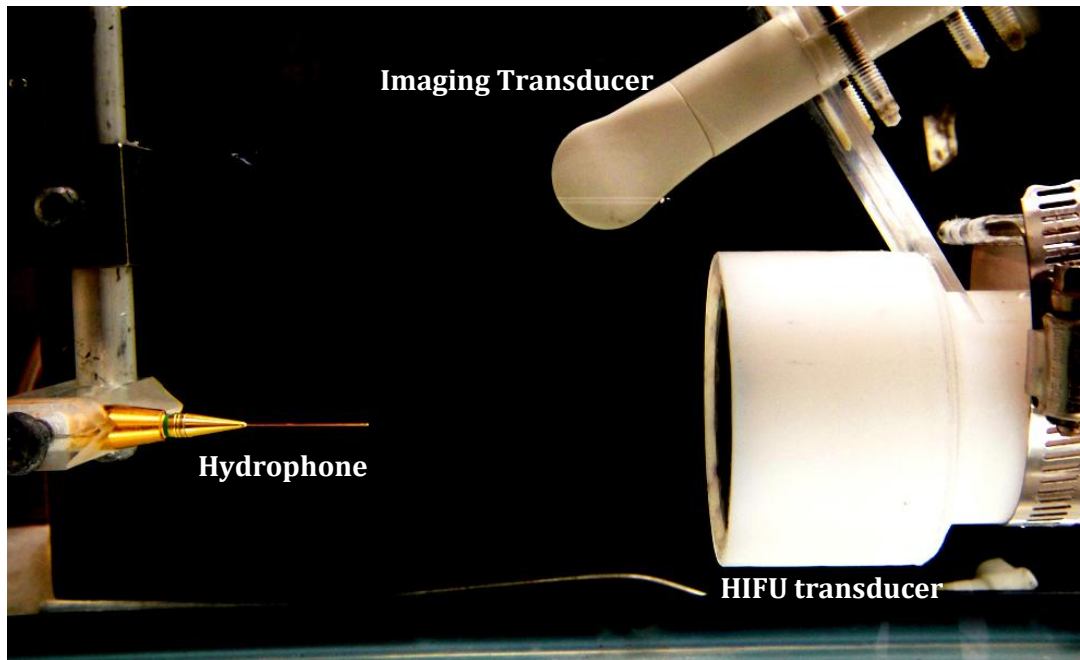
Figure 2.13: Hydrophone positioning with respect to Image guided HIFU system.
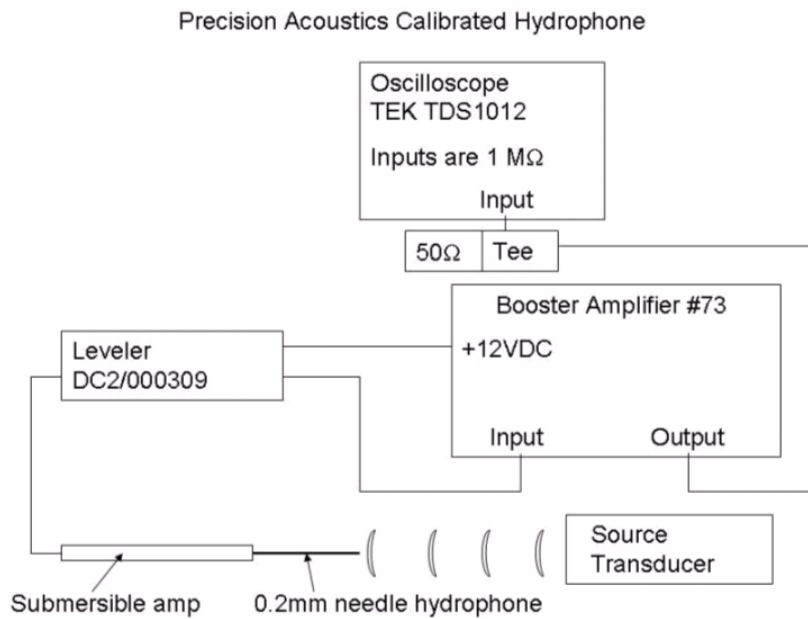
Figure 2.14: Schematics of Hydrophone micro-positioning system setup. Leveler in this setup is used to reduce the dynamic range of a signal. Booster amplifier in the figure amplifies the signal received by the hydrophone (figure partially duplicated from Prince and Link, 2006).
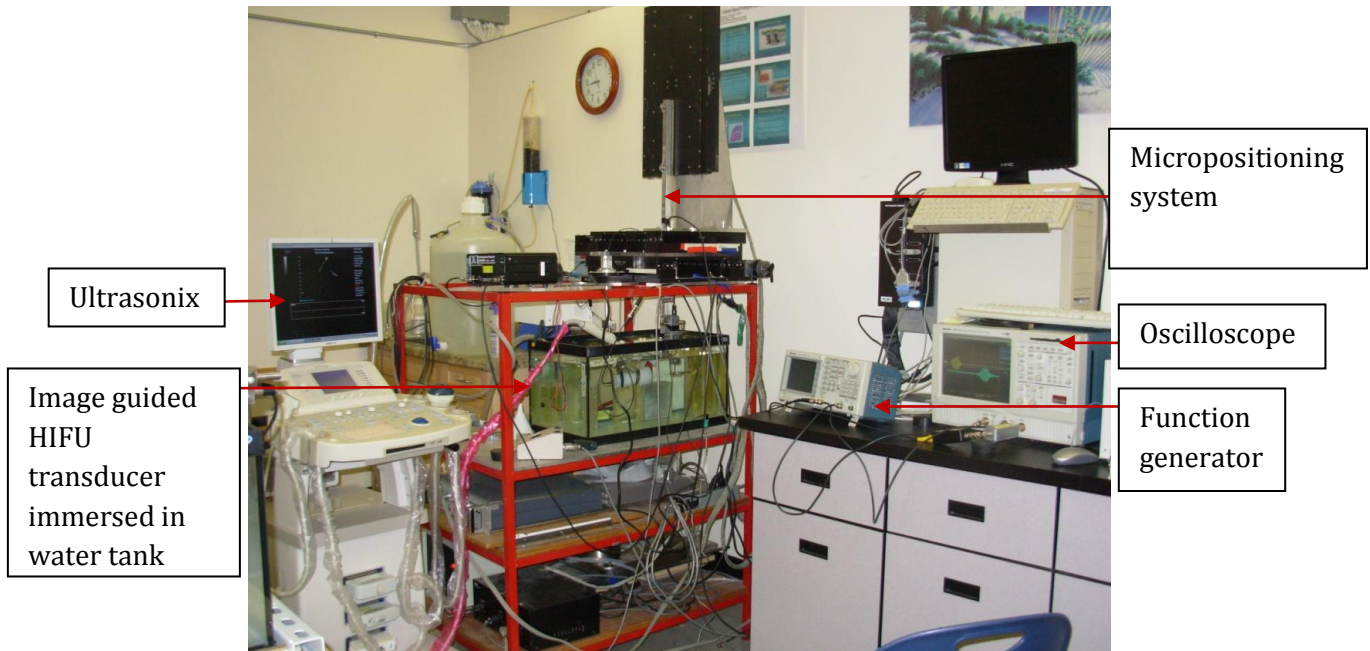
Figure 2.15: Apparatus used for alignment of imaging and therapy transducers apparatus

The data collected from the hydrophone voltage measurements in MATLAB is shown in figure 2.16.

After the position of the focal spot of the HIFU transducer was achieved, the precise position of the hydrophone tip was utilized in a B-mode (Figure 2.17), real-time ultrasound imaging to confirm that both the imaging and therapy transducers were aligned as well as to mark the focal spot using a template (Figure 2.18) overlaid on the screen of the ultrasound imager. In subsequent experiments, the template was overlaid on the ultrasound imager screen to locate the HIFU geometric focus during HIFU procedures, thereby guiding the HIFU focal energy to the desired region in the volume of interest.
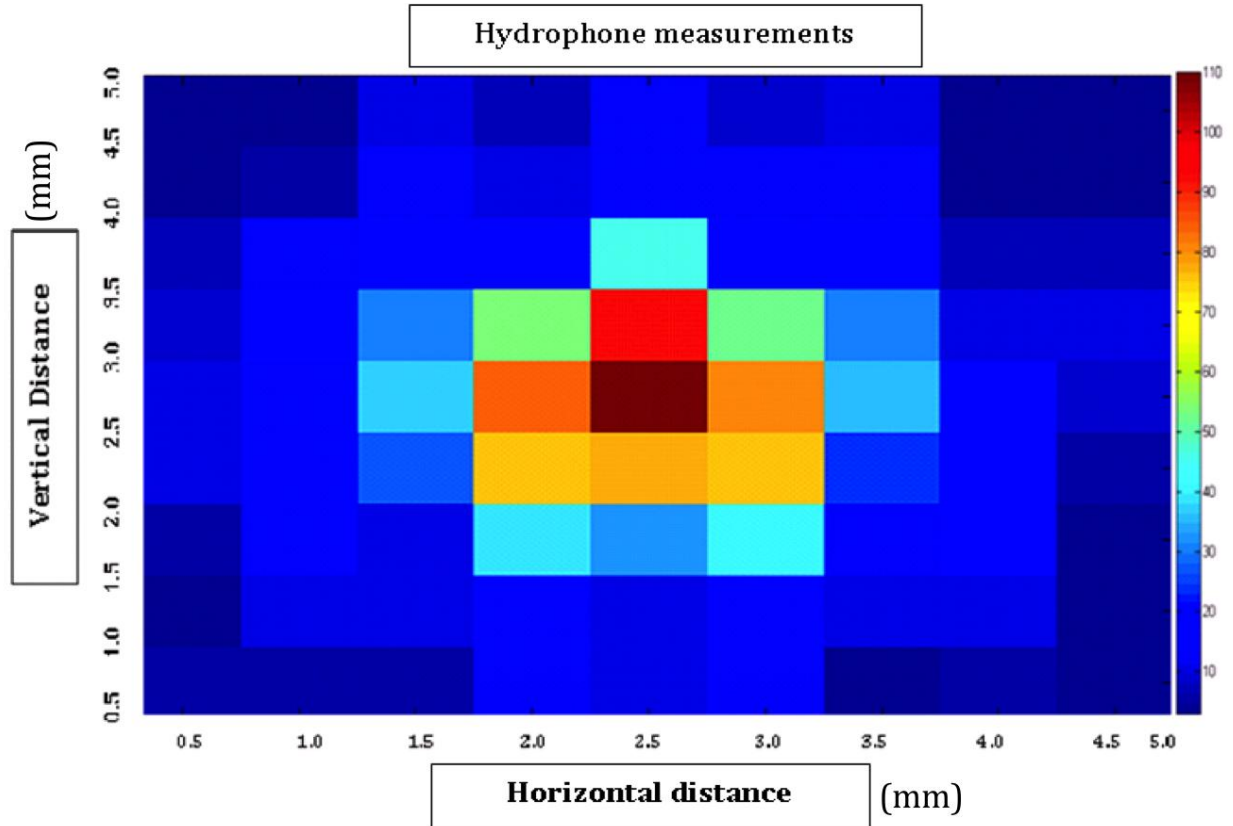
Figure 2.16: Hydrophone voltage measurements within a calculation area that is 75 mm away from HIFU transducer element. Both X and y range from -5 to +5 mm with a step size of 0.5 mm. The values on the color bar correspond to the hydrophone-recorded voltage in mV.
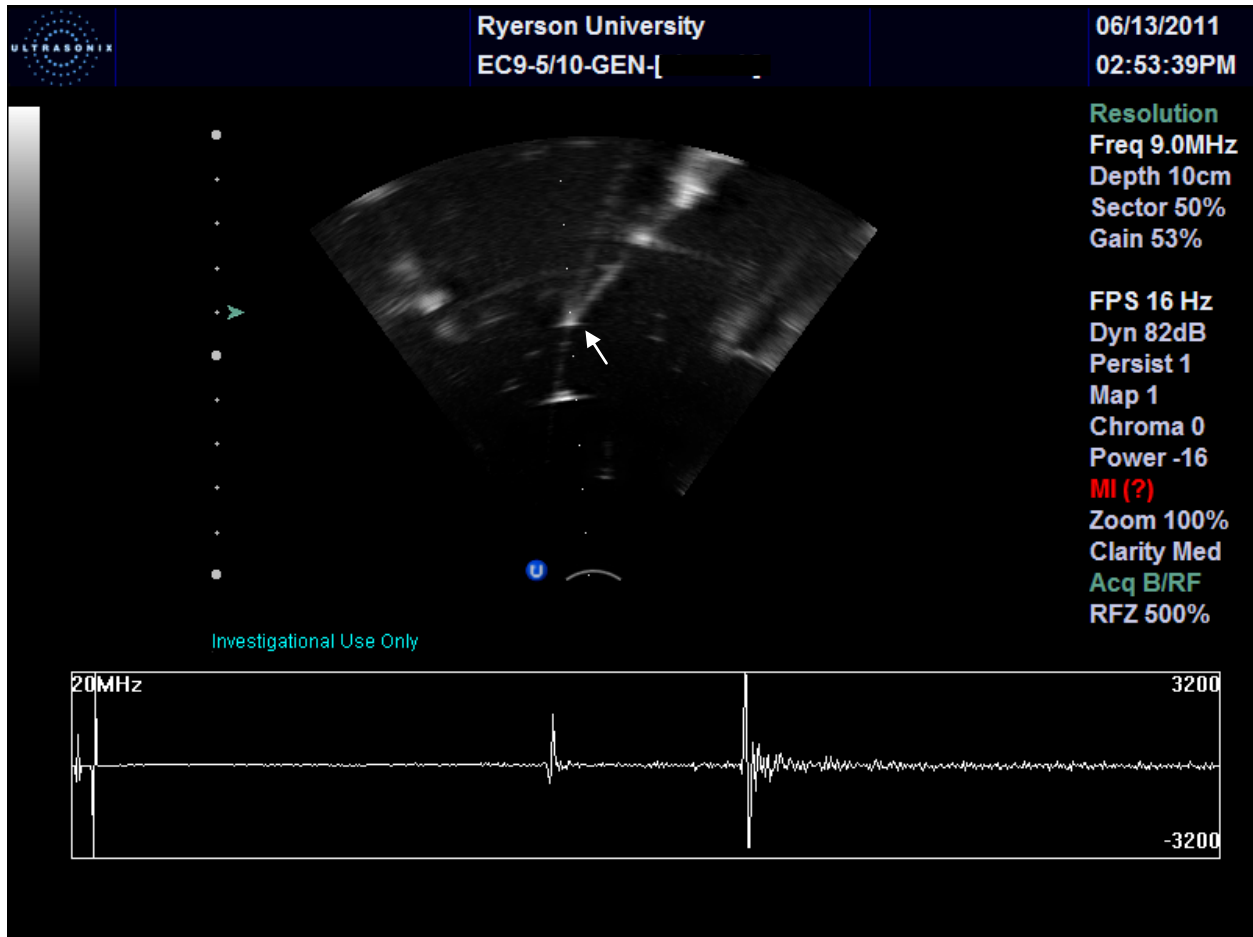
Figure 2.17: B mode image of the alignment of imaging and therapy transducers apparatus. Arrow indicates the tip of the Hydrophone needle. Position 0 indicates the highest recorded voltage zone
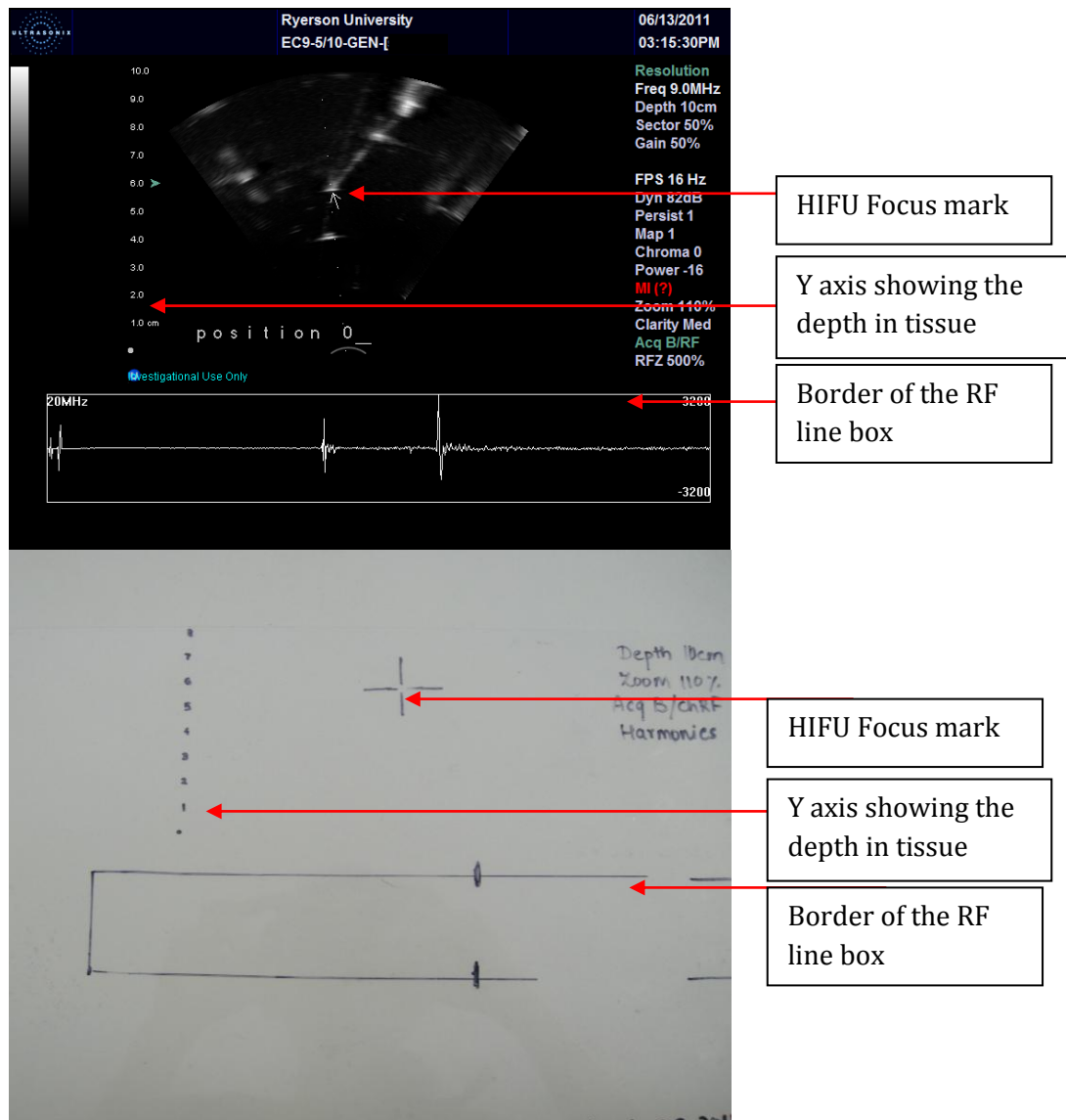
Figure 2.18: Template (bottom) with marked HIFU position (Ultrasound image (top) shown as a reference for all the marks when the template is overlain on the B- mode image of the Ultrasonix screen).

2.1.5. TESTING THE IMAGE-GUIDED HIFU SYSTEM

Testing of the image guided therapeutic HIFU system was carried out in tissue mimicking gel phantom and *ex vivo* tissue after alignment of the imaging and therapy transducers. The following materials and methods were used to test the image-guided HIFU system:

2.1.5.1 TISSUE-MIMICKING GEL PHANTOM

Gel Phantom was prepared using the procedure described by Iizuka et al. (1998). To prepare the gel phantom, a sufficient amount of degassed water was heated to 80 ^{0}C. Then, aqueous solution was prepared by dissolving type A gelatin porcine skin (Sigma-Aldrich Corp., St. Louis, MO)(15% by weight) in the hot water. When the solution was cooled down to 40 ^{0}C, formaldehyde with a mass that equals to 10% of the mass of gelatin was added to aid polymerization (Iizuka et al., 1998). Scatters were not added to the phantom. This allowed us to visualize the lesion being formed at the HIFU focus very clearly.

The gel phantom prepared in this project was utilized to test the image-guided HIFU system. This was achieved by the formation of cavitation activity at the HIFU focus using the therapeutic component of the system. The HIFU-induced effects were visualized in real time through the appearance of a hyperechoic region in an ultrasound B-mode image at around the geometric focus of the HIFU transducer, which was determined using a needle hydrophone when aligning the imaging and therapy transducers. The input peak-to-peak voltage was 600 mV, which corresponds to total acoustic power of about 90.8 W (as determined by the Onda power measurement) and free field focal intensity of 5587 W/cm^2 (as determined by the LATS simulation program). The sonication time for this experiment was 3 seconds.

2.1.5.2 TISSUE MODELS: *EX VIVO*

To further test the image-guided HIFU system, experiments with *ex vivo* tissue model (chicken breast) were conducted. A piece of chicken breast tissue was placed in a container with a coupling gel above it. The *ex vivo* tissue was brought under the coupling water tank that facilitates the propagation of ultrasonic waves from the imaging and therapy transducers to the tissue model.

In this experiment, the image-guided HIFU system was used to deliver an *in situ* focal intensity of approximately 2800 W/cm^2 (as determined by the Onda power measurement and ultrasound simulation program) for 5 seconds. Ultrasound B-mode imaging was used to guide the HIFU focus to the desired target depth of 1.5 cm. A 5-second exposure of in-situ focal intensity of

approximately 2800 W/cm^2 resulted in the formation of a thermal lesion inside the chicken breast tissue.

2.2 EX VIVO TISSUE EXPERIMENTS

This section describes the methodology for experiments conducted on the ex vivo tissue at varying ultrasound exposure conditions and varying microbubble concentrations.

2.2.1 MICROBUBBLE, ACOUSTIC INTENSITY, ULTRASOUND EXPOSURE TIME

The treatment parameters including microbubble concentration used in the current study, acoustic *in situ* intensity and HIFU exposure duration , are explained in detail in this section.

2.2.1.1 MICROBUBBLES

The Artenga$^{®}$ microbubbles have been used in the current study. The mean bubble diameter is 2 microns. These bubbles contain perflurocarbon enclosed in a lipid shell. 2.5ml microbubble solution in a standard syringe has a concentration of 1×10^9 microbubbles/ml (Artenga inc, 2008). The experiments were carried out at 6 different microbubble concentrations (0% bubble concentration in degassed water solution), 10%, 25%, 50%, 75% and 100% which is the actual highest concentration of the Artenga$^{®}$ microbubbles). The microbubble suspension was prepared according to the manufacturer's instruction (Artenga Inc, 2008). 0.2 ml microbubble solution was injected at the focus into the *ex vivo* tissue via 22 gauge needle.

2.2.1.2 ACOUSTIC INTENSITY

For the purpose of this study, the intensities ranging from 600 to 2300 W/ cm^2 were used. The lowest intensity at which the hyper echoic lesion appeared on the B-mode imaging was 649 W/cm$^{2.}$ Hence the lowest intensity chosen was 649 W/cm^2. The RF amplifier used in the current experiments has the range up to 100 Watts and hence the highest intensity chosen was 2316 W/cm^2. Lesions were created at 6 different intensities (694, 940, 1209, 1539, 1897 and 2316 W/cm^2). See Appendix A.

2.2.1.3 ULTRASOUND EXPOSURE TIME

A continuous wave exposure of 3 seconds, 5 seconds and 10 seconds time has been used in the current study.

2.2.2 TREATMENT DELIVERY AT VARYING ULTRASOUND EXPOSURE PARAMETERS AND MICROBUBBLE CONCENTRATIONS

2.2.2.1 VARYING ACOUSTIC INTENSITY

The HIFU treatment was delivered to the *ex vivo* chicken breast tissue. The lesion volume and peak temperature were measured at 6 different acoustic intensities (649, 940, 1209, 1539, 1879 and 2316 W/cm^2). The HIFU treatment was delivered in presence of the 0.2 ml 0% microbubble concentration (0.2 ml stabilized degassed water) and 0.2 ml 100% microbubble concentration (0.2 ml microbubble solution). Three trials were conducted at each intensity and microbubble concentration. The exposure duration was 5 seconds for each trial.

2.2.2.2 VARYING MICROBUBBLE CONCENTRATION

The HIFU treatment was delivered to the *ex vivo* tissue at 6 different intensities (section 2.2.1.2) and 6 different microbubble concentration 0%, 10%, 25%, 50%, 75% and 100% (section 2.2.1.1). Three trials were conducted at a given microbubble concentration and intensity. The exposure duration was 5 seconds for each trial.

2.2.2.3 VARYING ULTRASOUND EXPOSURE TIME

This set of experiment consists of HIFU exposure in presence of 0.2 ml 100% microbubble concentration at 3 different intensities (649, 1539 and 2316 W/cm^2). Three different exposure times were chosen. At a given intensity, the HIFU treatment was delivered for 3, 5 and 10 seconds. For each exposure time, 3 trials were conducted.

2.2.3 LESION VOLUME AND PEAK TEMPERATURE MEASUREMENT

This section describes the lesion volume cutting and size measurement technique used in this work. It also describes the temperature measurement technique using thermocouple.

2.3.3.1 LESION VOLUME MEASUREMENT

Tissue, where coagulated necrosis occurred, was white and the demarcation between the destroyed and unaffected tissue was sharp. The maximum length (L), width (W) and depth (D) in millimeters of the coagulated necrosis in the tissue was measured using ruler. The volume (V) in mm^3 was calculated according to the following formula adopted from ter Haar (1991).

$$V = \frac{\pi}{6} \; x \, L \; x \, W \; x \, D \tag{6}$$

Lesion cutting pattern and measurement technique is depicted in figure 2.19. After the lesion was created in the *ex vivo* tissue, the tissue was cut in a transverse plane (plane perpendicular to the HIFU beam) across the focal region to reveal the radial lesions (figure 2.19 a (ii) and figure 2.20). The lesion was then sliced perpendicular to the radial lesion at the center (figures 2.19 a (iii) and figure 2.21). The width and the depth of the lesion were assumed to be identical due to the radial symmetry of the lesions.

HIFU transducer

Direction of tissue slicing, orthogonal to HIFU beam (transverse plane)

i)

3 cm thick tissue

1.5 cm to focal depth

ii)

Direction of the tissue slicing is perpendicular to the transverse slice

iii)

a

b

Figure not to scale

w
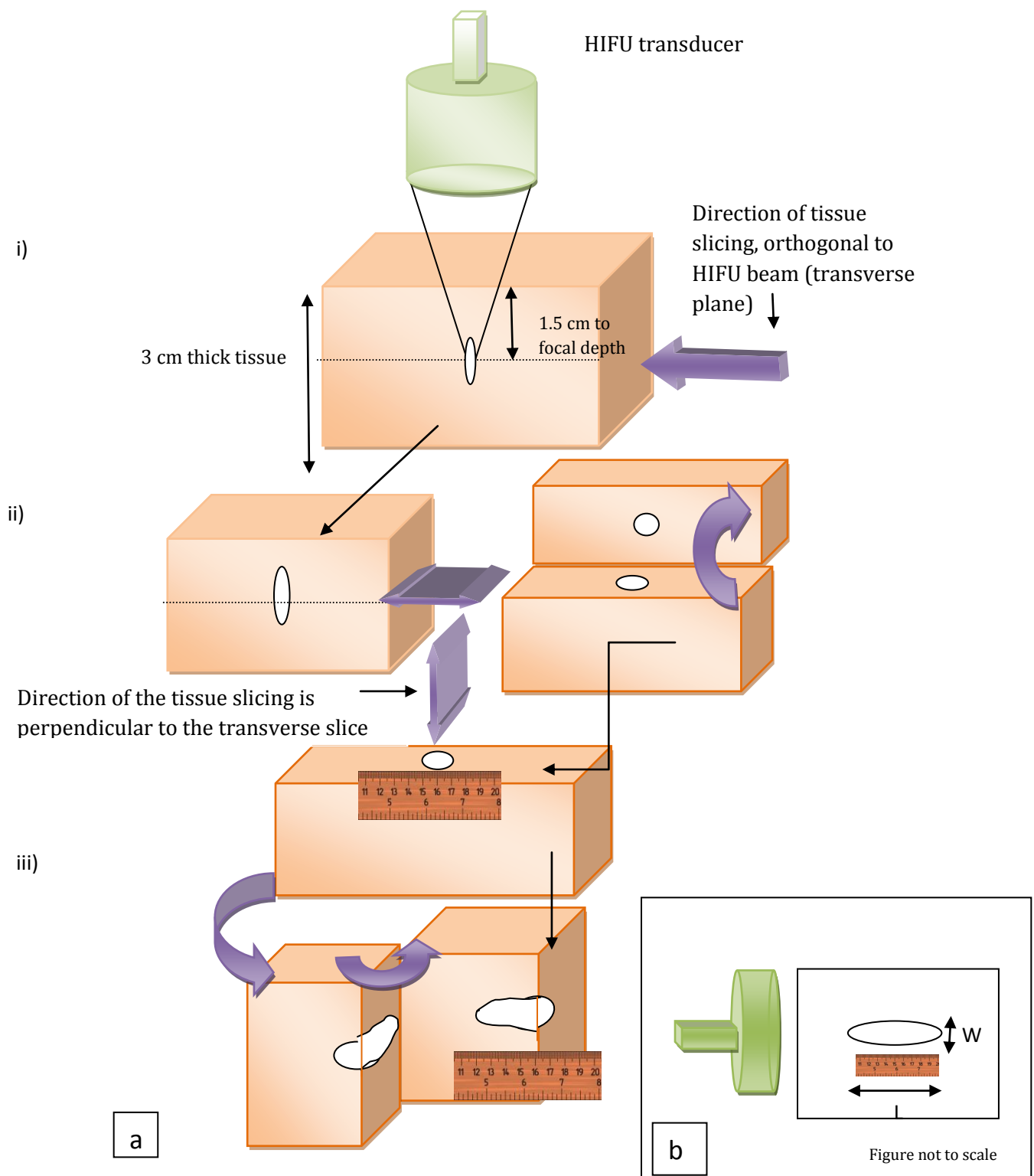
Figure 2.19: (a) Lesion cutting pattern and (b) size measurement technique.. The maximum length and, width were measured using the ruler.
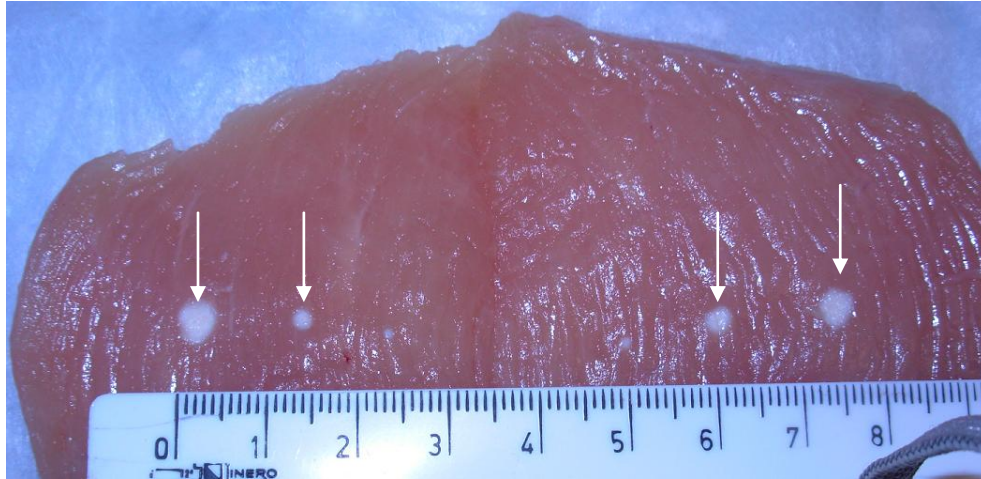
Figure 2.20: Ex vivo tissue sliced in a lateral plane (Perpendicular to HIFU beam). Arrows indicate the 2 lesions sliced in half at the transverse plane (perpendicular to HIFU beam).
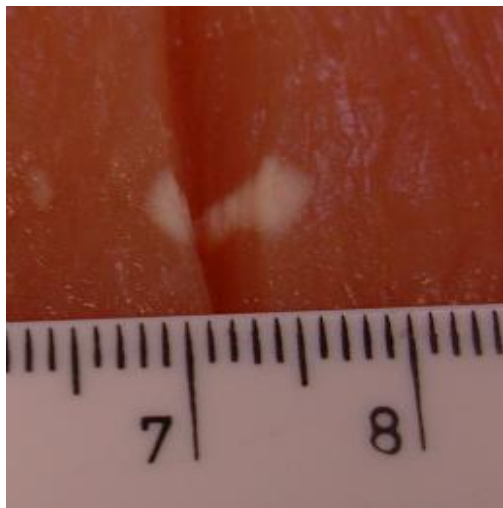
Figure 2.21: Ex vivo tissue sliced in a axial plane

2.2.3.2 PEAK TEMPERATURE MEASUREMENT

The tissue temperature of the location of the lesion was measured using k type calibrated thermocouples (these are made in house - the instructions for making this thermocouple in house are given in Appendix B). The thermocouple was calibrated against calibrated mercury in glass thermometer. It was inserted in the tissue at the HIFU focal zone under the guidance of the ultrasound imaging (figure 2.22). The thermocouple was placed at 1 mm from the focus (figure

2.23 and 2.24). Temperature was measured 5 seconds prior to starting the HIFU exposure (initial tissue temperature), during the exposure and for at least 60 seconds after the exposure. The actual temperature was recorded real time using multimeter that recorded temperature every second. Three trials were obtained for each exposure condition. The average of the peak temperature was calculated.
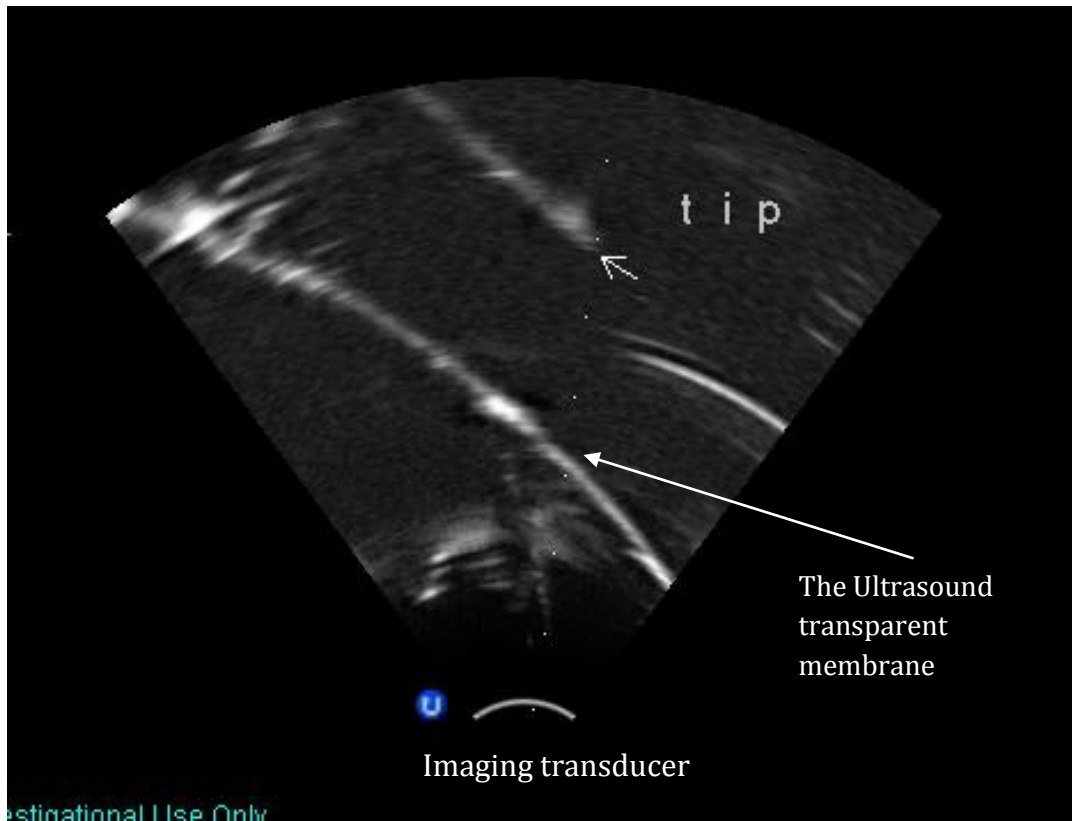
Figure 2.22: Thermocouple insertion in the tissue at the focal zone. B mode, image of the thermocouple insertion into the tissue. Arrow indicated the tip of the thermocouple.
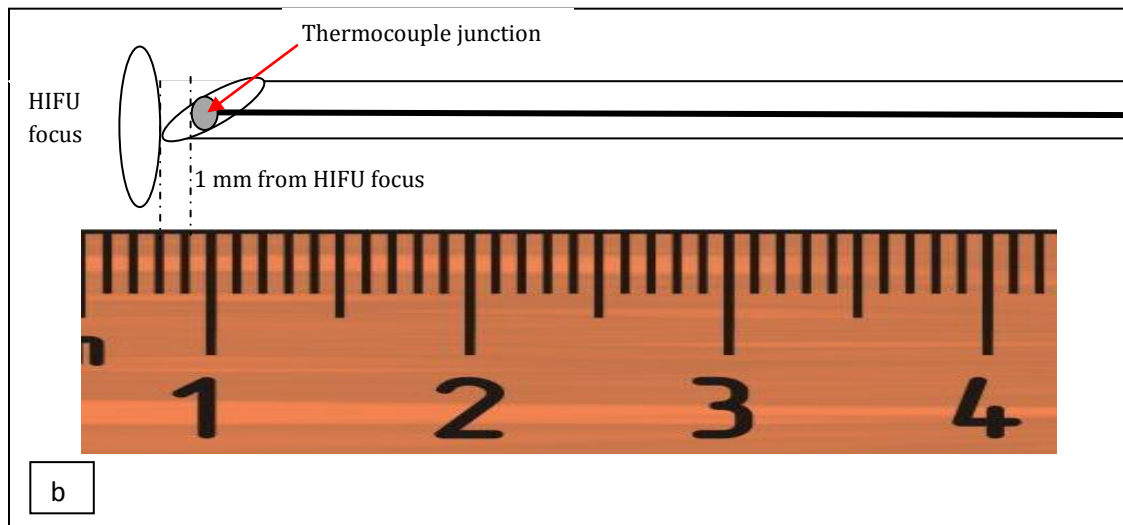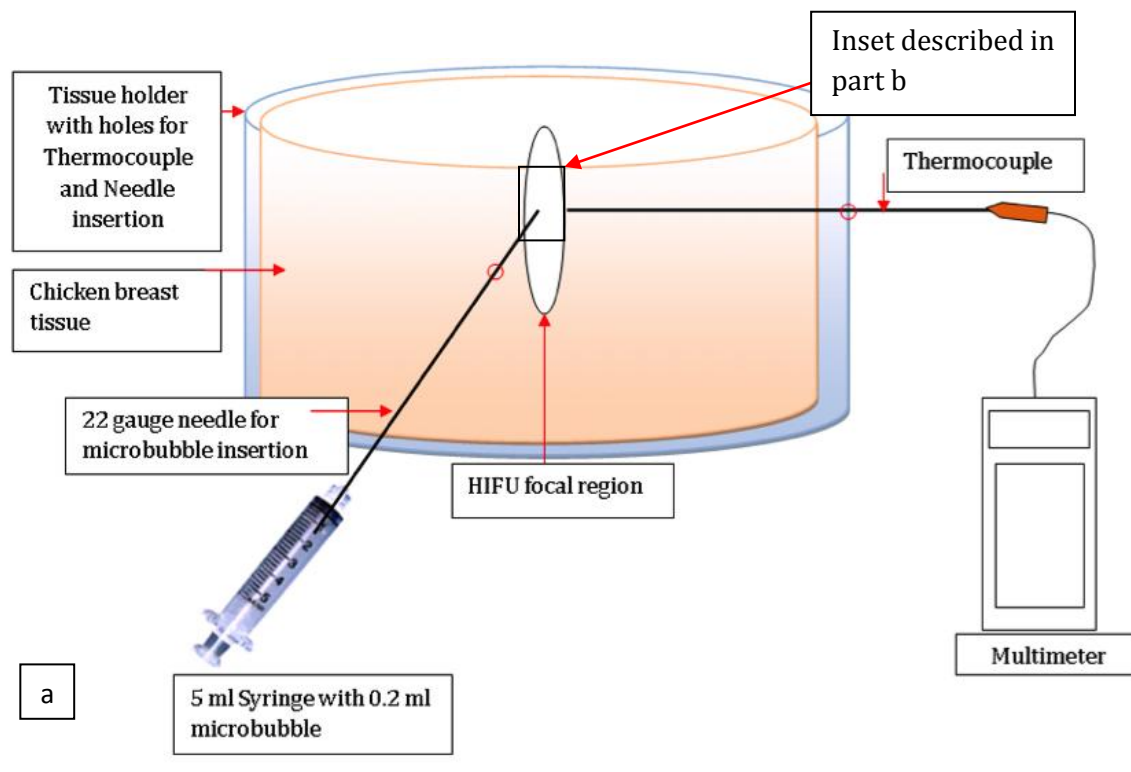
Figure 2.23(a) Schematic representation of the Thermocouple insertion technique at the focus(b) the magnified image of the inset from figure (a).
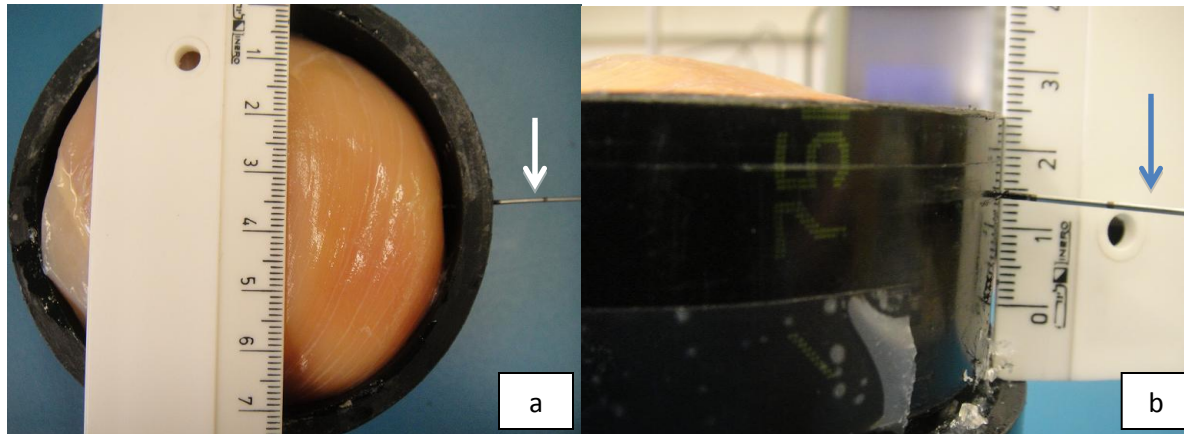
Figure 2.24: Thermocouple insertion technique. The tissue holder contains millimeter size holes for the passage of the thermocouples and Microbubble needles. (a) Top view of the tissue in a tissue holder with thermocouple inserted. (b) Side view of the tissue in a tissue holder with thermocouple inserted. Arrows indicate the thermocouple

2.3 STATISTICAL ANALYSIS

All data were processed by the statistic software SPSS. SPSS is a computer program used for survey authoring and deployment (IBM SPSS Data Collection), data mining (IBM SPSS Modeler), text analysis, statistical analysis, and collaboration and deployment (Field, 2005). A t-test was used for comparison among the groups. The difference was significant if the p-value was less than 0.05 (The confidence interval was chosen to be 95 %).

CHAPTER 3

RESULTS

Chapter 3 presents the results. It is divided in 2 parts. First section reports the results of the power measurements, calibration of the HIFU transducer and the development and alignment of the Image guided HIFU system. Second part presents the results from the experiments conducted on the *ex vivo* tissue at various ultrasound exposure conditions and microbubble concentrations.

3.1 DEVELOPMENT AND TESTING OF IMAGE GUIDED HIFU SYSTEM

3.1.1 POWER MEASUREMENT RESULTS

Power measurements using Onda radiation force power meter are shown in figure 3.1. The graph yields the acoustic output power (in W) for a given input peak to-peak voltage (in mV p-p). The net electric power and corresponding acoustic output is given in appendix A. This acoustic power will be used to calculate the in situ intensity using the LATS simulation.
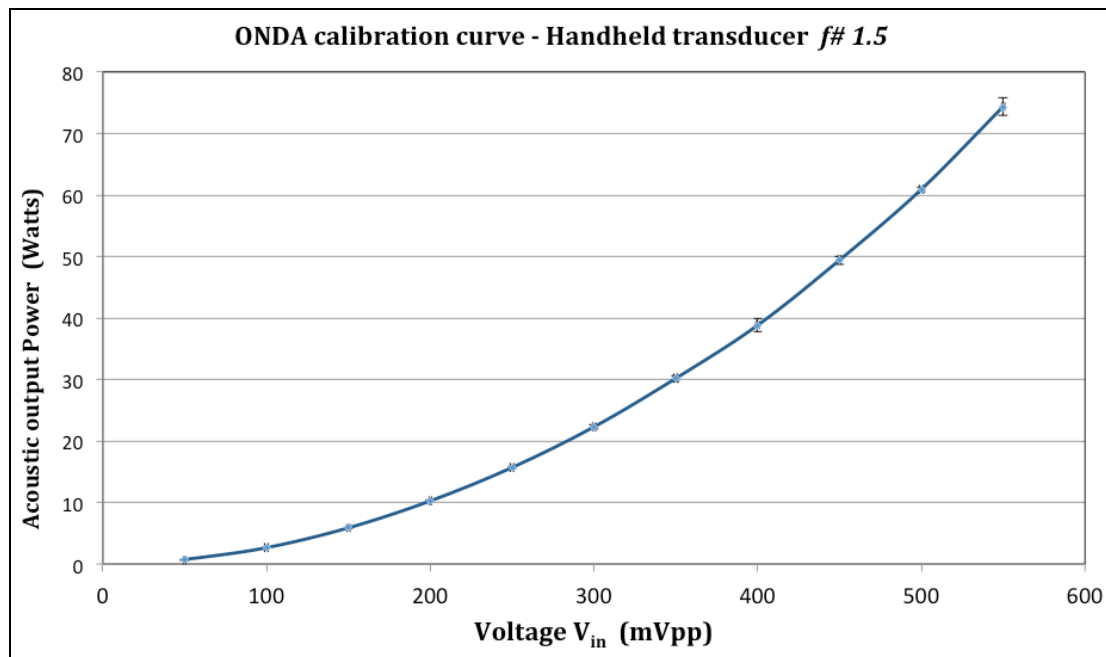
Figure 3.1Results of power measurements using Onda power meter: a graph of the output acoustic power vs. Input voltage

3.1.2 CALIBRATION TABLES

Combining the results of the ultrasound power measurements and the ultrasound field simulation program, a calibration table can be produced. Such a table gives the output acoustics power (W) and the *in situ* focal intensity in a water medium for a given input peak-to-peak voltage (mVp-p).

Calibration tables for HIFU transducer are provided in Appendix A. The output acoustic power in appendix A was obtained from figure 3.1, whereas the *in situ* focal intensities were obtained from the ultrasound simulation program LATS. The last values of the output acoustic levels in Appendix A are not shown because the Onda power meter is not sensitive to acoustic power levels below 0.6 W or above 100 W (Onda Corp. 2008). Figure 3.2 shows the free field intensity and *in situ* intensity vs. total acoustic power. The α effective in 1.5 cm tissue depth has a correction factor applied to it to account for 2 different mediums (water and tissue). It was obtained using the formula from Butt & Tavakkoli (2011) as shown below

$$\alpha_{effective} = \alpha_{cw} \frac{L_w}{L_w + L_t} + \alpha_{cw} \frac{L_t}{L_w + L_t} \tag{7}$$

where L_w and L_t denote the lengths along the Z-axis of water medium and tissue medium, respectively. α_{cw} is the actual attenuation coefficient of water medium and α_{ct} is the actual attenuation coefficient of tissue. For simulations with only 1 layer, it is apparent that $\alpha = \alpha_{cw} = \alpha_{ct}$. Lowest and the highest *in situ* intensities used in the current study are 649 W/cm^2 and 2316 W/cm^2.
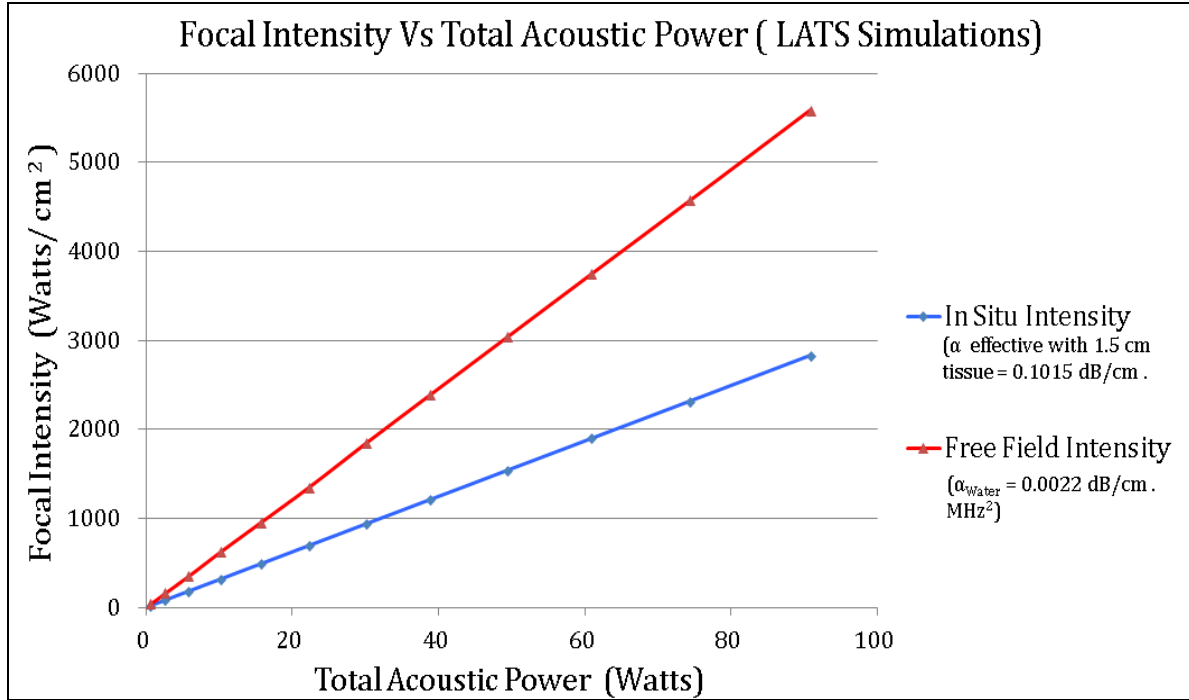
Figure 3.2: LATS in situ intensity simulations vs. total acoustic power for free field intensity (in water) and in situ intensity at 1.5 cm tissue depth.

3.1.3 TESTING OF THE IMAGE GUIDED HIFU SYSTEM

3.1.3.1 TESTING OF IMAGE GUIDED HIFU IN GEL PHANTOM

Figure 3.3 shows a B-mode ultrasound image of the tissue-mimicking gel phantom prior to being tested with the image-guided HIFU system. The arrow indicates the HIFU focal region marked using the template shown in figure 2.18. Figure 3.4 shows a B-mode ultrasound image of the tissue- mimicking gel phantom after a 3-second HIFU exposure of free field intensity 5587 W/cm^2. A hyperechoic region was observed very close to the HIFU focus immediately after the exposure (figure 3.4). Since there were no scatterers in the phantom, the ultrasound echo was very minimal and the image appears dark. The dotted line in the images is arbitrary line for the spatial selection of the ultrasound RF signal and its position may not represent the actual HIFU focal plane. Its placement is user dependent. It can be placed wherever it is necessary to collect the RF data or it can even be turned off. Hence subsequently it may not appear in the same plane

as the arrow. We did not need the RF data line hence the dotted line will be ignored in current study.
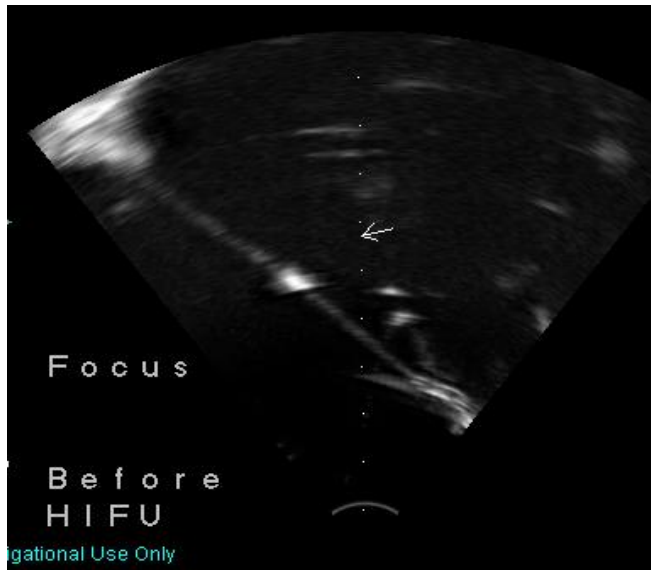
Figure 3.3: B-mode ultrasound image of the tissue-mimicking gel phantom prior to being exposed to HIFU. The arrow locates the position of the geometric focus of HIFU transducer as determined by the template.
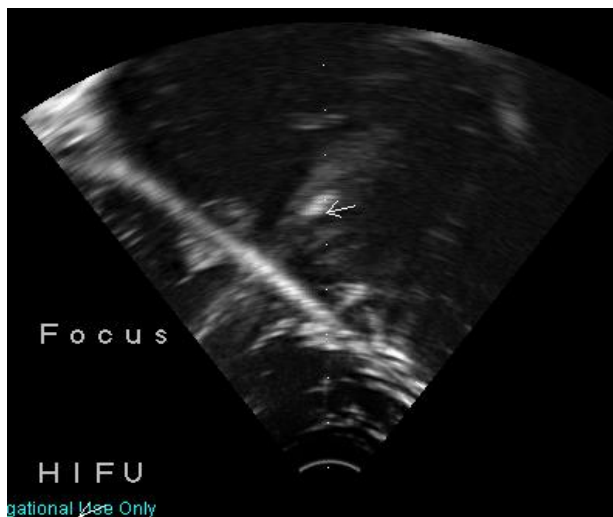
Figure 3.4: B-mode ultrasound image of the tissue-mimicking gel phantom after being exposed to HIFU. The arrow locates the position of the geometric focus of HIFU transducer as determined by the template.

3.1.3.1 TESTING OF IMAGE GUIDED HIFU IN *EX VIVO* TISSUE

Figure 3.5 shows the pre lesioning position of the HIFU focus indicated by an arrow that was placed using the template. The lesion was visible as a hyperechoic region on the B mode image as shown in figure 3.6.This was confirmed by cutting the tissue to examine the thermal lesion formed (figure 3.7).
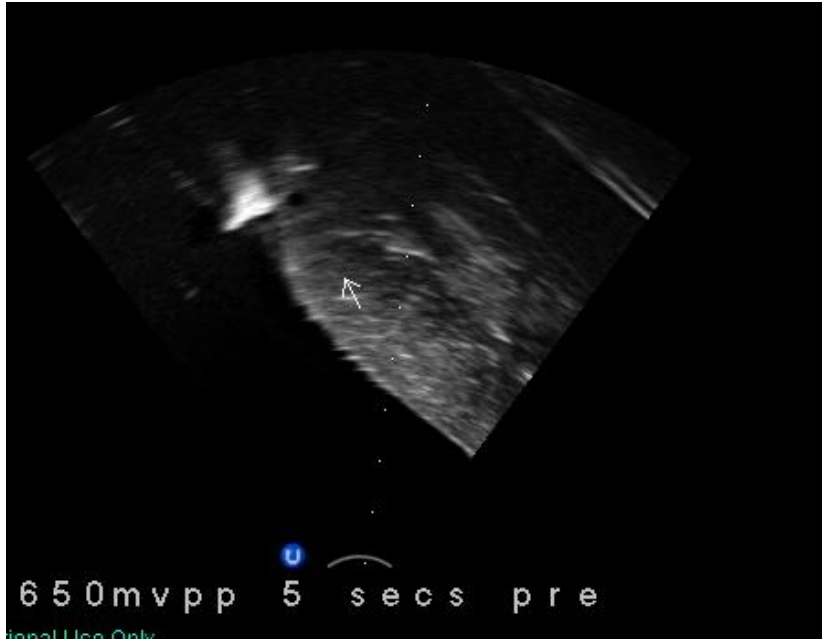
Figure 3.5: B-mode ultrasound image of the ex vivo chicken breast tissue prior to being exposed to HIFU. The arrow locates the position of the geometric focus of HIFU transducer as determined by the template.
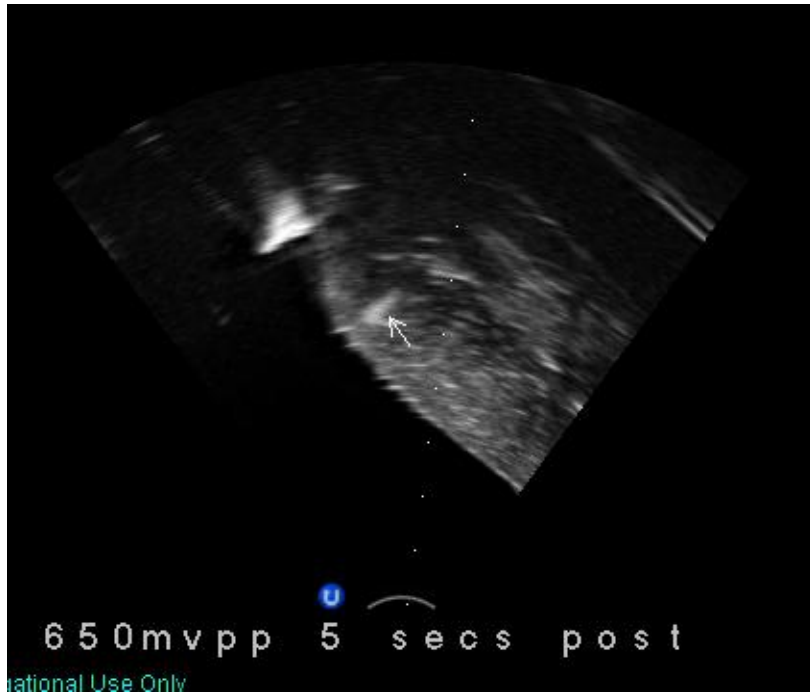
Figure 3.6: B-mode ultrasound image of the ex vivo chicken breast tissue after being exposed to HIFU. The arrow locates the position of the geometric focus of HIFU
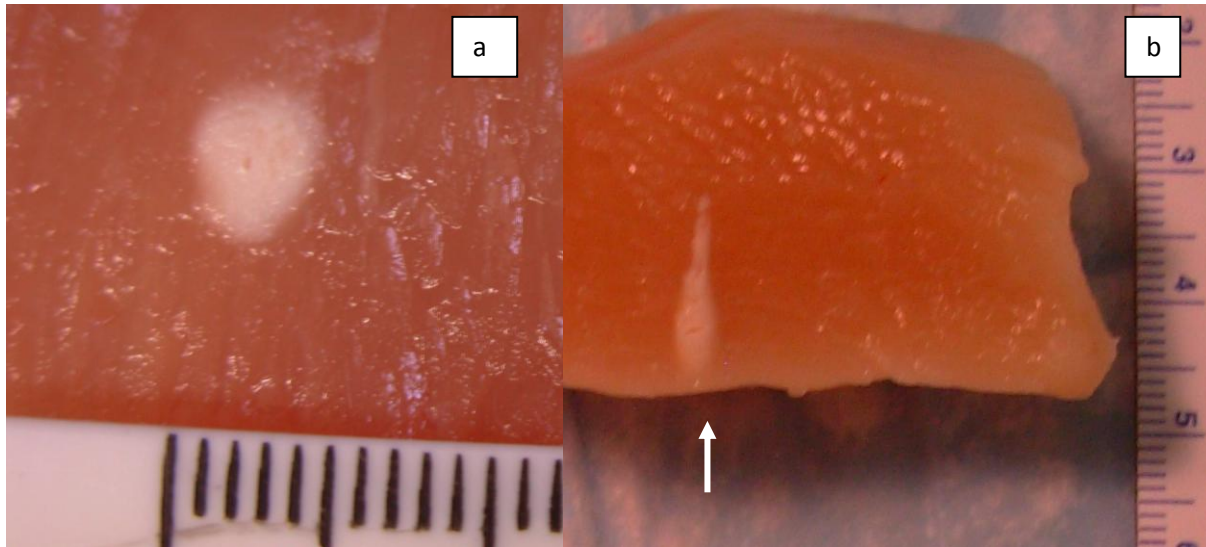
Figure 3.7: The ex vivo chicken breast tissue showing the thermal lesion. Figure (a) shows the lesion in plane perpendicular to HIFU beam. Figure (b) shows another lesion in the axial plane parallel to HIFU beam (Arrow indicating the direction of the HIFU beam).

3.2 *EX VIVO* EXPERIMENTS

This section reports on the lesion formed and peak temperature measurement. It will also report on the results from the *ex vivo* tissue experiments in absence and presence of microbubbles at various ultrasound exposure conditions and various microbubble concentrations.

3.2.1 DETERMINATION OF LESION SIZE AND PEAK TEMPERATURE

3.2.1.1 LESION SIZE

Figure 3.8 illustrates the lesion in lateral plane (plane perpendicular to the HIFU beam) at the focus. Figure 3.8 are representative images for the lesion size at intensity 649, 1530 and 2316 W/cm^2 in absence (0% concentration) (a, c and e) and presence (100% concentration) (b, d and f) of microbubbles respectively. The lesion size in axial plane is not shown. The maximum length and width for the lesions in figure 3.8 are shown in table 1. This table also contains the mean of the group and standard deviation on the group. Each group consists of three different trials under same ultrasound and microbubble conditions.
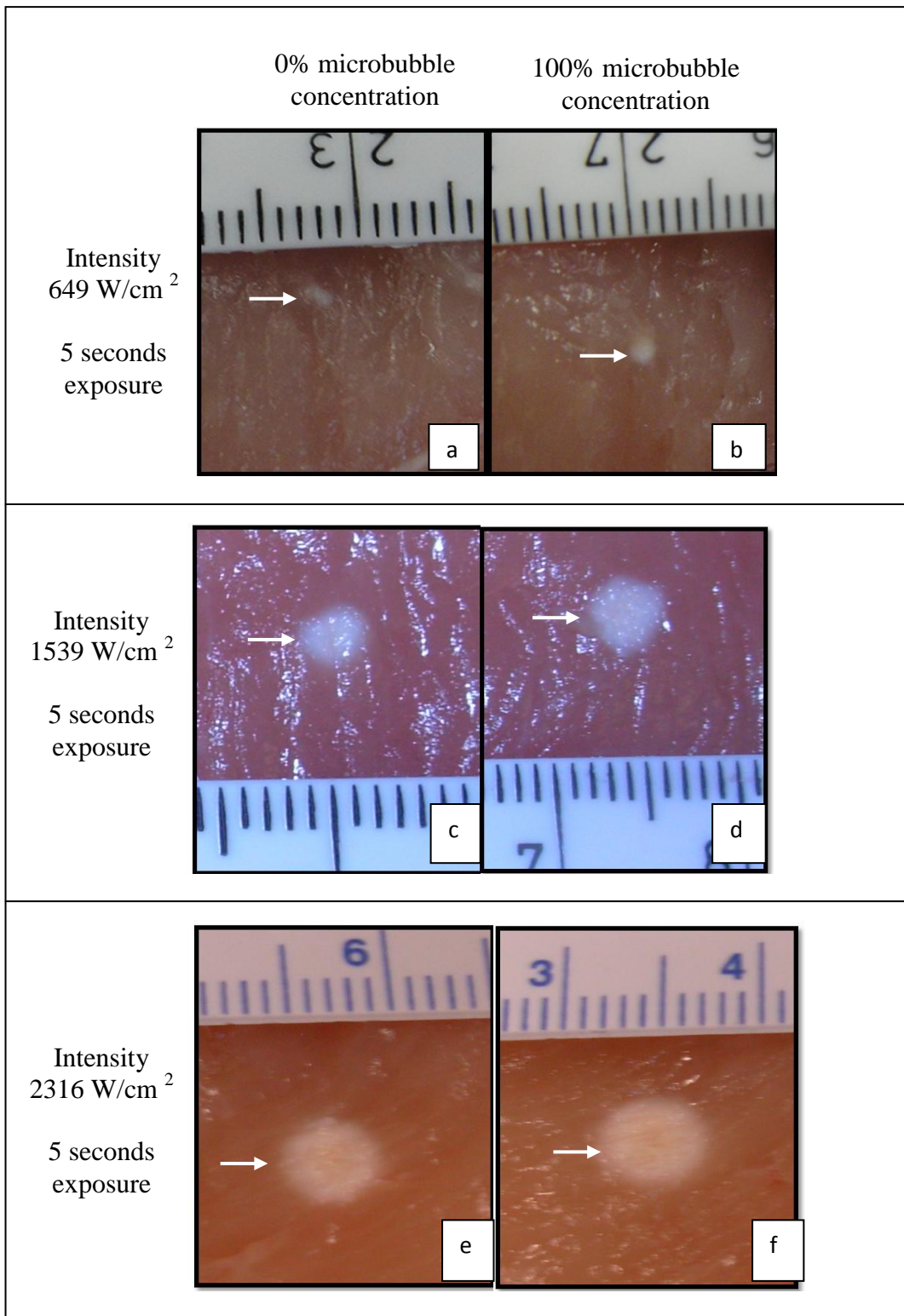
Figure 3.8: Lesion size in lateral plane for Intensity 649 W/cm^2 in absence (a) and presence (b) of microbubbles, Intensity 1539 W/cm^2 in absence (c) and presence (d) of microbubbles, Intensity 2316 W/cm^2 in absence (e) and presence (f) of microbubbles. Arrows indicate the position of the lesions.

Table 1: Maximum length and width of the specific lesions shown in figure 3.8. The table also gives the mean of each group along with the standard deviation.

	US alone (0 % Microbubble concentration – degassed water)		USMB (100 % Microbubble concentration)	
Intensity W/cm^2	*Maximum lesion length (mm)*	*Maximum lesion width (mm)*	*Maximum lesion length (mm)*	*Maximum lesion width (mm)*
649	7 (M=7.33, SD= ± 0.58)	1.5 (M= 1.16, SD= ± 0.29)	8 (M= 8 , SD=± 0)	1.5 (M=1.07, SD= ±0.12)
1539	11 (M= 11.50 , SD= ±0.50)	3 (M=2.33, SD=±0.21)	13 (M=13.33 , SD= ±0.58)	4 (M=3.67, SD=±0.12)
2316	15 (M= 14.44, SD= ± 0.58)	4.5 (M=4.37, SD=±0.35)	17 (M= 16.50, SD=± 0.50)	6 (M=6, SD=±0.17)

3.2.1.2 TEMPERATURE MEASUREMENT

Figure 3.9 shows the temperature at 3 different intensities 649, 1539 and 2316 W/cm^2 in absence (0% microbubble concentration) and presence (100% microbubble concentration) of microbubbles. The average of the peak temperatures were used for comparison among the groups. The temperature curves represent the temperature measured at 5 seconds prior to starting the HIFU exposure (base tissue temperature around 26 ⁰C), during the exposure (for 5 seconds) and for at least 60 seconds after the exposure. The x axis on all the graphs represents the exposure time in seconds. As seen in the graph first 5 seconds is a base line tissue temperature recorded at room temperature. Next 5 seconds on the *x* axis represents when the HIFU is turned on (from 5 seconds to 10 seconds on the *x* axis). The HIFU is turned off at 10 seconds. The temperature is recorded at least 60 seconds post HIFU. The temperature measurements were repeated 3 times at same exposure conditions. At each exposure condition, peak temperature was determined. The average of the peak temperature was taken for the comparisons of the results. Figure 3.9 a, c, e show the temperature profiles for intensities 649 , 1539 and 2316 W/cm^2 in absence of microbubbles respectively. It can be seen that the peak temperature rises as the intensity increases. Figure 3.9 a and b show the temperature profile at intensity 649 W/cm^2 in absence and presence of microbubbles respectively. The average peak temperature achieved in

the absence of microbubbles is 45.67 ^{o}C ($\pm$0.89^{o} C). The average of the peak temperature achieved in presence of 100% microbubbles was 52.67 ^{o}C ($\pm$1.53). The temperature rise of 7 ^{o}C was noted at this intensity. Similar trend of temperature rise was noted for other intensities (figure 39 c, d, e and f). It can be seen that the temperature rises as the intensity increases as well as in presence of the microbubbles. Moreover, as seen in figure 3.9 the temperature profile at intensity 649 W/cm^{2} seem uniform without much deviation in the profile. However as the intensity increases the temperature is more non uniform and higher uncertainties in the profile can be noted.
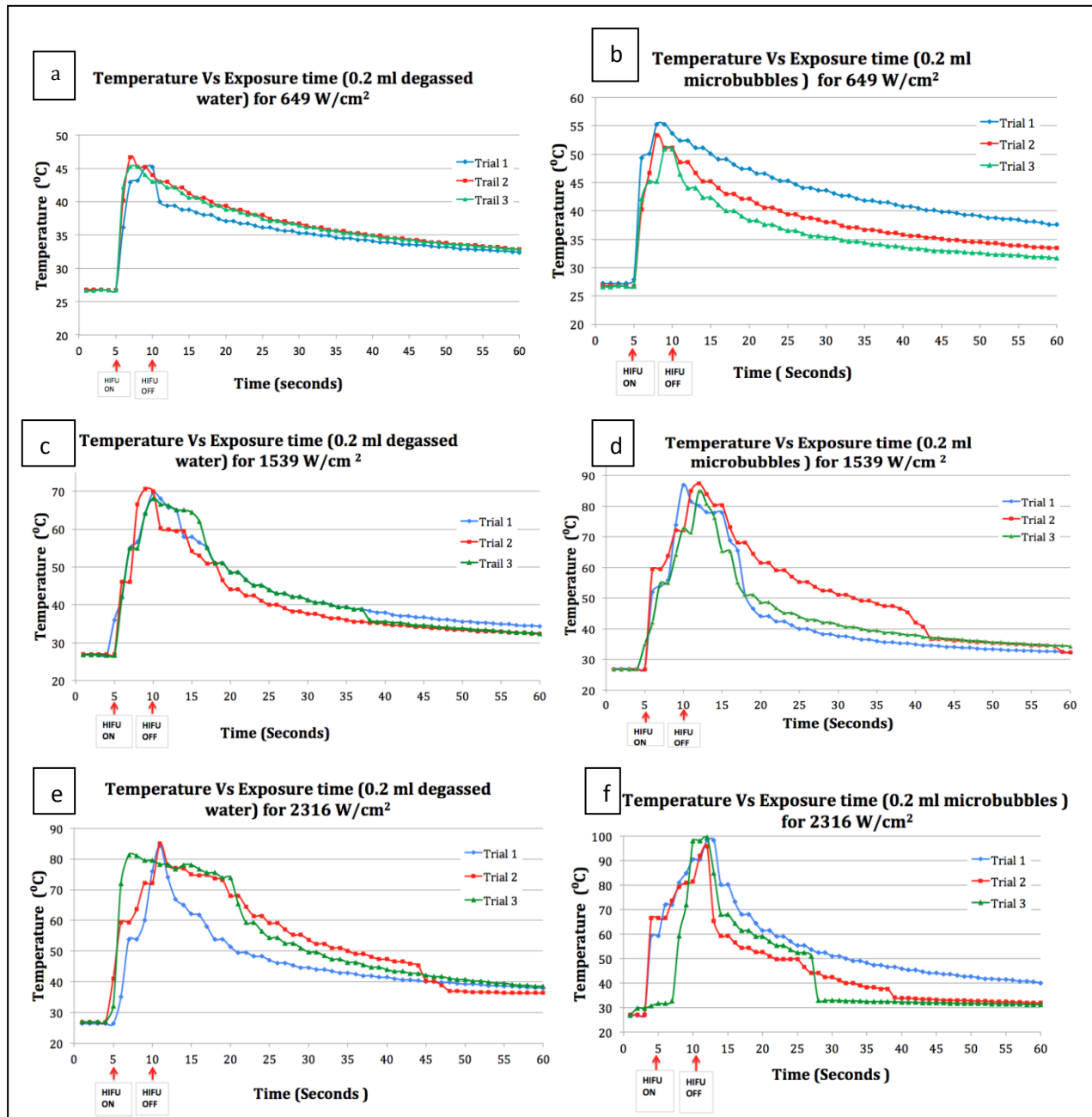
Figure 3.9: Temperature measurements at Intensity 649 W/cm² in absence (a) and presence (b) of microbubbles, Intensity 1539 W/cm² in absence (c) and presence (d) of microbubbles, Intensity 2316 W/cm² in absence (e) and presence (f) of microbubbles. Each line in a graph represents three temperature measurements at different occasions at same exposure conditions. The average of the peak temperatures was taken to compare the results.

3.2.2 HIFU INTENSITY AND MICROBUBBLE CONCENTRATION

Lesion volume and peak temperature was measured at *in situ* intensities ranging from 600 to 2300 W/cm^2 and microbubble concentrations ranging from 0% to 100% for 5-second exposure. Figure 3.10 shows the lesion volume in mm^3 as a function of acoustic intensity in W/cm^2 at various microbubble concentrations. The error bars in the graphs indicate the standard deviation, of three temperature measurements under same exposure conditions, using SPSS software. It can be seen, as the intensity increases, the lesion volume increases. At intensities ranging from 1200 to 2300 W/cm^2, the lesion volume increases approximately by a factor of 2 for ultrasound-microbubble (USMB) with 100% microbubble concentration treated group compared to ultrasound alone (0% microbubble concentration). The difference in lesion volume is statistically significant for these range of intensities ($p < 0.05$). For intensities ranging from 600 to 1000 W/cm^2, the lesion volume increase is very small regardless of the microbubble concentration. This difference was not statistically significant ($p > 0.05$). It can also been seen, at intensity 1897 W/cm^2, 0% microbubble concentration produces lesion volume of 125 mm^3. Similar lesion volume can be obtained with 100% microbubble concentration at 1539 W/cm^2.

At intensity 2300 W/cm^2 the lesion volume increases steadily as the microbubble concentration increases. Lesion volume is similar for 0% and 10% microbubble concentration. For instance the difference in the lesion volume across all intensities is 2.91 mm^3 $\pm$ 4.29mm^3. However, the difference in the lesion volume is statistically significant for 10%, 25%, 50% and 75% microbubble concentration for 2316 W/cm^2. Again, for 75% and 100% microbubble concentration, there is no large difference in lesion volume at particular intensity. For 75% and 100% concentrations the difference in lesion volume is 7.20 mm^3 $\pm$ 7.60mm^3 across all intensities. At intensity 1500 W/cm^2 as the microbubble concentration increases from 0 to 25%, there seems to be no significant increase in lesion volume. Similarly from 50% to 100% microbubble concentration at 1539 W/cm^2, the increase in lesion volume is very small. At intensities from 600 to 1000 W/cm^2, no statistical difference is observed among the groups ($p < 0.05$).
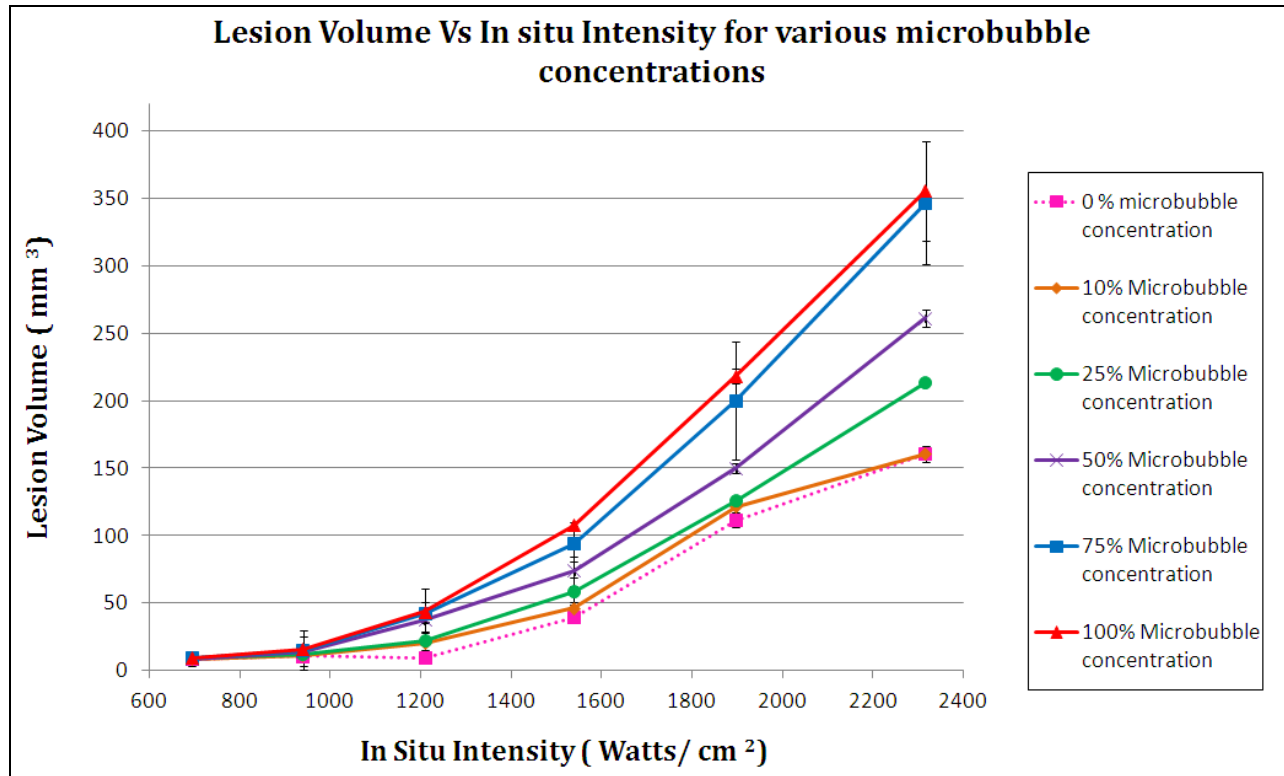
Figure 3.10: Lesion volume vs. in situ intensity at various microbubble concentrations. The error bars represent the standard deviation of a group with 3 trials under same treatment conditions. Pink dotted line, showing the lesion volume curve for 0% microbubble concentration, starts to plateau around 1900 W/cm² whereas the red line indicating 100% microbubble concentration follows a steep rise.

Figure 3.11 shows the peak temperature vs. *in situ* intensity. Unlike the lesion volume, the difference in the peak temperature rise for each group was statistically significant ($p<0.05$) for 0% and 100% microbubble concentration. For intensities ranging from 1200 to 2300 W/cm², the temperature rise is approximately 10 to 16 °C for USMB treated group compared to US alone. However, the peak temperature rise for intensities from 600 to 1000 W/cm² is approximately 5 to 7 °C.

As for peak temperature at various microbubble concentrations for different intensities ranging from 600 to 2300 W/cm², there seems to be steady increase in the temperature. It can be seen that at 2300 W/cm² there is statistically significant rise in peak temperature from 0% to 100% microbubble concentration.
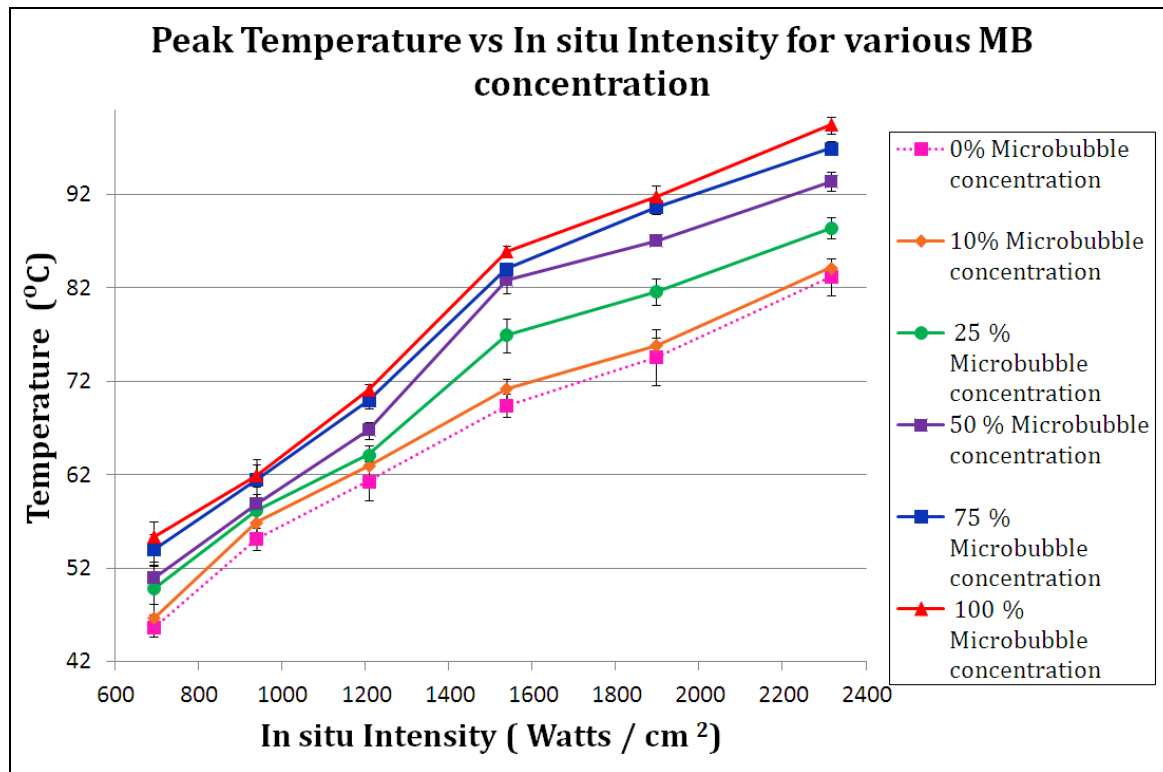
Figure 3.11: Peak temperature vs. in situ intensity at various microbubble concentration. The error bars represent the standard deviation of a group with 3 trials under same treatment conditions. Pink dotted line, showing the temperature curve for 0% microbubble concentration, follows a modest rise whereas the red line indicating 100% microbubble concentration follows a steep rise from 1200 to 1500 W/cm².The 70% concentration and 100% concentration gives comparable values of temperature. Similarly 0% and 10% microbubble concentration gives comparable values of temperature.

3.2.3 HIFU INTENSITY AND HIFU EXPOSURE TIME

Figure 3.12 and 3.13 shows the lesion volume and peak temperature as a function of HIFU exposure duration respectively. Each point represents the average of three trials conducted under same conditions. The graphs show the lesion volume and peak temperature that were measured for intensities 649, 1539 and 2316 W/cm² for 3, 5 and 10 seconds HIFU exposure each. It can be seen from Figure 3.12 that the lesion volumes at 5 seconds and 10 seconds are similar for 2316 W/cm². Three seconds exposure duration yields small lesion volume regardless of microbubble concentration or intensity. On the other hand, from Figure 3.13 a slight increase in peak

63

temperature can be seen at 10 seconds exposure duration compared to 5 seconds exposure duration. Although there is clear rise in temperature at 2316 W/cm^2 with microbubble from 5 to 10 seconds, the lesion volume is comparable.
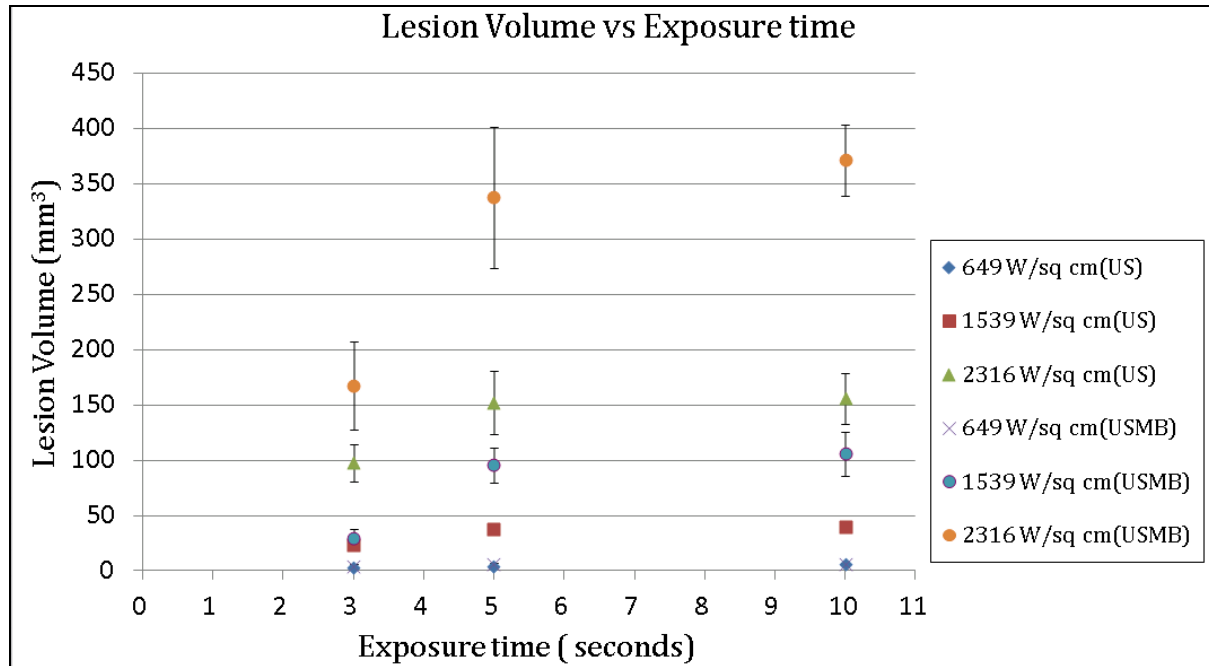
Figure 3.12: Lesion volume vs. Exposure time at 0 and 100 % microbubble concentration for 649, 1539 and 2316 W/cm^2 intensities at 3, 5 and 10 seconds HIFU exposure duration. The error bar represents a standard deviation for 3 trials in each group with same treatment conditions.
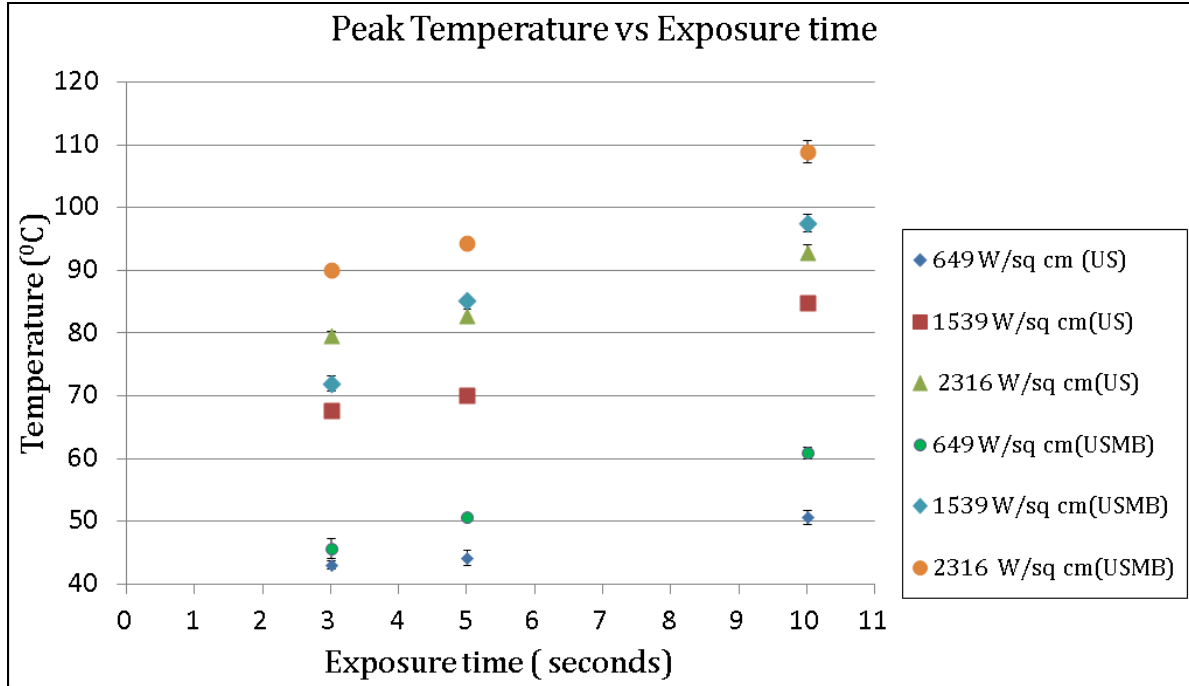
Figure 3.13: Peak Temperature vs. Exposure time at 0 and 100% microbubble concentration for 649, 1539 and 2316 W/cm^2 intensities at 3, 5 and 10 seconds HIFU exposure duration. . The error bar represents a standard deviation for 3 trials in each group with same treatment conditions.

3.2.4 RELATIONSHIP BETWEEN LESION VOLUME AND TEMPERATURE

The scatter plot of the lesion volume as a function of peak temperature for all the microbubbles concentration (0% to 100%) and the intensities (649 to 2316 W/cm ^{2}) are shown in figures 3.14 and 3.15 respectively. These graph show that the lesion volume increases as the temperature increases. This holds true for temperature of up to 70°C. The variability of the lesion volume is less below 65°C to 75°C. The variability of the lesion volume is increases over 70°C temperature. At temperatures higher than 70 °C, the lesion volume appears to increase at slightly higher rate. Similarly, figure 3.16 shows the scatter plot of the lesion volume as a function of the peak temperature at intensities 649, 1539 and 2316 W/cm^2 with 0% and 100% microbubble concentration for all the trials at 3, 5 and 10 seconds exposure duration. The variability of the lesion volume is again less under 70°C and the variability is greater for temperatures over 70°C.

65
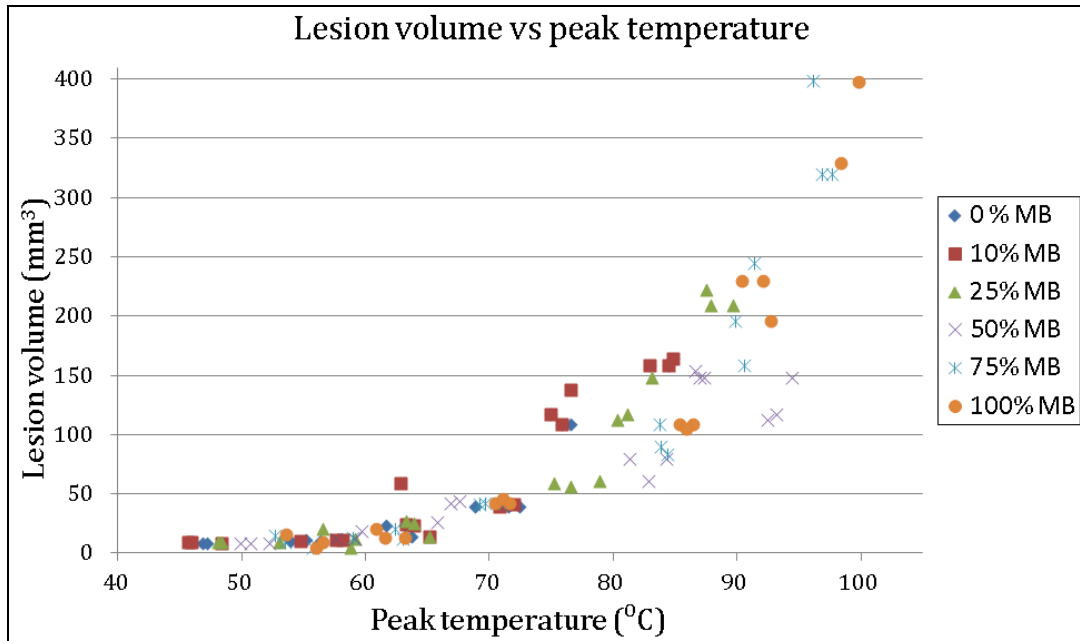
Figure 3.14: Scatter plot for lesion volume vs. peak temperature for all intensities represented at all microbubble concentration. The data points represent all the trials of the treatments. Color coding of the data points represents the microbubble concentration.
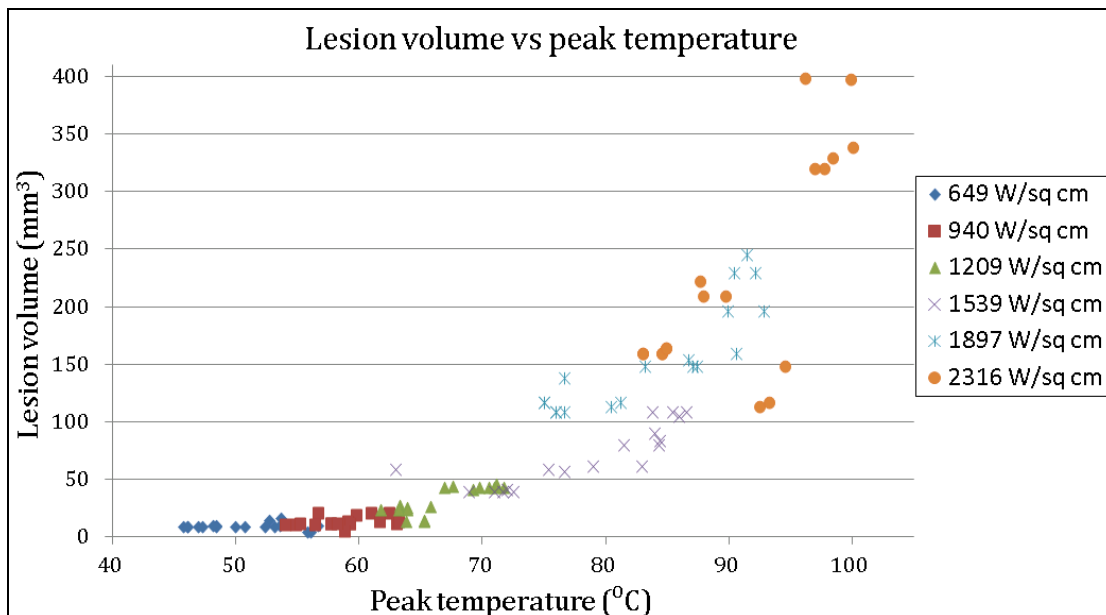
Figure 3.15: Scatter plot for lesion volume vs. peak temperature for all microbubble concentration represented at all intensities. The data points represent all the trials of the treatments. Color coding of the data points represents the focal intensities.
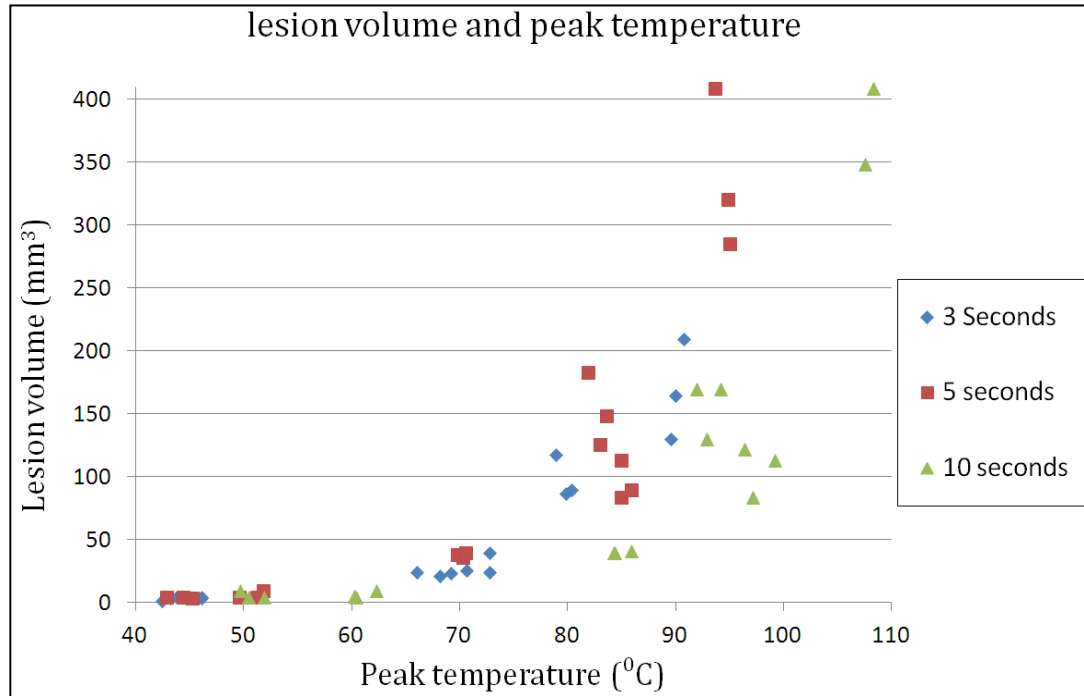
Figure 3.16: Scatter plot for lesion volume vs. peak temperature for intensities 649, 1539 and 2316 W/cm^2 for 0% and 100% microbubble concentration at 3, 5 and 10 seconds exposure duration. The graph contains the data points for all the trials of the treatment. Color coding of the data points represent the exposure duration.

CHAPTER 4

DISCUSSIONS

The current study investigated the use of contrast agents to enhance HIFU ablation. We have measured bubble-enhanced lesion volume and temperature rise in an *ex vivo* tissue model as a function of several parameters. Our observations are similar to the earlier work of Lele (1987), Hynynen (1991), Clarke and ter Haar (1997), and Holt and Roy (2001). The current section discuses the results obtained from the *ex vivo* tissue experiments. We discuss the mechanisms for the enhanced heating and potential reasons for increase in lesion volume. We also discuss the limitations of the current study and propose some solutions.

All data in this project were taken at room temperature 26 $^{\circ}$C and presented by the mean and its standard deviation of three measurements unless specified otherwise. An *ex vivo* chicken breast tissue model has been used in this study. Compared to the artificial gel phantoms, the *ex vivo* tissue model is closer to the *in vivo* conditions in terms of tissue composition. The temperature rise and lesion volume at the focus for various US exposure and microbubble concentrations were studied. We have used the lesion volume calculation method adapted from ter Haar et al. (1991). This model is better suited for the current experiments as we measured the lesion volume by slicing the tissue and measured the length and width with ruler. Other methods of lesion volume measurements are discussed latter. Maximum length and width was measured.

4.1 MICROBUBBLE ASSISTED LESION FORMATION AND TEMPERATURE RISE

4.1.1 MICROBUBBLE CONCENTRATION AND FOCAL INTENSITY

HIFU causes temperature to increase because ultrasound energy is converted to heat as the tissue absorbs the energy. Presence of microbubbles in current study increased the lesion volume and temperature. With regards to the mechanism by which microbubbles in the ultrasound field cause heating, two factors may be involved: (1) heating by oscillation or explosion of microbubble contrast agents exposed to HIFU, and (2) cavitation bubbles generated by HIFU exposure (Umemura et al., 2001; Holt and Roy, 2001; Kaneko et al., 2003; Matsumoto et al., 2005; Miller et al., 1996; Baker et al., 2001; Kennedy et al., 2003). Although the presence of the microbubble

agent was associated with higher temperatures and more tissue damage, it cannot be predicted for sure as to how much of the differences between groups can be attributed to cavitation and how much to attribute to microbubble oscillation (inducing temperature rise). In general, the behavior of acoustic cavitation is complicated and unpredictable, but Tran et al. (2003) reported that microbubbles could increase the cavitation caused by HIFU by lowering the cavitation threshold. To detect and analyze cavitation, we would need to use a second ultrasound probe for listening only. This is called passive cavitation detection. We did not try to detect or analyze cavitation in the present study.

The lesion volume and temperature increased as the intensity and microbubble concentration increases as shown in figures 3.10 and 3.11. Similar phenomenon were observed by Zhang et al., (2011) and Holt and Roy (2001). Other investigations have shown that microbubbles lead to a higher and faster temperature rise (Holt and Roy, 2001; Umemura et al., 2002). These findings showed that the introduction of microbubble could lead to complete necrosis of the target tissue. Mechanisms for microbubble-assisted heating were presented, modeled, and estimated by Holt and Roy (2001), who showed similar results to the earlier work of Lele (1987), Hynynen (1991), and Clarke and ter Haar (1997). Modeling estimates from Holt and Roy demonstrated that the heat deposition from bubbles can explain the measured temperature rises quantitatively. The role of inertial cavitation in enhancing the heating rate was also shown by Farny et al. (2010).

The cause of increased heating in the presence of bubbles has been hypothesized as viscous damping of noninertially cavitating bubbles (explained by Holt and Roy, 2001), absorption of high frequencies created from inertial cavitation, and/or an increase in acoustic path length due to scattering (Holt and Roy, 2001). These mechanisms help microbubble contrast agents to increase thermal effect of HIFU (Chapelon et al., 1992; Chen et al., 2003). We believe that this was the mechanism of microbubble-assisted HIFU ablation in our study. In our current study, we found that as the concentration of the Artenga® microbubbles increases, until certain level larger volume of the target tissue was destroyed. So, the volume of necrosis in USMB group was greater regardless of the ultrasound intensity and exposure duration. Cigar shape was noticed for almost all the lesions. However, the lesion shape changed to tadpole like in presence of microbubbles. The lesion width was symmetrical for the lesions without the microbubbles. The

radial symmetry was lost in most of the lesions (towards transducer side) created in presence of the microbubbles.

Microbubbles are regarded as effective cavitation nuclei (Chen et al., 2003). The bubble implosion can generate shock waves, high-velocity liquid jets, free radical species and strong shear forces that can damage cells and tissues. As shown in figure 3.10, lesion volume increases for USMB group and the increase in lesion volume is steep as the intensity increases. On the other hand the measured lesion volume values plateaus at intensities greater than 1500 W/cm^2 for treatment without the microbubbles. This could possibly occur due to limited extent of the HIFU beam width. The HIFU beam width, as discussed in chapter 1, is only few millimeters in diameter for highly focused ultrasound transducers. The local elevations of the temperatures are created in this focal area where the thermal dose is deposited. The lesion size is dependent on the deposited thermal dose (explained in chapter 1) and the heat conduction in tissue (ter Haar et al., 1989). This thermal dose will increase with the increase in exposure duration and intensity. However, after reaching certain threshold there will be no further increase in heat conduction leading to plateauing of the lesion volume (Figure 3.10, 0% microbubble concentration curve). Significant lesion volume increase can be seen at intensities greater than 1200 W/cm^2 (p<0.05), however, the lesion volume does not increase greatly at intensities between 600 to 1000 W/cm^2 (p>0.05). Lesion size is determined by the exposure duration and focal intensity (ter Haar et al., 1989). Lesion formation during HIFU therapy is a complex process, which involves both thermal and cavitation effects. The initial lesion is formed thermally (Holt and Roy, 2001). Further, Holt and Roy (2001) showed that the boiling of the tissue may cause the lesion shape transformation and advancement. In USMB treated tissues, the enhanced heating from inertial cavitation generated bubbles may be the dominant mechanism for lesion formation.

Investigations of temperature changes at various intensities have shown that the presence of microbubbles lead to a higher temperature rise (Holt and Roy, 2001; Umemura et al., 2002). We have established that through our study as well. It is well known that; microbubbles also assist in the onset of cavitation (Blomley et al., 2001; Yu et al., 2004; Unger et al., 2002), thus leading to a larger production of free radicals such as hydroxyl . It has been believed that free radicals alone could induce necrosis and they could also extend the volume of the HIFU-induced lesion (Goldberg et al., 2002; Prat et al., 1994; Huber et al., 2001). The ultrasound intensity used in this

study ranges above and below the known cavitation thresholds (Fry, 1991). Therefore, we concluded that both thermal effects and cavitation were intensified by the administration of the microbubble agent during HIFU thus resulting in an enhancement of the HIFU therapy.

4.1.2 MICROBUBBLE ASSISTED HIFU LESION AND EXPOSURE DURATION

Zhang et al., (2011) recently showed that the lesion volume increase with the exposure duration. Our study shows similar results. However, as seen in figure 3.12, the lesion volume increases from 3 to 5 seconds exposure. No significant difference in lesion volume was recorded for 5 and 10 seconds. As depicted in figure 3.12, the lesion volume in the *ex vivo* tissue at all intensities seem to be similar for 5 second and 10 second exposure. For e.g. consider intensity 2316 W/cm^2, the lesion volume in absence of microbubbles produce similar volume at 5 second and 10 second exposure. Similarly in presence of microbubbles the lesion volume achieved at 5 and 10 seconds are not very different. However, the peak temperatures achieved at these conditions show a notable difference (Figure 3.13). This phenomenon could be explained by the boiling of tissue (vapor cavities produced due to overheating of the tissue) (Khokhlova et al., 2005). The tissue boiling might increase the temperature while preventing its dissipation through the gas bubble. The heat conduction may be prevented due to the voids created at the tissue boiling site as well as shielding the focus from the HIFU energy by scattering or reflecting the ultrasound energy and hence reducing the rate of increase in the lesion volume (Khokhlova et al., 2005).

4.1.3 RELATIONSHIP BETWEEN LESION VOLUME AND TEMPERATURE

We have studied the relationship between the lesion volume size and the temperature rise for all the microbubble concentrations, focal intensities and exposure durations. This analysis is unique to our study. In figures 3.14 and 3.15, until 70 $^\circ$C there appears very little variability in the lesion volume as a function of temperature. Lesion formation under 70 $^{\mathbf{o}}$C may be created due to thermal effect. This could be because of both direct thermal effects from HIFU due to high pressures created at the focus as well as thermal effect induced due to enhanced heating from bubbles. At temperatures greater than 70 $^\circ$C, the lesion volume increases. However, large variability in the lesion volume above 70 $^{\mathbf{o}}$C can be seen. This increase in the lesion volume variability above 70°C cannot be explained solely due to thermal effect. It appears that there are

71

other mechanisms (microbubble induced heat and cavitation) involved in enhancing the lesion volume above this 70 ⁰C threshold. Similar trend was noticed in figure 3.16. Curve fitting was not applied to these data. We did not find a suitable model that was appropriate to test the curve fitting for this data.

4.2 LIMITATIONS

We discuss some limitations of this study and propose potential solutions to those limitations in this section. In this study we have used the volume of ellipsoid to measure the volume of the lesion. It was especially difficult to cut the lesion in axial plane due to uncertainty of determining the exact location of the lesion in the tissue from the surface. However, the focal depth in tissue was known (1.5 cm), hence the tissue was sliced at 1.5 cm depth in the plane perpendicular to the HIFU beam. A ruler was used to measure the maximum length and width of the lesion. Volume of ellipsoid is a simple calculation (ter Haar, 1991) and easy to implement hence we have used this method. However, there are several drawbacks to this method. Using ruler to measure the length and width is a crude measurement and will not give an exact lesion volume and the values of the measurement will vary from one observer to other. In literature, several methods are discussed for determining lesion volume. Sedelaar el al., (2000) proposed the application of the three dimensional contrast enhanced ultrasound to measure volume of the affected tissue after the HIFU treatment for localized prostate cancer. MRI has been used for lesion volume calculation in several studies (Köhler et al., 2009;Zhang et al., 2011).Whole mount method involves the fixation of the tissue in formalin and then sectioning the tissue. Later identifying the lesions and measuring the dimensions of the lesions (Karavitakis et al., 2011). We used a software based lesion volume calculation to compare it to our current method. This method involves a matlab based code that will enable us to import the actual jpeg image of the lesion. The boundaries of the lesion will be user defined and the code will compute the volume in 3D. We did not have enough data (photos of the lesions), hence this method was not implemented in current work. It has been recommended as a future work. We collected the data on lesion volume using a simple method using ruler measurements. We believe that further investigations should concentrate on understanding the relationship between the ultrasound exposure and the true size of ablation, thus enabling the prediction of the actual necrosis volume.

The comparatively small values for the standard deviations and the narrow ranges of peak temperatures indicated stable tissue model. However, *in vivo*, conditions change drastically due to breathing of the subject, blood flow, position of the tumor in the body, and tissue type. This suggests that HIFU should be administered on an individual basis when extending the study to *in vivo* situations. The limitation of the present study is that it was performed in normal chicken breast tissue. Further studies in malignant tissue should be performed in future.

We have used a thermocouple in our present experiments. The measurements may not represent an actual temperature achieved. An error in temperature measurement using a thermocouple is mainly caused by the viscous loss at the interface between the thermocouple and the tissue medium (Fry and Fry, 1954). Result of the effect is a much steeper temperature rise initially where the time scale of this effect is a fraction of a second. After the early steep rise, the temperature elevation is mainly caused by acoustic absorption. It should be noted that the temperature rise results obtain by the multi-meter is limited by the response time, which is about 0.2 s. Thus, the early rise due to the viscous loss is not registered. The disparity between theory and experimental data for time less than 1 s may be caused by the error due to the viscous loss (Chen et al., 2009). The direct determination of temperature rise and cavitation in situ under high intensity ultrasound treatment is very difficult. Other methods for determining the lesion temperature include using MRI thermometry (Kahn et al., 1998; Köhler et al., 2009).

CHAPTER 5

CONCLUSIONS AND FUTURE WORK

5.1. CONCLUSIONS

Microbubble contrast agents in combination with HIFU therapy enhanced the therapeutic effect by increasing the focal temperature of the tissue and in turn increasing the lesion volume. The efficacy of the HIFU therapy in combination with microbubbles can be controlled through ultrasound/ microbubble exposure parameters. This effect depended on the HIFU intensity and microbubble concentration and the ultrasound exposure duration.

- As the HIFU intensity increases the peak temperature of the focal region increases causing increase in the lesion volume.
- As the microbubble concentration increases, the peak temperature increases along with the lesion volume without plateauing.
- As the exposure duration of the treatment increases from 3 to 10 seconds, the peak temperature increases. However the lesion volume increases from 3 to 5 seconds. Lesion volume yields same values for 5 and 10 seconds.

In *ex vivo* tissue model, a shorter time or lower acoustic intensity is required in presence of microbubble contrast agents, to produce the same effects; thus, the treatment time needed for HIFU therapy may be shortened, and the incidence of adverse effects may decrease. Although many problems remain unresolved, with additional improvement, HIFU combined with a contrast agent may offer a useful treatment approach that will provide real clinical benefit through enhancing efficiency and safety of the HIFU treatments.

5.2. FUTURE WORK

The current study uses maximum width and length of the lesion in order to measure its volume, which may be an overestimation of the actual volume. In future, an algorithm for lesion volume calculation using a computer simulation program such as matlab can be designed in order to allow calculating the 3D volume accurately from the imported 2D image or histological slices of

the lesion. We developed a matlab program in order to test the accuracy of the lesion volume measurements. This program required importing full length axial image of the lesion. However, we did not have enough data to compare the results as we did not have full length axial image of the lesions. Figure 5.1 shows the comparison between the volume obtained by the matlab program by importing the 2D axial images calculating volume in 3D rotational geometry and the lesion volume estimated for the current study along with the lesion volume derived from the same ellipsoid formula but using average of the length and width of the lesion .
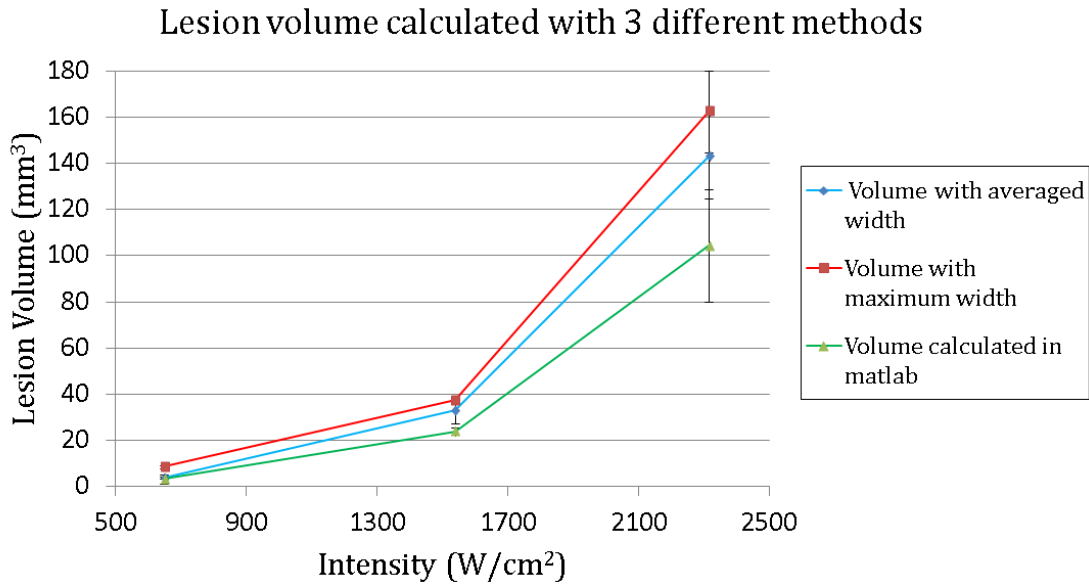
Figure 5.1: Lesion volume calculated with 3 different methods.

Moreover, more controlled methods of lesion volume calculation (discussed in chapter 4) can also be implemented to test the accuracy of the matlab algorithm discussed here. Further studies are recommended for *in vivo* situations in presence of blood vessels where the effect of the microbubbles can be studied to determine the optimal conditions for microbubble assisted HIFU treatments. Work is needed to build an ex vivo tissue model with blood vessels. More studies are needed to study the effects of clinically approved microbubbles such as Definity® and Optison®.

APPENDICES

Appendix A: Calibration table for the HIFU system

Input Voltage (mVpp)	Output Electric Power (Watts)	Output Acoustic power (Watts)	In situ Intensity (Watts / cm^2)	Free Field Intensity (Watts/cm^2)
50.00	1.00	0.63	19.77	36.90
100.00	3.00	2.66	82.70	160.00
150.00	8.00	5.88	183.10	354.00
200.00	13.50	10.25	319.40	627.50
250.00	19.00	15.69	488.70	953.60
300.00	27.00	22.29	649.30	1350.00
350.00	36.00	30.18	940.20	1852.00
400.00	45.50	38.82	1209.00	2387.00
450.00	57.00	49.41	1539.00	3039.00
500.00	69.00	60.91	1897.00	3747.00
550.00	83.55	74.37	2316.00	4571.00
600.00	96.00	90.83	2829.00	5587.00

HIFU system block diagram
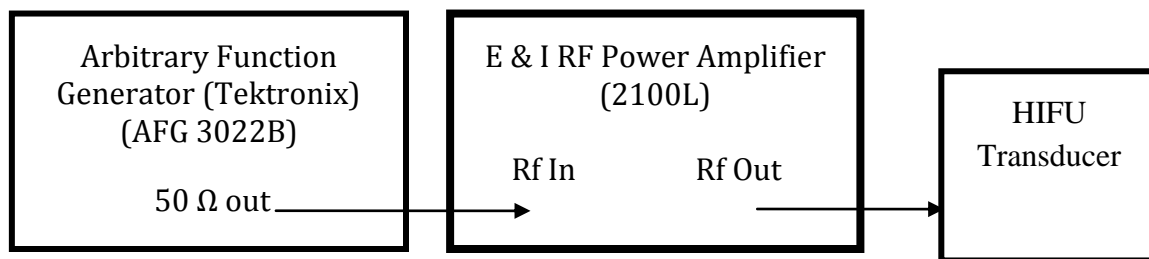
E & I RF power amplifier has an inbuilt power meter that gives us the output electric power for a certain input voltage. Onda power meter was utilized to determine the Output acoustic power for a certain input voltage.

Appendix B: Thermocouple construction instructions

Arthur Worthington, Dept of Physics, Ryerson University
September 2000

(1) Cut matching 114 cm lengths of 76.2 μm chromel and alumel wires(California Fine Wire, Grover Beach, CA, USA);. Tape each end of one wire to a desk or counter top. Tape the other wire on top of the first.

(2) Hold the double end of the wires in a vise and place the other double end in an electric drill. Keep a slight but steady tension on the wires and run the drill for about 60 seconds to twist the wires together tightly. Do not allow the wires to kink.

(3) Remove the wires from the drill carefully and allow them to relax the twist but do not allow them to kink.

(4) Cut the tape from one end and strip a little of the insulation with a match or lighter. Cut back the stripped twisted wires so that there is only a small uninsulated length left. Strip the other end and place in the clamp on top of the Thermocouple Welder (thermocouple welder welds thermocouple wires together to form a uniform bead junction, consistent in size and quality, without detrimental oxide layers). Figure below shows the thermocouple welder. Turn the power on and turn on "Charge". Touch the first end of the wires to the carbon post under glycerol on top of the welder to form the weld. Examine under a microscope to confirm the weld bead. Check that the resistance of the two wires, through the junction, is about 300 Ω.

(5) Cut the plastic hub from a hyperdermic needle and hold the needle in plastic forceps whose handle is held in a small vise. Pass the welded end of the thermocouple through the bore..With a very small needle (e.g. 27 gauges) it may be necessary to pass the wires through the needle before welding the junction.

(6) Push the junction slightly out of the needle and coat it with crazy glue. Pull the junction back so that it is just inside the bore.

(7) Cut a piece of clear 22 gauge PVC tubing(Alpha Wire, Elizabeth, NJ, USA) so that it is long enough to go from the hub of the needle to almost the other end of the thermocouple wires. Push the tubing onto a 18 gauge needle. Mount the needle onto a plastic syringe from which the finger grips have been cut. Use a short section of rubber hose to connect the syringe to the aspirator on a cold water tap. Turn on the tap to apply a vacuum to the tubing feed a sufficiently long piece of suture through the tubing. Remove the tubing from the needle and tie the suture to the stripped end of the wires. Pull the wires through the tubing and crazy glue the tubing to the remainder of the hub.

(8) Cut the wires if necessary, strip the insulation, and connect the wires to a type K thermocouple plug. Make sure that the wires are under Teflon washers: metal washers will tear and break these very fine wires. Check that the thermocouple works with a digital thermometer It should read room temperature. Hold the sharp end of the needle between your fingers and watch the reading increase. If the reading goes down, the wires are connected to the wrong terminals in the plug.

(9) After constructing the thermocouple, double check its calibration by comparing its readings with a calibrated digital thermocouple for a few temperatures within the range of 5 $^{\circ}$C to 90° C.
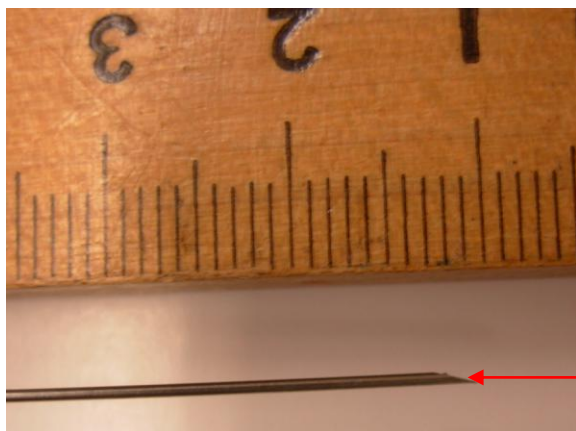
A 22 gauge needle with the thermocouple inside.

Thermocouple

Alligator clip holding the other end of the thermocouple twisted wire.

Tip of the twisted thermocouple immersed on to the carbon rod inside the mineral oil

Mineral oil

.001

.0025   CHARGER   ON

THERMOCOUPLEWELDER   POWER   ON
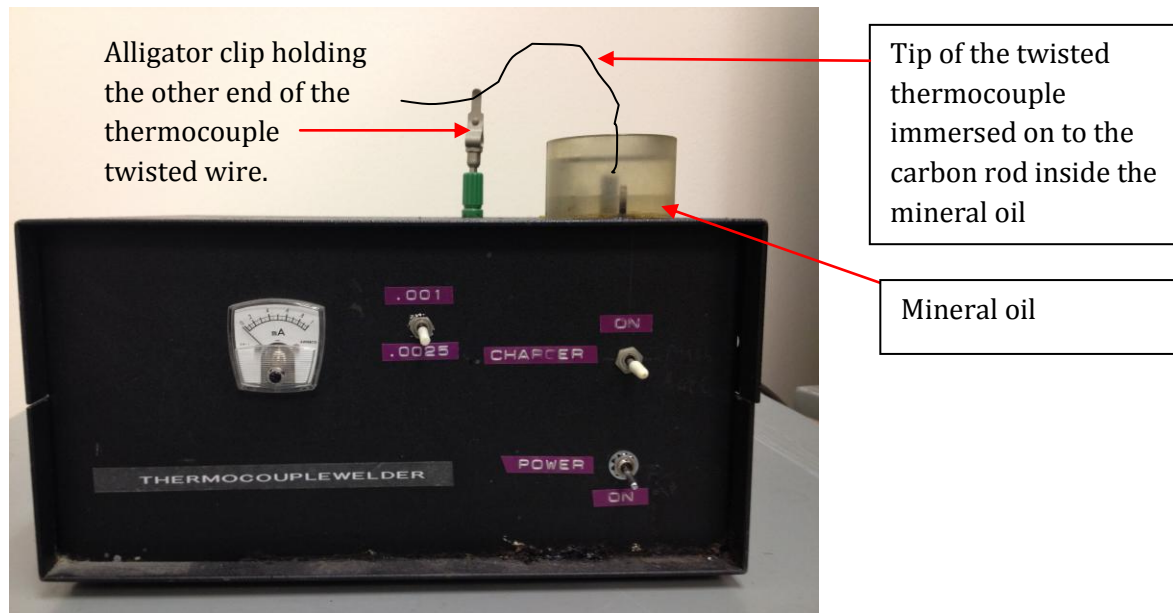
Thermocouple welder.

REFERENCES

Alongi, F., Russo, G., Spinelli, A., Borasi, G., Scorsetti, M., Gilardi, M. C., et al. (2011). Can magnetic resonance image-guided focused ultrasound surgery replace local oncology treatments? A review. *Tumori, 97*(3), 259.

Apfel, R. E., & Holland, C. K. (1991). Gauging the likelihood of cavitation from short-pulse, low-duty cycle diagnostic ultrasound. *Ultrasound in Medicine & Biology, 17*(2), 179-185.

Bailey, M. R., Blackstock, D. T., Cleveland, R. O., & Crum, L. A. (1998). Comparison of electrohydraulic lithotripters with rigid and pressure-release ellipsoidal reflectors. I. acoustic fields. *The Journal of the Acoustical Society of America, 104*(4), 2517.

Bailey, M. R., Blackstock, D. T., Cleveland, R. O., & Crum, L. A. (1999). Comparison of electrohydraulic lithotripters with rigid and pressure- release ellipsoidal reflectors. II. cavitation fields. Journal of the Acoustical Society of America, 106(2), 1149-1160.

Baker, K. G., Robertson, V. J., & Duck, F. A. (2001). A review of therapeutic ultrasound: Biophysical effects. *Physical Therapy, 81*(7), 1351.

Bao, S., Thrall, B. D., Gies, R. A., & Miller, D. L. (1998). In vivo transfection of melanoma cells by lithotripter shock waves. *Cancer Research, 58*(2), 219-221.

Bao, S., Thrall, B. D., & Miller, D. L. (1997). Transfection of a reporter plasmid into cultured cells by sonoporation in vitro. *Ultrasound in Medicine and Biology, 23*(6), 953-959.

Bednarski, M. D., Lee, J. W., Callstrom, M. R., & Li, K. C. P. (1997). In vivo target-specific delivery of macromolecular agents with MR- guided focused ultrasound. *Radiology, 204*(1), 263-268.

BIOPAC Systems Inc. (2005). Compound Action Potential: Nerve Conduction BIOPAC User Manual. Goleta, CA.

Blomley, M. J., Cooke, J. C., Unger, E. C., Monaghan, M. J., & Cosgrove, D. O. (2001). Microbubble contrast agents: A new era in ultrasound. *BMJ (Clinical Research Ed.), 322*(7296), 1222-1225.

Bommannan, D., Menon, G. K., Okuyama, H., Elias, P. M., & Guy, R. H. (1992). Sonophoresis. II. examination of the mechanism(s) of ultrasound-enhanced transdermal drug delivery. *Pharmaceutical Research, 9*(8), 1043-1047.

Bommannan, D., Okuyama, H., Stauffer, P., & Guy, R. H. (1992). Sonophoresis. I. the use of high-frequency ultrasound to enhance transdermal drug delivery. *Pharmaceutical Research, 9*(4), 559-564.

Bradley, J.N. (1962). Shock Waves in Chemistry and Physics. Methuen, London, 246–263.

Bradley, J. N., & Raymond J. Emrich, R. (1963). Shock waves in chemistry and physics. *American Journal of Physics, 31*(3), 224.

Brookes, M., & Dyson, M. (1985). Stimulation of bone repair by ultrasound. *International Journal of Rehabilitation Research, 8*(Supplement), 73.

Brujan, E. A., Ikeda, T., & Matsumoto, Y. (2005). Jet formation and shock wave emission during collapse of ultrasound-induced cavitation bubbles and their role in the therapeutic applications of high-intensity focused ultrasound. *Physics in Medicine and Biology, 50*(20), 4797-4809.

Burov, A.K. (1956). High intensity ultrasonic vibrations for action on animal and human malignant tumours. Dokl. Akad. Nauk. SSR 106, 239–241.

Butt, F. & Tavakkoli, J. (2011). Linear Acoustic and Temperature Simulation (LATS) User Manual (Version 1.1). Ryerson University, Toronto, ON, Canada.

Byl, N. N. (1995). The use of ultrasound as an enhancer for transcutaneous drug delivery: Phonophoresis. *Physical Therapy, 75*(6), 539.

Canadian Cancer Society. (2011). Canadian cancer statistics. Retrieved September 2, 2011 from the CCS. http://www.cancer.ca/Ontario/About%20cancer/Cancer%20statistics/Stats%20at%20a%20glance/General%20cancer%20stats.aspx?sc_lang=en&r=1

Catane, R., Beck, A., Inbar, Y., Rabin, T., Shabshin, N., Hengst, S., et al. (2007). MR-guided focused ultrasound surgery (MRgFUS) for the palliation of pain in patients with bone metastases-- preliminary clinical experience. *Annals of Oncology : Official Journal of the European Society for Medical Oncology / ESMO, 18*(1), 163-167.

Chapelon, J. Y., Margonari, J., Theillere, Y., Gorry, F., Vernier, F., Blanc, E., et al. (1992). Effects of high-energy focused ultrasound on kidney tissue in the rat and the dog. *European Urology, 22*(2), 147-152.

Chaussy, C., & Thuroff, S. (2000). High-intensity focused ultrasound in prostate cancer: Results after 3 years. *Molecular Urology, 4*(3), 179-182.

Chen, D., Fan, T., Zhang, D., & Wu, J. (2009). A feasibility study of temperature rise measurement in a tissue phantom as an alternative way for characterization of the therapeutic high intensity focused ultrasonic field. *Ultrasonics, 49*(8), 733-742.

Chen, W., Lafon, C., Matula, T. J., Vaezy, S., & Crum, L. A. (2003). Mechanisms of lesion formation in high intensity focused ultrasound therapy. *Acoustics Research Letters Online, 4*(2), 41.

Cheng, S., Zhou, X., Tang, Z., Yu, Y., Bao, S., & Qian, D. (1997). Iodized oil enhances the thermal effect of high-intensity focused ultrasound on ablating experimental liver cancer. *Journal of Cancer Research and Clinical Oncology, 123*(11), 639-644.

Clarke, R. L., & ter Haar, G. R. (1997). Temperature rise recorded during lesion formation by high-intensity focused ultrasound. *Ultrasound in Medicine & Biology, 23*(2), 299-306.

Clement, G. T. (2004). Perspectives in clinical uses of high-intensity focused ultrasound. *Ultrasonics, 42*(10), 1087.

Cobbold, R. S. C. (2007). Foundations of biomedical ultrasound. Oxford University Press.

Coleman, D. J., Lizzi, F. L., & Driller, J. (1985). Therapeutic ultrasound in the treatment of glaucoma. I. experimental model. *Ophthalmology, 92*(3), 339-346.

Coleman, D. J., Lizzi, F. L., & Driller, J. (1985). Therapeutic ultrasound in the treatment of glaucoma. II. clinical applications. *Ophthalmology, 92*(3), 347-353.

Coleman, D. J., Lizzi, F. L., & Torpey, J. H. (1985). Treatment of experimental lens capsular tears with intense focused ultrasound. *British Journal of Ophthalmology, 69*(9), 645-649.

Cosgrove, D. (2006). Ultrasound contrast agents: An overview. *European Journal of Radiology, 60*(3), 324-330.

Cranston D, TER Haar G.R, & Kennedy J.E. (2003). *High intensity focused ultrasound: Surgery of the future?*. England: British Institute of Radiology.

Crum, L. A. (1980). Measurements of the growth of air bubbles by rectified diffusion. *The Journal of the Acoustical Society of America, 68*(1), 203.

Crum, L. A., Roy, R. A., Dinno, M. A., Church, C. C., Apfel, R. E., Holland, C. K., et al. (1992). Acoustic cavitation produced by microsecond pulses of ultrasound: A discussion of some selected results. *Journal of the Acoustical Society of America, 91*(2), 1113-1119.

Dalecki, D. (2004). Mechanical bioeffects of ultrasound. *Annual Review of Biomedical Engineering, 6*(1), 229-248.

Dayton, P., Klibanov, A., Brandenburger, G., & Ferrara, K. (1999). Acoustic radiation force in vivo: A mechanism to assist targeting of microbubbles. *Ultrasound in Medicine & Biology, 25*(8), 1195-1201.

Delius, M., Denk, R., Berding, C., Liebich, H. G., Jordan, M., & Brendel, W. (1990). Biological effects of shock waves: Cavitation by shock waves in piglet liver. *Ultrasound in Medicine & Biology, 16*(5), 467-472.

Dijkmans, P. A., Juffermans, L. J. M., Musters, R. J. P., van Wamel, A., ten Cate, F. J., van Gilst, W., et al. (2004). Microbubbles and ultrasound: From diagnosis to therapy. *European Journal of Echocardiography : The Journal of the Working Group on Echocardiography of the European Society of Cardiology, 5*(4), 245-256.

Dubinsky, T. J., Cuevas, C., Dighe, M. K., Kolokythas, O., & Hwang, J. H. (2008). High-intensity focused ultrasound: Current potential and oncologic applications. *AJR.American Journal of Roentgenology, 190*(1), 191-199.

Dunn, F., Averbuch, A. J., & O'Brien Jr., W. D. (1977). Primary method for the determination of ultrasonic intensity with the elastic sphere-Radiometer. *Acustica, 38*(1), 58-61.

Dyson, M., Woodward, B., & Pond, J. B. (1971). Flow of red blood cells stopped by ultrasound. *Nature, 232*(5312), 572-573.

Farny, C. H., Glynn Holt, R., & Roy, R. A. (2010). The correlation between bubble-enhanced HIFU heating and cavitation power. *, 57*(1) 175-184.

Feng, F., Mal, A., Kabo, M., Wang, J. C., & Bar-Cohen, Y. (2005). The mechanical and thermal effects of focused ultrasound in a model biological material. *The Journal of the Acoustical Society of America, 117*(4 Pt 1), 2347.

Flynn, H.G.(1964). Physics of acoustic cavitation in liquids. In Physical Acoustics, ed. WP Mason, vol. 1B, chapter 9. New York: Academic

Flynn, H. G. (1982). Generation of transient cavities in liquids by microsecond pulses of ultrasound. *The Journal of the Acoustical Society of America, 72*(6), 1926 - 1932.

Frenkel,V. (2011).Editor: "Therapeutic Ultrasound: Mechanisms to Applications". Nova Science Publishers, Inc. Hauppauege, NY.

sFrenkel, V. (2008). Ultrasound mediated delivery of drugs and genes to solid tumors. *Advanced Drug Delivery Reviews, 60*(10), 1193-1208.

Frenkel, V., & Li, K. C. P. (2006). Potential role of pulsed-high intensity focused ultrasound in gene therapy. *Future Oncology (London, England), 2*(1), 111-119.

Fry, F. J. (1958). Precision high intensity focusing ultrasonic machines for surgery. *American Journal of Physical Medicine, 37*(3), 152-156.

Fry, W. J., Barnard, J. W., Fry, E. J., Krumins, R. F., & Brennan, J. F. (1955). Ultrasonic lesions in the mammalian central nervous system. *Science (New York, N.Y.), 122*(3168), 517-518.

Fry, W. J., & Fry, F. J. (1960). Fundamental neurological research and human neurosurgery using intense ultrasound. *IRE Transactions on Medical Electronics, ME-7*, 166-181.

Fry, F. J., Kossoff, G., Eggleton, R. C., & Dunn, F. (1970). Threshold ultrasonic dosages for structural changes in the mammalian brain. *The Journal of the Acoustical Society of America, 48*(6), 1413.

Gelet, A., Chapelon, J. Y., Bouvier, R., Pangaud, C., & Lasne, Y. (1999). Local control of prostate cancer by transrectal high intensity focused ultrasound therapy: Preliminary results. *The Journal of Urology, 161*(1), 156-162.

Gianfelice, D., Khiat, A., Amara, M., Belblidia, A., & Boulanger, Y. (2003). MR imaging-guided focused US ablation of breast cancer: Histopathologic assessment of effectiveness-- initial experience. *Radiology, 227*(3), 849.

Goldberg, S. N., Girnan, G. D., Lukyanov, A. N., Ahmed, M., Monsky, W. L., Gazelle, G. S., et al. (2002). Percutaneous tumor ablation: Increased necrosis with combined radio-frequency ablation and intravenous liposomal doxorubicin in a rat breast tumor model. *Radiology, 222*(3), 797.

Hasegawa, T., & Yosioka, K. (1975). Acoustic radiation force on fused silica spheres and intensity determination. *Journal of the Acoustical Society of America, 58*(3), 581-585.

Hedrick, W. R., Hykes, D. L., Starchman, D. E. (2004). Ultrasound physics and instrumentation. St. Louis, MO: Elsevier Mosby.

Hill, C. R., & ter Haar, G. R. (1995). Review article: High intensity focused ultrasound--potential for cancer treatment. *The British Journal of Radiology, 68*(816), 1296.

Holt, R. G., & Roy, R. A. (2001). Measurements of bubble-enhanced heating from focused, MHz-frequency ultrasound in a tissue-mimicking material. *Ultrasound in Medicine & Biology, 27*(10), 1399-1412.

Huber, P. E., & Debus, J. (2001). Tumor cytotoxicity in vivo and radical formation in vitro depend on the shock wave-induced cavitation dose. *Radiation Research, 156*(3), 301-309.

Humphrey, V. F. (2007). Ultrasound and matter--physical interactions. *Progress in Biophysics and Molecular Biology, 93*(1-3), 195-211.

Hynynen, K. (1991). The threshold for thermally significant cavitation in dog's thigh muscle in vivo. *Ultrasound in Medicine & Biology, 17*(2), 157-169.

Hynynen, K., Pomeroy, O., Smith, D. N., Huber, P. E., McDannold, N. J., Kettenbach, J., et al. (2001). MR imaging-guided focused ultrasound surgery of fibroadenomas in the breast: A feasibility study. *Radiology, 219*(1), 176.

Iizuka, M. N., Sherar, M. D., & Vitkin, I. A. (1999). Optical phantom materials for near infrared laser photocoagulation studies. *Lasers in Surgery and Medicine, 25*(2), 159-169

Janzen, N., Zisman, A., Pantuck, A. J., Perry, K., Schulam, P., & Belldegrun, A. S. (2002). Minimally invasive ablative approaches in the treatment of renal cell carcinoma. *Current Urology Reports, 3*(1), 13-20.

Kaneko, Y., Maruyama, T., Takegami, K., Watanabe, T., Mitsui, H., Hanajiri, K., et al. (2005). Use of a microbubble agent to increase the effects of high intensity focused ultrasound on liver tissue. *European Radiology, 15*(7), 1415-1420.

Kennedy, J. E., Wu, F., ter Haar, G. R., Gleeson, F. V., Phillips, R. R., Middleton, M. R., et al. (2004). High-intensity focused ultrasound for the treatment of liver tumours. *Ultrasonics, 42*(1-9), 931-935.

Kennedy, J. E. (2005). High-intensity focused ultrasound in the treatment of solid tumours. *Nature Reviews Cancer, 5*(4), 321-327.

Kessel, D., Jeffers, R., Fowlkes, J. B., & Cain, C. (1994). Porphyrin-induced enhancement of ultrasound cytotoxicity. *International Journal of Radiation Biology, 66*(2), 221-228.

Kim, H. J., Greenleaf, J. F., Kinnick, R. R., Bronk, J. T., & Bolander, M. E. (1996). Ultrasound-mediated transfection of mammalian cells. *Human Gene Therapy, 7*(11), 1339-1346.

Köhrmann, K. U., Michel, M. S., Gaa, J., Marlinghaus, E., & Alken, P. (2002). High intensity focused ultrasound as noninvasive therapy for multilocal renal cell carcinoma: Case study and review of the literature. *The Journal of Urology, 167*(6), 2397-2403.

Kossoff, G. (1965). Balance technique for the measurement of very low ultrasonic power outputs. *The Journal of the Acoustical Society of America, 38*(5), 880.

Kratzik, C., Schatzl, G., Lackner, J., & Marberger, M. (2006). Transcutaneous high-intensity focused ultrasonography can cure testicular cancer in solitary testis. *Urology, 67*(6), 1269-1273.

Lake, A. M., Hall, T. L., Kieran, K., Fowlkes, J. B., Cain, C. A., & Roberts, W. W. (2008). Histotripsy: Minimally invasive technology for prostatic tissue ablation in an in vivo canine model. *Urology, 72*(3), 682-686.

Lafon, C., Zderic, V., Noble, M., Yuen, J., Kaczkowski, P., Sapozhnikov,O., Chavrier, F., Crum, L.& Vaezy, S. (2005). Gel phantom for use in high-intensity focused ultrasound dosimetry. Ultrasound in Medicine and Biology, 31(10), 1383-1389.

Lawrie, A., Brisken, A. F., Francis, S. E., Tayler, D. I., Chamberlain, J., Crossman, D. C., et al. (1999). Ultrasound enhances reporter gene expression after transfection of vascular cells in vitro. *Circulation, 99*(20), 2617-2620.

Lee, H. M., Hong, J. H., & Choi, H. Y. (2006). High-intensity focused ultrasound therapy for clinically localized prostate cancer. *Prostate Cancer and Prostatic Diseases, 9*(4), 439-443.

Lele, P.P. (1987). Effects of ultrasound on solid mammalian tissues and tumors in vivo. In: Repacholi MH, Grandolfo M, Rindi A, eds. Ultrasound: Medical Applications, Biological Effects and Hazard Potential. New York: Plenum.275–306.

Leighton, T. G. (1994). The acoustic bubble. *The Journal of the Acoustical Society of America, 96*(4), 2616.

Lizzi, F. L., Coleman, D. J., Driller, J., Franzen, L. A., & Jakobiec, F. A. (1978). Experimental, ultrasonically induced lesions in the retina, choroid, and sclera. *Investigative Ophthalmology & Visual Science, 17*(4), 350.

Lynn, J.G., Putnam, T.J., 1944. Histological and cerebral lesions produced by focused ultrasound. Am. J. Pathol. 20, 637–649.

Lynn, J.G., Zwemmer, R.L., Chick, A.J., Miller, A.F., 1942. A new method for the generation and use of focused ultrasound in experimental biology. J. Gen. Physiol. 26, 179–193.

Madersbacher, S., Kratzik, C., Susani, M., Marberger, M., Foster, R. S., Bihrle, R., et al. (1994). Tissue ablation in benign prostatic hyperplasia with high intensity focused ultrasound. *Journal of Urology, 152*(6 I), 1956-1961.

Mashouf, S. (2009). An Enhanced Numerical Model to Simulate Nonlinear Continuous Wave Ultrasound Propagation and the Resulting Temperature Response. Unpublished master's thesis, Ryerson University, Toronto, ON, Canada.

Matsumoto, Y., Allen, J. S., Yoshizawa, S., Ikeda, T., & Kaneko, Y. (2004). Medical ultrasound with microbubbles. *Experimental Thermal and Fluid Science, 29*(3), 255-265.

McDannold, N., Vykhodtseva, N., & Hynynen, K. (2006). Targeted disruption of the blood-brain barrier with focused ultrasound: Association with cavitation activity. *Physics in Medicine and Biology, 51*(4), 793-807.

Melodelima, D., Chapelon, J. Y., Theillère, Y., & Cathignol, D. (2004). Combination of thermal and cavitation effects to generate deep lesions with an endocavitary applicator using a plane transducer: Ex vivo studies. *Ultrasound in Medicine & Biology, 30*(1), 103-111.

Miller, D. L., & Thomas, R. M. (1996). Contrast-agent gas bodies enhance hemolysis induced by lithotripter shock waves and high-intensity focused ultrasound in whole blood. *Ultrasound in Medicine & Biology, 22*(8), 1089-1095.

Miller, M. W., Miller, D. L., & Brayman, A. A. (1996). A review of in vitro bioeffects of inertial ultrasonic cavitation from a mechanistic perspective. *Ultrasound in Medicine & Biology, 22*(9), 1131-1154.

Mitragotri, S. (2005). Healing sound: The use of ultrasound in drug delivery and other therapeutic applications. *Nature Reviews.Drug Discovery, 4*(3), 255-260.

Mitragotri, S., Blankschtein, D., & Langer, R. (1995). Ultrasound-mediated transdermal protein delivery. *Science, 269*(5225), 850-853.

Mitragotri, S., Edwards, D. A., Blankschtein, D., & Langer, R. (1995). A mechanistic study of ultrasonically-enhanced transdermal drug delivery. *Journal of Pharmaceutical Sciences, 84*(6), 697-706.

Mourad, P. D., Lazar, D. A., Curra, F. P., Mohr, B. C., Andrus, K. C., Avellino, A. M., et al. (2001). Ultrasound accelerates functional recovery after peripheral nerve damage. *Neurosurgery, 48*(5), 1136-1141.

Nightingale, K. R., Kornguth, P. J., Walker, W. F., McDermott, B. A., & Trahey, G. E. (1995). A novel ultrasonic technique for differentiating cysts from solid lesions: Preliminary results in the breast. *Ultrasound in Medicine & Biology, 21*(6), 745-751.

O'Neil, H. T. (1949). Theory of focusing radiators. *The Journal of the Acoustical Society of America, 21*(5), 516.

Onda Corporation. (2008). Onda RFB-2000 Radiation Force Balance Operating Manual. Sunnyvale, California, USA.

Oosterhof, G. O. N., Cornel, E. B., Smits, G. A. H. J., Debruyne, F. M. J., & Schalken, J. A. (1997). Influence of high-intensity focused ultrasound on the development of metastases. *European Urology, 32*(1), 91-95.

Parsons, J. E., Cain, C. A., & Fowlkes, J. B. (2005). Characterizing pulsed ultrasound therapy for production of cavitationally-induced lesions. *AIP Conference Proceedings, , 754* 178-180.

Parsons, J. E., Cain, C. A., Abrams, G. D., & Fowlkes, J. B. (2006). Pulsed cavitational ultrasound therapy for controlled tissue homogenization. *Ultrasound in Medicine & Biology, 32*(1), 115-129.

Pernot, M., Pernot, M., Tanter, M., Tanter, M., Bercoff, J., Bercoff, J., et al. (2004). Temperature estimation using ultrasonic spatial compound imaging. *, 51*(5) 606-615.

Pilla, A. A., Mont, M. A., Nasser, P. R., Khan, S. A., Figueiredo, M., Kaufman, J. J., et al. (1990). Non-invasive low-intensity pulsed ultrasound accelerates bone healing in the rabbit. *Journal of Orthopaedic Trauma, 4*(3), 246-253.

Poliachik, S. L., Chandler, W. L., Mourad, P. D., Bailey, M. R., Bloch, S., Cleveland, R. O., et al. (1999). Effect of high-intensity focused ultrasound on whole blood with and without microbubble contrast agent. *Ultrasound in Medicine & Biology, 25*(6), 991-998.

Prat, F., Chapelon, J. Y., Abou el Fadil, F., Sibille, A., Theillière, Y., Ponchon, T., et al. (1994). Focused liver ablation by cavitation in the rabbit: A potential new method of extracorporeal treatment. *Gut, 35*(3), 395-400.

Prince, J. L. & Links, J. M. (2006). Medical Imaging: Signals and systems. Upper Saddle River, NJ: Pearson Prentice Hall

Prosperetti, A. (1998). Physics of acoustic cavitation in liquids: H. G. Flynn's review 35 years later. *The Journal of the Acoustical Society of America, 103*(5), 2970.

Roberts, W. W., Hall, T. L., Ives, K., Wolf, J. S., Fowlkes, J. B., & Cain, C. A. (2006). Pulsed cavitational ultrasound: A noninvasive technology for controlled tissue ablation (histotripsy) in the rabbit kidney. *The Journal of Urology, 175*(2), 734-738.

Rooney, J.A., & Nyborg, W.L. (1972). Acoustic radiation pressure in a traveling plane wave field. Am. J. Phys. 40:1825–30

Rooney, J.A. (1973). Determination of acoustic power outputs in the microwatt -milliwatt range. Ultrasound Med. Biol. 1:13–16

Rosenschein, U., Gaul, G., Erbel, R., Amann, F., Velasguez, D., Stoerger, H., et al. (1999). Percutaneous transluminal therapy of occluded saphenous vein grafts: Can the challenge be met with ultrasound thrombolysis? *Circulation, 99*(1), 26.

Rosenschein, U., Roth, A., Rassin, T., Basan, S., Laniado, S., & Miller, H. I. (1997). Analysis of coronary ultrasound thrombolysis endpoints in acute myocardial infarction (ACUTE trial): Results of the feasibility phase. *Circulation, 95*(6), 1411-1416.

Sapareto, S. A., & Dewey, W. C. (1984). Thermal dose determination in cancer therapy. *International Journal of Radiation Oncology, Biology, Physics, 10*(6), 787.

Schäfer, S., Kliner, S., Klinghammer, L., Kaarmann, H., Lucic, I., Nixdorff, U., et al. (2005). Influence of ultrasound operating parameters on ultrasound-induced thrombolysis in vitro. *Ultrasound in Medicine & Biology, 31*(6), 841.

Shehata, I. A. (2011). Treatment with high intensity focused ultrasound: Secrets revealed. *European Journal of Radiology,*

Sokka, S. D., King, R., & Hynynen, K. (2003). MRI-guided gas bubble enhanced ultrasound heating in in vivo rabbit thigh. *Physics in Medicine and Biology, 48*(2), 223-241.

Statistics Canada, Canadian Cancer Society, Canadian Electronic Library (Firm), Public Health Agency of Canada, & ebrary, I. (2011). *Canadian cancer statistics 2011: Featuring colorectal cancer* .Retrieved September 2, 2011 from the CCS http://www.cancer.ca/Ontario/About%20cancer/Cancer%20statistics/Stats%20at%20a%20glance/General%20cancer%20stats.aspx?sc_lang=en&r=1

Stewart, E. A., Gedroyc, W. M. W., Tempany, C. M. C., Quade, B. J., Inbar, Y., Ehrenstein, T., et al. (2003). Focused ultrasound treatment of uterine fibroid tumors: Safety and feasibility of a noninvasive thermoablative technique. *American Journal of Obstetrics and Gynecology, 189*(1), 48-54.

Takahi Hasegawa, & Katuya Yosioka. (1975). Acoustic radiation force on fused silica spheres, and intensity determination. *The Journal of the Acoustical Society of America, 58*(3), 581.

Tata, D. B., Dunn, F., & Tindall, D. J. (1997). Selective clinical ultrasound signals mediate differential gene transfer and expression in two human prostate cancer cell lines: LnCap and PC-3. *Biochemical and Biophysical Research Communications, 234*(1), 64-67.

ter Haar, G. (1995). Ultrasound focal beam surgery. *Ultrasound in Medicine & Biology, 21*(9), 1089-1100.

ter Haar, G. (2001). High intensity focused ultrasound for the treatment of tumors. *Echocardiography (Mount Kisco, N.Y.), 18*(4), 317-322.

ter Haar, G. (2001). Acoustic surgery. *Physics Today, 54*(12), 29.

ter Haar, G. (2007). Therapeutic applications of ultrasound. *Progress in Biophysics and Molecular Biology, 93*(1-3), 111-129.

ter, Haar, G., Clarke, R. L., Vaughan, M. G., & Hill, C. R. (1991). Trackless surgery using focused ultrasound: Technique and case report. *Minimally Invasive Therapy & Allied Technologies, 1*(1), 13-19.

ter Haar, G., & Coussios,C .(2007). High intensity focused ultrasound: Physical principles and devices. *International Journal of Hyperthermia*, 23(2), 89-104.

ter Haar, G., Rivens, I., Chen, L., & Riddler, S. (1991). High intensity focused ultrasound for the treatment of rat tumours. *Physics in Medicine and Biology, 36*(11), 1495.

Tezel, A., & Mitragotri, S. (2003). Interactions of inertial cavitation bubbles with stratum corneum lipid bilayers during low-frequency sonophoresis. *Biophysical Journal, 85*(6), 3502-3512.

Thüroff, S., Chaussy, C., Vallancien, G., Wieland, W., Kiel, H. J., Le Duc, A., et al. (2003). High-intensity focused ultrasound and localized prostate cancer: Efficacy results from the european multicentric study. *Journal of Endourology, 17*(8), 673-677.

Tran, B. C., Jongbum Seo, Hall, T. L., Fowlkes, J. B., & Cain, C. A. (2003). Microbubble-enhanced cavitation for noninvasive ultrasound surgery. *, 50*(10) 1296-1304.

Umemura, S., Kawabata, K., Hashiba, K. (2001).Enhancement of ultrasonic absorption by microbubbles for therapeutic application. In: Proceedings of the Ultrasonics Symposium. Atlanta, Ga: Institute of Electrical and Electronics Engineers, 1311–1314.

Unger, E. C., Matsunaga, T. O., McCreery, T., Schumann, P., Sweitzer, R., & Quigley, R. (2002). Therapeutic applications of microbubbles. *European Journal of Radiology, 42*(2), 160-168.

Unger, E. C., Porter, T., Culp, W., Labell, R., Matsunaga, T., & Zutshi, R. (2004). Therapeutic applications of lipid-coated microbubbles. *Advanced Drug Delivery Reviews, 56*(9), 1291-1314.

Vaezy, S., Shi, X., Martin, R. W., Chi, E., Nelson, P. I., Bailey, M. R., et al. (2001). Real-time visualization of high-intensity focused ultrasound treatment using ultrasound imaging. *Ultrasound in Medicine & Biology, 27*(1), 33-42.

Vaezy, S., & Zderic, V. (2007). Hemorrhage control using high intensity focused ultrasound. *International Journal of Hyperthermia : The Official Journal of European Society for Hyperthermic Oncology, North American Hyperthermia Group, 23*(2), 203.

Vallancien, G., Harouni, M., Guillonneau, B., Veillon, B., & Bougaran, J. (1996). Ablation of superficial bladder tumors with focused extracorporeal pyrotherapy. *Urology, 47*(2), 204-207.

Vaughan, M. G., ter Haar, G. R., Hill, C. R., Clarke, R. L., & Hopewell, J. W. (1994). Minimally invasive cancer surgery using focused ultrasound: A pre-clinical, normal tissue study. *The British Journal of Radiology, 67*(795), 267.

Visioli, A. G., Rivens, I. H., ter Haar, G. R., Horwich, A., Huddart, R. A., Moskovic, E., et al. (1999). Preliminary results of a phase I dose escalation clinical trial using focused ultrasound in the treatment of localised tumours. *European Journal of Ultrasound : Official Journal of the European Federation of Societies for Ultrasound in Medicine and Biology, 9*(1), 11-18.

von Eschenbach, A. C. (2004). A vision for the national cancer program in the united states. *Nature Reviews.Cancer, 4*(10), 820-828.

Warden, S. J., Fuchs, R. K., Kessler, C. K., Avin, K. G., Cardinal, R. E., & Stewart, R. L. (2006). Ultrasound produced by a conventional therapeutic ultrasound unit accelerates fracture repair. *Physical Therapy, 86*(8), 1118.

William J. Fry, & Ruth Baumann Fry. (1954). Determination of absolute sound levels and acoustic absorption coefficients by thermocouple Probes—Experiment. *The Journal of the Acoustical Society of America, 26*(3), 311.

Wood, R. W., & Loomis, A. L. (1928). The physical and biological effects of high-frequency sound-waves of great intensity. (phil. mag., sept., 1927). *Journal of the Franklin Institute, 205*(1), 151-153.

Wu, F., Wang, Z., Chen, W., Bai, J., Zhu, H., & Qiao, T. (2003). Preliminary experience using high intensity focused ultrasound for the treatment of patients with advanced stage renal malignancy. *The Journal of Urology, 170*(6 Pt 1), 2237-2240.

Wu, F., Wang, Z., Chen, W., Wang, W., Gui, Y., Zhang, M., et al. (2004). Extracorporeal high intensity focused ultrasound ablation in the treatment of 1038 patients with solid carcinomas in china: An overview. *Ultrasonics Sonochemistry, 11*(3-4), 149-154.

Wu, F., Wang, Z., Chen, W., Zou, J., Bai, J., Zhu, H., et al. (2004). Extracorporeal focused ultrasound surgery for treatment of human solid carcinomas: Early chinese clinical experience. *Ultrasound in Medicine & Biology, 30*(2), 245-260.

Wu, J., & Nyborg, W. L. (2008). Ultrasound, cavitation bubbles and their interaction with cells. *Advanced Drug Delivery Reviews, 60*(10), 1103-1116.

J. Wu, J., Nyborg, W.L.(2007). Emerging Therapeutic Ultrasound, World Scientific Co., Hackensack, New Jersey, USA.

Xu, Z., Fowlkes, J. B., Rothman, E. D., Levin, A. M., & Cain, C. A. (2005). Controlled ultrasound tissue erosion: The role of dynamic interaction between insonation and microbubble activity. *Journal of the Acoustical Society of America, 117*(1), 424-435.

Xu, Z., Ludomirsky, A., Eun, L. Y., Hall, T. L., Tran, B. C., Fowlkes, B., et al. (2004). Controlled ultrasound tissue erosion. *IEEE Transactions on Ultrasonics, Ferroelectrics and Frequency Control, 51*(6), 726-736.

Yang, X. (2004). In Roy R., Holt R.(Eds.), *Bubble dynamics and size distributions during focused ultrasound insonation* ASA.

Yang, X., Roy, R. A., & Holt, R. G. (2004). Bubble dynamics and size distributions during focused ultrasound insonation. *The Journal of the Acoustical Society of America, 116*(6), 3423.

Yock, P. G., & Fitzgerald, P. J. (1997). Catheter-based ultrasound thrombolysis. *Circulation, 95*(6), 1360.

Young F. (1989). Cavitation. New York:McGraw-Hill.

Young, F. R., &. Strasberg, M. (1992). Cavitation. *The Journal of the Acoustical Society of America, 91*(6), 3591.

Yu, T., Wang, G., Hu, K., Ma, P., Bai, J., & Wang, Z. (2004). A microbubble agent improves the therapeutic efficiency of high intensity focused ultrasound: A rabbit kidney study. *Urological Research, 32*(1), 14-19.

Zderic, V., and Vaezy, S. (2007). Hemorrhage control using high intensity focused ultrasound, Int. J. Hypertherm. 23 (2),1–9

Zhi B. Wang, Feng Wu, Zhi L. Wang, & Chuan Liu. (1998). Concept of biological focal field and its importance in tissue resection with high‐intensity focused ultrasound. *The Journal of the Acoustical Society of America, 103*(5), 2869.